Raytheon

Raytheon Systems Company

SPECIAL SENSOR MICROWAVE / IMAGER

(SSM/I)

USER'S INTERPRETATION GUIDE

FOURTH EDITION
(Revision A)

Contract Number F04701-96-C-0026

April 1999

Contracting Agency:

Department of the Air Force
Space and Missile Systems Center (SMC)

FOREWORD
TO THE FOURTH EDITION

This represents the 4th Edition of the SSM/I User's Interpretation Guide. The primary impetus behind issuing this edition was that most of the figures in previous versions were of poor image quality. We have replaced those outdated images with higher quality DIGS (DMSP Image Generation System) output images. We also set out to create new figures and graphs, where possible, using standard office automation tools, rather than scanned out of other references. Here is a summary of the changes:

- Section 2 was reorganized and augmented with new graphs and the latest radiative transfer naming conventions.

- Section 3 is changed very little, except that a few of the images and tables were re-created. Unfortunately, the exploded view of the SSM/I sensor is still of poor quality.

- Section 4 was changed to reflect some recent changes in the ground processing software supplied to the weather centrals (AFWA, FNMOC). Also included for historical reference is the history of Specter and its eventual migration to DIGS.

- All the images in Section 5 were updated to DIGS format.

- Algorithms in Section 6 were changed to include corrections coordinated in late 1997 and early 1998. Where necessary, the images were updated to DIGS format.

- The case study in Section 7 is a discussion of the same synoptic situation as in previous editions, except that the SSM/I images have been upgraded to DIGS output.

In addition to the contributors to previous editions (see next page), I would like to thank James Austin, Mary Dahm, Scott Turek and Justin Armstrong for their assistance in compiling this latest revision. Finally, special thanks to Dr. Jeff Haferman at FNMOC for providing corrections to some of the algorithm citations in Section 6.

Tim Davis
Raytheon Systems Company
April 1999

Acknowledgements
(from previous editions)

The authors wish to thank the many helpful individuals who reviewed the very rough first draft and provided numerous useful corrections and suggestions. These included Lt Col Al Adams (SSD/MWA), Dick Armstrong (NSIDC), Marie Colton (FNOC), Vince Falcone (AFGL), Lt Col Charles Holliday (AFGWC), Jim Hollinger (NRL), Tom Lee (NOARL), Elena Lobl (Hughes), Bruce Miers (ASL), Jim Peirce (Hughes), and Lt Col Michael Zimmerman (AFGWC). We are especially grateful to Capt Dawn Stewart (Det 19, 15 WS) and Capt Randall Skov (AWS/DOT), who provided us with the case study in Section 7. Portions of Section 7 are quoted directly from the work of Captains Stewart and Skov.

Kerry Grant
John Heinrichs
Hughes Aircraft Company
April 1, 1991

TABLE OF CONTENTS

1. Introduction

The purpose of this guide is to familiarize operational personnel with the Special Sensor Microwave/Imager (SSM/I) sensor system, the data it provides, and how to make the best use of this information to support mission requirements.

The SSM/I is a passive microwave sensor carried aboard Defense Meteorological Satellite Program (DMSP) platforms (see Figure 1-1).

Supplementing existing sensors (most of which operate in the infrared or visible ranges) with microwave instruments has been an objective of scientists and operational meteorologists since the theory of microwave remote sensing was first advanced. Section 2 of this guide describes some basic aspects of this theory, covering the nature of electromagnetic radiation and the basic processes by which it is generated and modified by the Earth-atmosphere system.

The first U.S. space-based passive microwave sensors were NASA instruments, including the Electronically Scanning Microwave Radiometer (ESMR), flown aboard Nimbus 5 and 6, and the Scanning Multi-channel Microwave Radiometer (SMMR) on Nimbus 7. Based on this experience, the Department of Defense procured several SSM/I sensors to enhance its capability to determine and predict terrestrial, oceanic, and atmospheric conditions. The first SSM/I to become operational was launched aboard DMSP F8 in June, 1987. As of this edition, the newest on-orbit SSM/I sensor is aboard DMSP F14, which launched in April, 1997. Section 3 describes the SSM/I sensor system and how it functions, and explains its unique sensor-to-Earth geometry.

Section 4 describes methods by which SSM/I data are ingested, processed, and distributed to users. The results of this processing include raw data (imagery) and environmental data records (EDRs; see Table 1-1), both of which can be displayed by a variety of systems or retrieved for use by applications software.

EDR Abbreviation	EDR Description
SM	Soil moisture
SW	Ocean surface wind speed
TYPE	Surface type
ST	Surface temperature
CWO	Cloud water content
RR	Rain rate
IC	Ice concentration
IA	Ice age
IE	Ice edge flag
WVO	Integrated columnar water vapor
RF	Rain flag
SND	Snow depth

Table 1-1. SSM/I derived environmental products

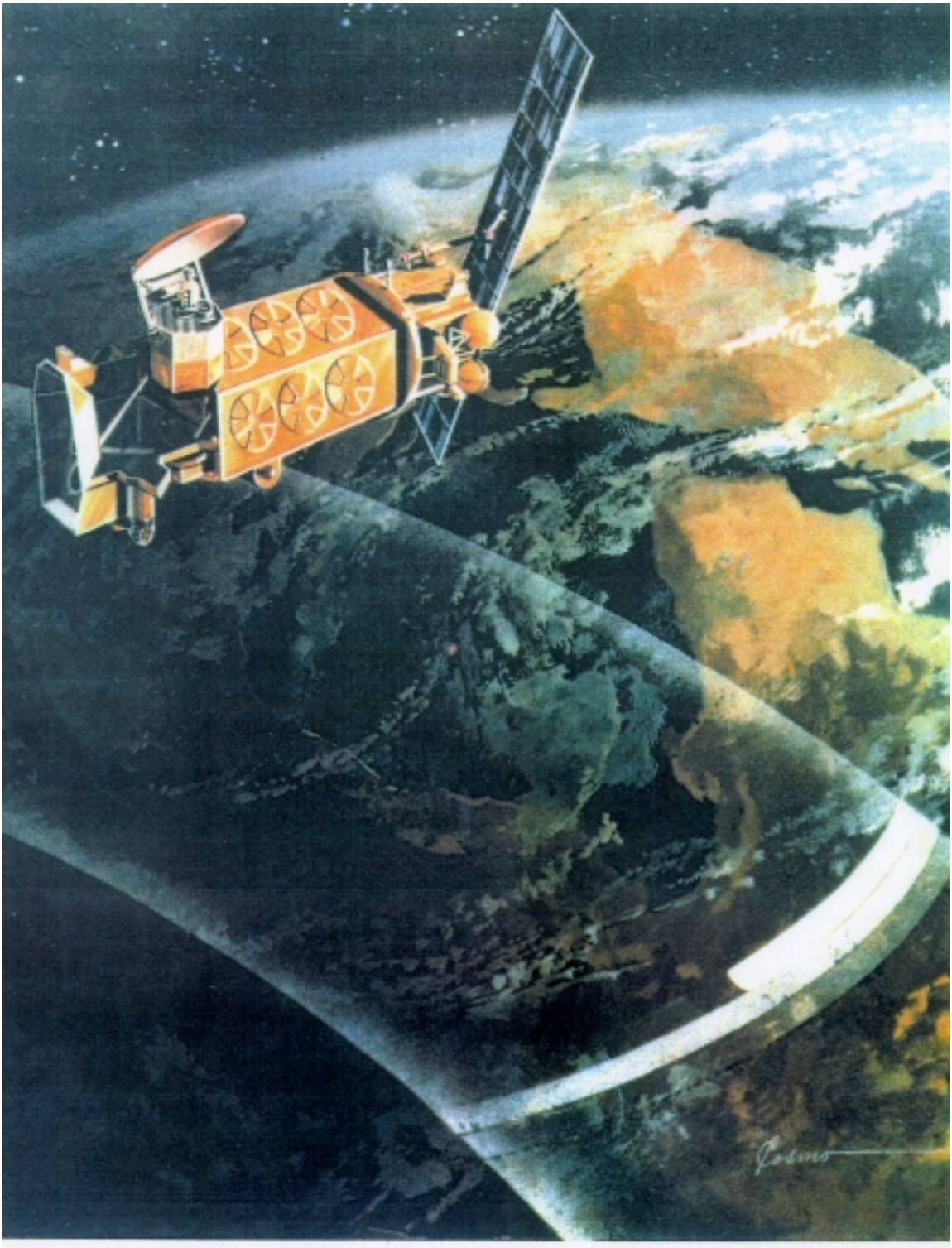

Figure 1-1. The DMSP 5D-2 satellite in a fully deployed operational configuration. The SSM/I is the cylindrical object mounted on the upper surface of the platform on the end farthest from the solar panels. A representation of the curved scans and swath boundaries is superimposed on the Earth's surface.

Because of the relative novelty of passive microwave data, and because of the significant differences in the way microwave radiation is generated and modified by the surface and atmosphere, interpretation of data from the SSM/I differs considerably from that of data from the more traditional infrared (IR) and visible sensors. An extensive discussion of how to interpret SSM/I data can be found in Sections 5 (Sensor Data Records) and 6 (Environmental Data Records).

Finally, Section 7 provides a case study to assist SSM/I users in interpreting the data in a real situation.

2. Microwave Remote Sensing Theory

The SSM/I sensor, like most passive remote sensors, receives information by detecting electromagnetic waves. The various properties of these waves are influenced by the Earth-atmosphere system. Consequently, one can infer the conditions in the system by observing the manner in which the waves are generated and modified.

2.1 The Nature of Electromagnetic Radiation

Electromagnetic (EM) waves are coupled oscillations of an electric field (***E***) and a magnetic field (***B***). These two components oscillate at right angles to each other. Figure 2.1-1 illustrates an EM wave propagating through space (in the z direction).

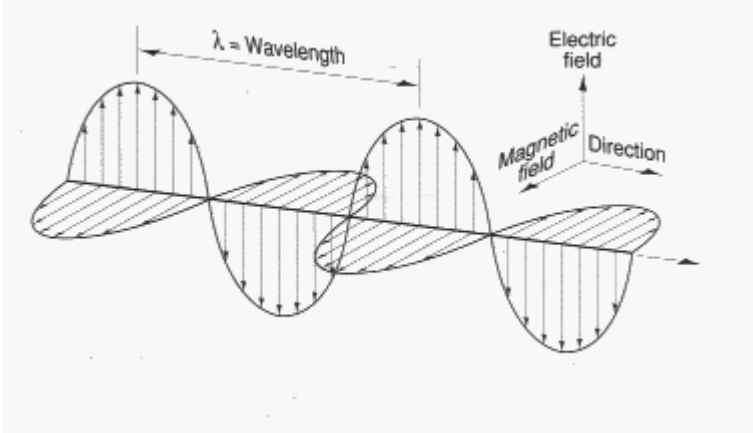

Figure 2.1-1. Model of electromagnetic wave propagation showing electric and magnetic fields perpendicular to each other.

In this example the electric field is confined to the x-axis and the magnetic field is perpendicular to it. In general, the fields are not confined to a particular plane, although ***E*** and ***B*** are always perpendicular to each other. As one can see, EM waves oscillate up and down much like water waves. They are characterized by a frequency (ν), wavelength (λ), and velocity. Frequency is defined as the number of times a wave peak passes a given point in one second, and wavelength as the distance between peaks. The velocity is the speed of light (c), which has a value of approximately 3×10^8 meters/second in a vacuum. It is slightly slower in all other media. The three parameters above are related by:

$$c = \nu \lambda .$$

From this relation, one may note that as the frequency increases, the wavelength becomes shorter. Frequency is measured in cycles per second or hertz (Hz), and wavelength is measured in meters (m), centimeters (cm), millimeters (mm), micrometers ($\mu m = 10^{-6}$ m),

or Angstroms (1Å = 10^{-10} m), depending upon the portion of the electromagnetic spectrum to which one is referring.

The direction in which the electric component of the wave in Figure 2.1-1 oscillates is fixed. In this special case, the wave is said to be linearly polarized (or plane polarized). The polarization of an EM wave simply tells one its orientation in space. Most EM waves are not polarized at all, and the direction of oscillation varies randomly (although the magnetic component is always 90 degrees to the electric component). If an EM wave is linearly polarized such that the electric component of oscillation is contained in a plane defined by a line from the sensor to the Earth and a line normal to the surface at that point, it is termed vertically polarized. If the electric component is perpendicular to this plane, it is termed horizontally polarized.

Since all EM waves travel at the same speed in a given medium (c),[1] in a general sense they differ from each other only in frequency (and thus wavelength). The EM spectrum categorizes these waves according to frequency (or wavelength). Figure 2.1-2 shows the part of the EM spectrum presently used for remote sensing. As seen in the figure, different frequency intervals are grouped together and given specific names (the microwave region, the infrared region, etc.). These regions overlap and are often further subdivided (for example, the radio region is subdivided into bands). The only real physical difference between these regions is their frequencies.

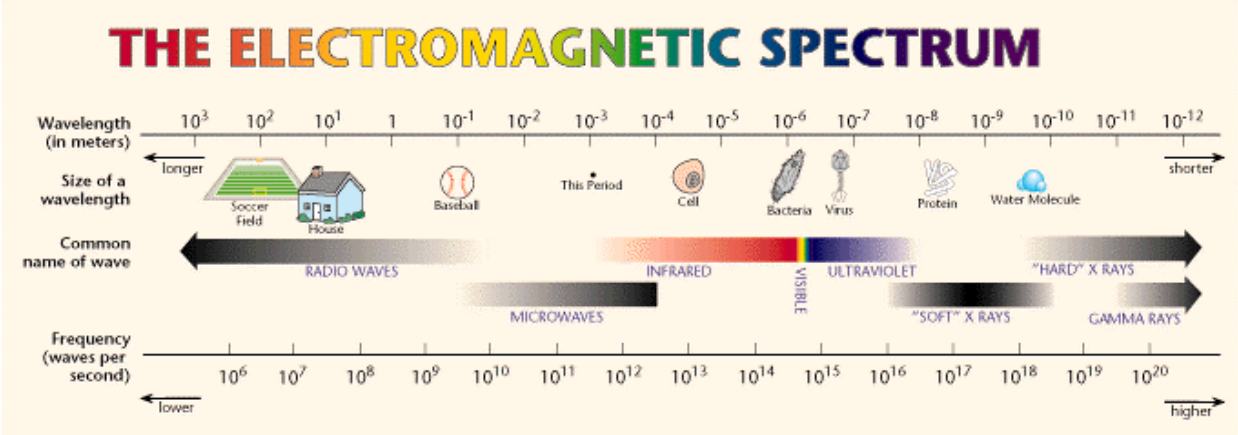

Figure 2.1-2. Electromagnetic spectrum with some illustration of the size scales involved.

There are three regions of particular interest to remote sensing. They are the microwave region (frequencies from about 300 MHz to 300 GHz, or wavelengths from 1 meter to 1 millimeter), the thermal infrared region (wavelengths from 2 μm to an arbitrary upper limit of 1000 μm), and the visible region (wavelengths from roughly 0.4 to 0.7 μm or 4000-7000 Å). The SSM/I measures in the microwave portion of the spectrum at four discrete frequencies: 19, 22, 37 and 85 GHz. The DMSP Operational Linescan System (OLS) consists of a thermal infrared sensor with a band from 10 to 13 μm and a visible

[1] This is not true of a plasma (ionized gas) medium; however, plasma effects are not a primary concern for microwave applications.

sensor with a band from 4000 to 11000 Å (0.4 to 1.1 μm). The OLS measures energy at a higher frequency (shorter wavelength) than the SSM/I.

2.2 Interactions Between Matter and Electromagnetic Waves

Passive remote sensors, such as the SSM/I and the OLS, infer conditions in the atmosphere and on the surface by measuring features in the EM spectrum induced by matter. There are four primary mechanisms in which matter interacts with EM waves: emission, absorption, reflection (or scattering), and transmission. How a particular piece of matter will interact with a given wave depends upon the wavelength of the radiation and the nature of the matter. From a remote sensing perspective, one is concerned with microwaves, thermal IR, and visible light interacting with the surface of the Earth and with atmospheric constituents. Each of the mechanisms of interaction occurs in both the Earth's surface and atmosphere; however, some mechanisms dominate specific regimes. For example, the surface of the Earth is primarily an emitter of microwaves and thermal IR. The atmosphere is transparent to many wavelengths, yet it strongly absorbs and scatters others.

To gain a better understanding of these processes two discussions are useful: Planck's blackbody radiation law (and other laws based on it) and the absorption, emission, and scattering of radiation by gases. Planck's law describes the thermal emission of radiation from the Earth's surface and atmosphere, and the gas theory shows how the atmosphere modifies this emission.

2.3 Planck's Law

All matter with a temperature above absolute zero emits radiation. The emission of radiation due to a body's temperature is called thermal emission. The nature of the radiation emitted (both quantity and frequency) is governed primarily by the temperature of the body. Planck's blackbody radiation law relates the distribution of energy emitted as radiation to its temperature and wavelength (or frequency) by either of the following two formulas:

$$M_e(\lambda, T) = 2\pi hc^2 / [\lambda^5(e^x - 1)] \qquad \textit{(wavelength domain)}$$

or

$$M_e(\nu, T) = 2\pi h\nu^3 / [c^2(e^x - 1)] \qquad \textit{(frequency domain)}$$

where

M_e = spectral radiant exitance (Watts $m^{-2} \cdot \mu m^{-1}$)
λ = wavelength (m)
ν = frequency (Hz)
T = Temperature (K)
c = speed of light in vacuum ($\sim 3.0 \times 10^8$ m s^{-1})
$x = hc/\lambda kT$ *(for wavelength domain formula)*
$x = h\nu/kT$ *(for frequency domain formula)*
h = 6.63 x 10^{-24} J · s (Planck's constant)
k = 1.38 x 10^{-23} J · K^{-1} (Boltzmann's constant)

A **blackbody** is a hypothetical mass of material which 1) completely absorbs all incident radiation and 2) emits all radiation into all directions at all wavelengths at the maximum possible for the given temperature. For this document, we will use the term **spectral radiant exitance**, $M_e(\lambda, T)$, defined as the power radiated into a hemisphere per unit area at a given wavelength and temperature (Vincent, 1990). Figure 2.3-1 is a graph of M_e vs. wavelength for emitters of various temperatures. The **total radiant exitance**, M_{total}, of a given blackbody is represented by the area under its spectral exitance curve. Three key features are immediately apparent in this figure:

- M_{total}, the total area under the Planck curve, increases with increasing temperature. That is, the warmer the source, the more energy it gives off.
- As the temperature of the source increases, the wavelength at which the blackbody emits the most radiation (λ_{bmax}) decreases.
- At either end (the "wings") of the curve, the values should be fairly easily modeled since they are virtually straight lines.

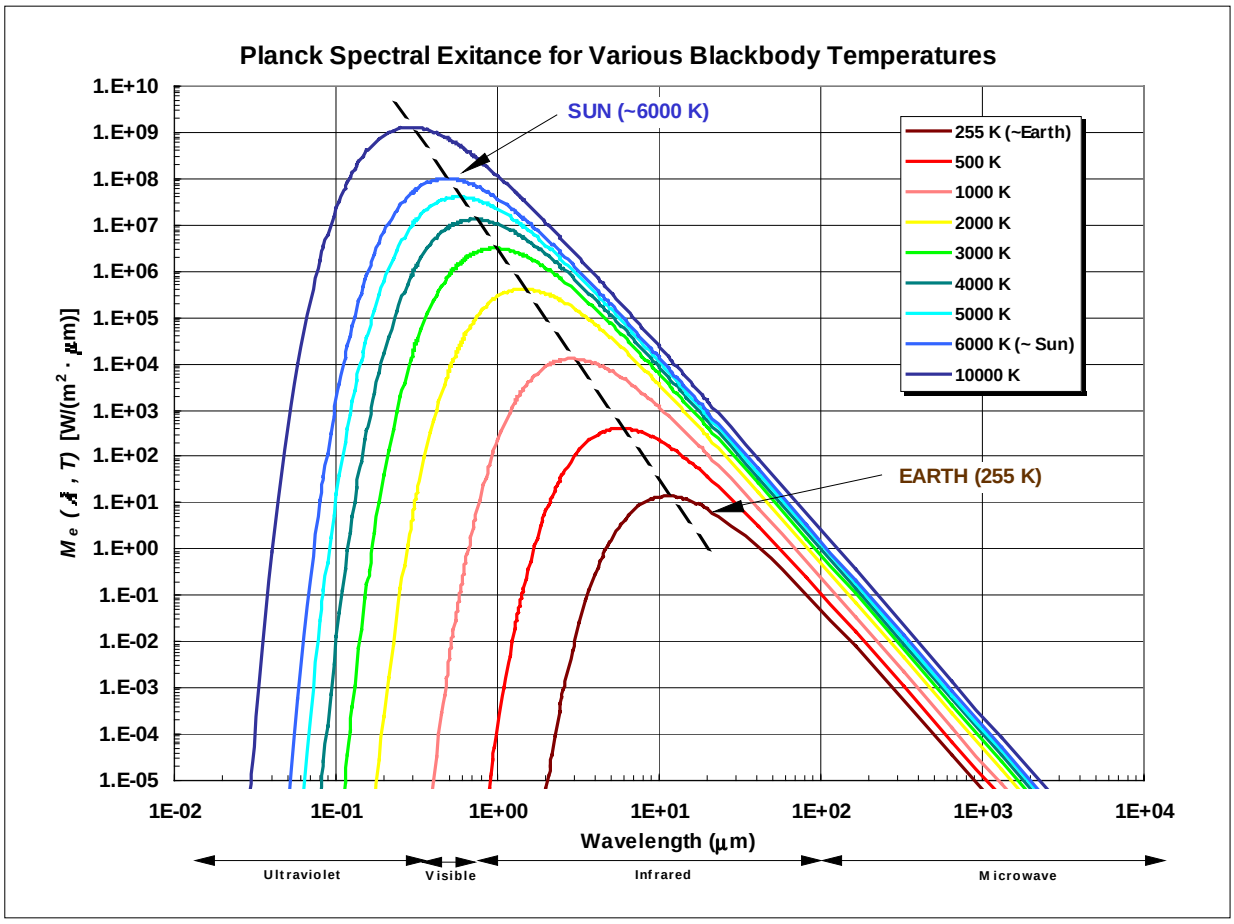

Figure 2.3-1. Planck curves of spectral radiant exitance. The dashed black line connects peaks for each curve shown to illustrate the linear relationship between blackbody temperature and the wavelength of peak exitance.

These three observations gave rise to three relationships which were derived from Planck's Law: the Stefan-Boltzmann Law, Wien's Displacement Law, and the Rayleigh-Jeans approximation.

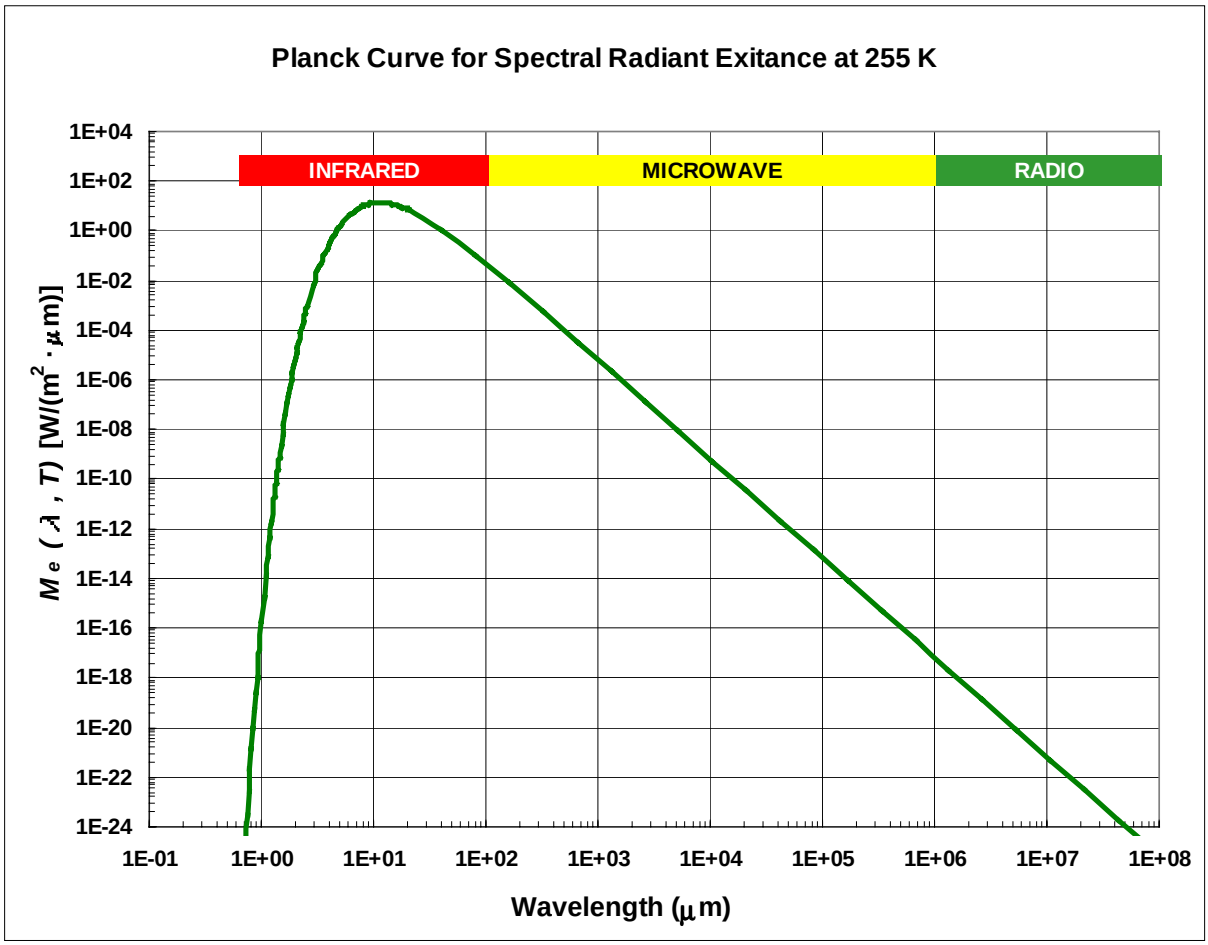

Figure 2.3-2. Blackbody model of the Earth-atmosphere system. Notice the nearly linear relationship between M_e and wavelength in the microwave portion of the spectrum.

2.3.1 The Stefan-Boltzmann Law

Total radiant exitance, M_{total} (the total power in watts emitted by a blackbody per unit area) increases as the fourth power of the temperature (Stefan-Boltzmann's law),

$$M_{total} = \sigma T^4,$$

where

M_{total} = the total exitance from a blackbody

σ = the Stefan-Boltzmann constant[2]
T = Temperature (Kelvins)

This is derived by integrating Planck's equation over all wavelengths and corresponds to the area under a Planck curve at a given blackbody temperature. As a practical example, if an iron bar is heated to higher and higher temperatures, it glows more brightly.

2.3.2 Wien's Displacement Law.

The wavelength at which a blackbody emits the most radiation is given by

$$\lambda_{max} = 2897\ \mu\text{m} \cdot \text{K} / T,$$

where

λ_{max} = brightest wavelength (μm),
T = temperature (Kelvins).

Thus, if the mean temperature of the Earth-atmosphere system is 255 K, the wavelength at which the brightest emissions occur is 2897 / 255 = 11.4 μm. Building on the iron bar example, as the temperature increases, not only does the iron glow brighter, but it also changes colors from a dull red to orange, to bright yellow. The color change is due to λ_{max} decreasing from red toward yellow (lower wavelength).

2.3.3 Rayleigh-Jeans approximation.

When designing sensors to extract information about the Earth from its radiation, it is reasonable to look at the regions where the Earth emits most of its radiant energy. DMSP's primary sensor, the Operational Line Scanner (OLS), does this by monitoring the visible and infrared (thermal emission) portions of the spectrum. While λ_{max} for the Earth occurs in the infrared, a significant portion of Earth's emitted radiation resides in the microwave region of the spectrum. Planck's law describes these emissions and is the model used to generate Figure 2.3-2. Notice in this figure that at the Earth's mean temperature, the relationship between brightness and frequency in the microwave portion (~10^2 to 10^6 μm) of the spectrum is roughly linear. As a result, one can make an important and useful simplification to Planck's law in this region, namely the Rayleigh-Jeans approximation, which states

$$M_e(\lambda, T) = 2\pi kTc / \lambda^4 \qquad \textit{(wavelength domain)}$$
$$M_e(\nu, T) = 2\pi kT\nu^2 / c^2 \qquad \textit{(frequency domain)}$$

where we defined all symbols in section 2.3. This approximation is linear in temperature and useful when the frequency is < 120 GHz (for a body at 300 K or less). SSM/I calibrations depend on the Rayleigh-Jeans approximation.

[2] The Stefan-Boltzmann constant, $\sigma = 5.672 \times 10^{-8}\ \text{W} \cdot \text{m}^{-2} \cdot \text{deg}^{-4}$

2.4 Absorption, Emission, and Scattering by the Atmosphere

Thermal emission of electromagnetic energy from the Earth's surface and atmosphere is not the end of the remote sensing story. The emitted energy is modified on its way to the sensor by the atmosphere itself. *How* it is modified allows us to infer some of the most important information about the weather: the presence of water vapor, rain, and clouds. The atmosphere modifies the thermal spectrum by selective absorption, emission, and scattering of EM energy.

The SSM/I gathers information about various atmospheric components by exploiting known changes in the thermal spectrum due to these three processes. Carbon dioxide, oxygen, water vapor, and liquid water reveal themselves to remote sensing devices through absorption and emission of EM radiation. Liquid and solid water are also detectable through scattering.

When a gas gains or loses energy, it does so by absorbing or emitting energy at a specific frequency unique to the kind of gas involved. One may thus positively identify specific gases by detecting the emission or absorption of radiation at the wavelength(s) unique to that gas. Gases have many energy states and absorb (and emit) energy at many frequencies. Whether an ensemble of molecules in a gas emits or absorbs at a particular frequency depends upon a number of factors, among them the temperature and pressure

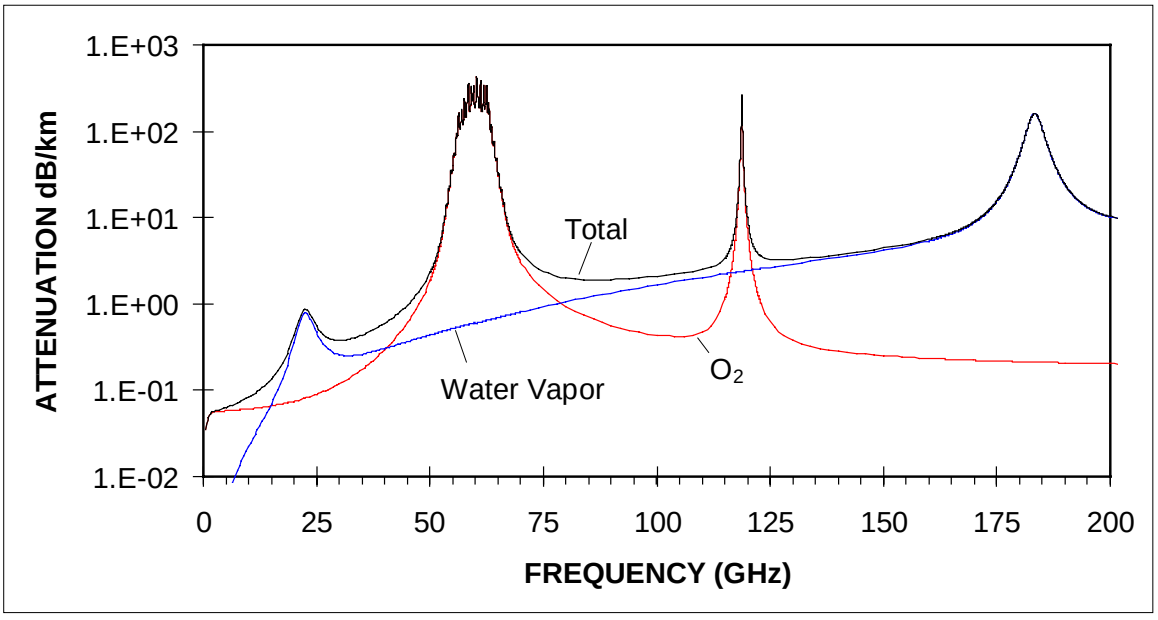

Figure 2.4-1. Atmospheric absorption in the microwave region (Liebe, et al., 1991; Meeks and Lilley, 1963; Gaut and Reifenstein, 1971).

of the gas and the brightness of the incident radiation. The emission and absorption features of a gas are known simply as its spectral lines. These spectral lines have a finite bandwidth, broadened by the Doppler effect (since the molecules are in motion), pressure, and other factors.

Figure 2.4-1 shows the absorption of microwaves due to atmospheric gases from 0 to 200 GHz. In general, absorption increases with increasing frequency. This explains why lower frequencies are more sensitive to surface phenomena and higher frequencies are more atmospheric sensitive. Water vapor has spectral lines at 22.2 GHz and 183.3 GHz. Oxygen has a family of lines centered near 60 GHz and a single line at 118.8 GHz.

Clouds are visible to humans because they scatter energy in the visible portion of the spectrum. Rain is detectable by radar because it scatters energy in the radar region. How much a particle in the atmosphere scatters a wave is a function of the particle's size and the wavelength of the radiation. Unlike absorption or emission, which occur only at specific wavelengths, scattering occurs over all wavelengths within a certain range. Rayleigh scattering is strongest when the diameter of the particle is approximately one-tenth the wavelength being scattered. Raindrops, for example, range in size from 0.5 mm to 7 mm; this is why weather radar systems are engineered so that wavelengths typically fall within the 1-10 cm range.

Absorption, emission, and scattering are important processes to the SSM/I. Three other concepts are needed to complete the story: emissivity, polarization, and the concept of brightness temperatures.

2.5 Emissivity, Brightness Temperatures, and Polarization

Real substances rarely behave like perfect blackbodies. The radiation emitted by a substance at a particular temperature will not be exactly the same as that emitted by a perfect blackbody at the same temperature. The ratio of actual exitance of a material (M_{actual}) to the expected blackbody exitance ($M_{blackbody}$) is the emissivity ε:

$$\text{emissivity} = \varepsilon = M_{actual} / M_{blackbody}$$

Emissivity ranges between 0 and 1, so the measured brightness of an object is always less than or equal to its expected blackbody brightness. Since one can relate brightness of an object at a particular wavelength to its temperature, an object's emissivity affects its apparent temperature in the same way:

$$T_b = \varepsilon T_{actual}$$

where

T_{actual} = the thermometric temperature of the object,
T_b = the radiometric temperature of the object (also known as the brightness temperature),

ε = the emissivity of the object.

The temperature measured by the SSM/I is the *brightness temperature* of the object at the wavelength being measured. The brightness temperature differs from the actual thermometric temperature of the object by the factor ε, the emissivity. Therefore, objects with a low emissivity (such as water) will appear much colder to the SSM/I than they actually are. If an object has a high emissivity (ε = 1), the SSM/I and a thermometer would both measure the same temperature.

Variations of surface brightness temperatures can exist due to emissivity variations, even in the absence of thermometric temperature changes. To maintain thermal equilibrium of a surface the emissivity plus the reflectivity (R) must equal 1 ($\varepsilon + R = 1$). The following shows that the brightness temperatures of land and ocean surfaces are dramatically different, even though their thermometric temperatures are identical. Assume an atmospheric brightness temperature (T_{sky}) of 50 K.

$$T_{surface} = (\varepsilon_{surface})(T_{surface}) + (R_{surface})(T_{sky})$$

T_{land}	=	(0.9)290	+	(0.1)50	=	266K
T_{ocean}	=	(0.4)290	+	(0.6)50	=	146 K.

Thus materials with the same nominal temperature of 290 K can have strikingly different apparent brightness temperatures.

The emissivity of an object may change depending upon a variety of conditions. Knowledge of the emissivity of substances and the way in which they change allows one to calculate a number of environmental parameters. For example, the emissivity of water increases with an increase of wind speed (see more on this in Section 5). Accordingly, an increase in the brightness temperature over the ocean may indicate an increase in wind speed.

The orientation in which the radiation is emitted may also affect its brightness temperature. In other words, the emissivity of an object may be a function of the polarization of the emitted radiation. Measurement of the amount of polarization can be performed by using two channels at the same frequency: one which detects vertically polarized energy, and another which detects horizontally polarized energy. Usually an EM wave is not polarized purely in the vertical or horizontal plane. In fact, it may not be polarized at all. In this case, both the vertical channel and the horizontal channel will each detect part of the energy from the wave. If the wave is closer to being vertically polarized than horizontally polarized, then the vertical channel will detect the most energy. The difference between the brightness of an object in the vertical channel and in the horizontal channel provides useful information about it.

Each of the concepts discussed - Planck's law, absorption, emission, scattering, emissivity, polarization, and brightness temperatures - can be integrated into a single theory of radiative transfer.

2.6 Radiative Transfer in the Atmosphere

The radiation incident on the SSM/I feedhorn is a mixture of energy created from and modified by many separate sources. Chief among these are radiation emitted by the surface in the direction of the sensor, radiation emitted by the atmosphere in the direction of the sensor, and radiation emitted by the atmosphere in a downward direction which is subsequently reflected by the surface back to the sensor. Radiation from each of these sources is subjected to absorption and scattering by intervening layers of the atmosphere. Figure 2.6-1 diagrams the paths radiation may take to the sensor. Along each path the radiation is subject to absorption and scattering. One can consider the final brightness value (at the sensor) to be a sum of two components: the brightness due to the surface (reduced by the absorption and scattering of the atmosphere), and the brightness due to the atmosphere. Polarization helps to separate the two sources, since emission from the atmosphere is not polarized. The first term takes into account not only the emission from

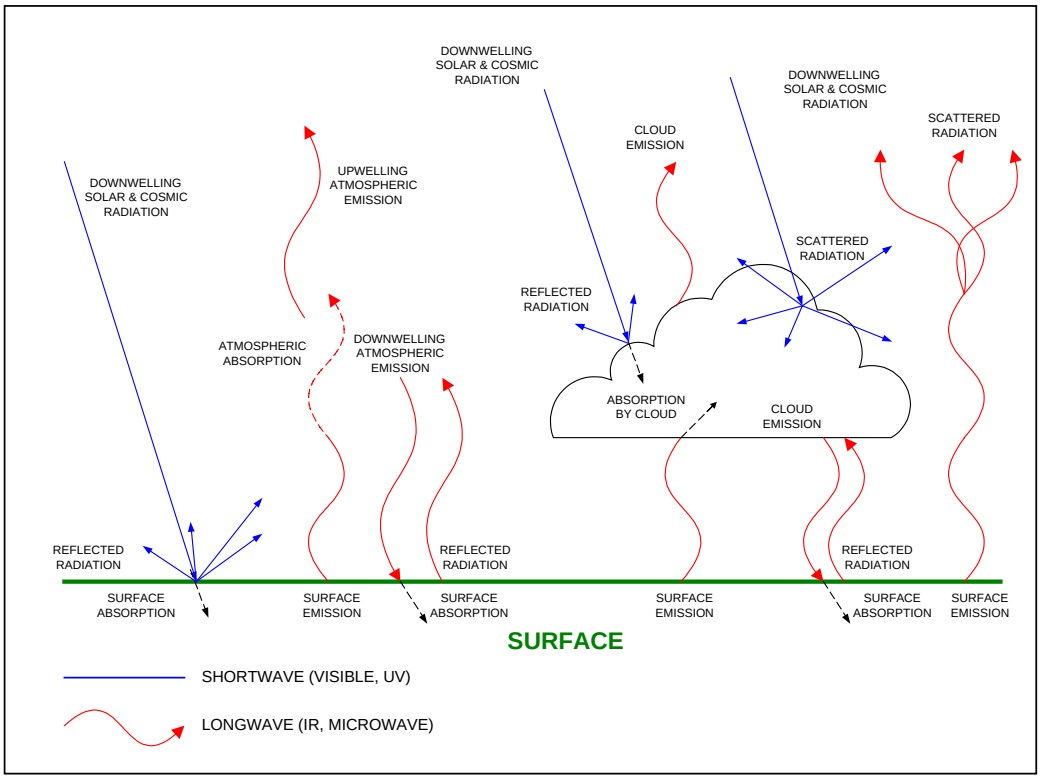

Figure 2.6-1. Radiative transfer processes.

the surface itself, but also emission downwards by the atmosphere (called downwelling radiation) which is reflected back up to the sensor. The brightness due to the atmosphere (upwelling radiation) is in itself a sum of the contributions from each point along the path between the surface and the sensor. By breaking the atmosphere into thin layers and summing the contributions from each of the layers, one may calculate the brightness due to the atmosphere. The contribution from each layer is the difference between the radiation emitted by the layer and the radiation scattered (or absorbed) by the layer.

How a given layer in the atmosphere emits or absorbs radiation is a function of many factors, including frequency, temperature, emissivity, absorption, and size of the material. Detailed knowledge of these factors, and the processes governing them, allow one to build mathematical models of radiative transfer. By setting up certain initial conditions on the surface and in the atmosphere, these models can predict the final brightness values at the sensor. Basically, SSM/I processing solves this problem in reverse. The final brightness values are known. What is required is to solve for the conditions on the surface and in the atmosphere. If the solution is successful, SSM/I derived estimates of environmental parameters match the reality on Earth.

3. The SSM/I Sensor System

3.1 Functional Description of the SSM/I

Radiation reaching the SSM/I from the Earth is directed from a 0.65 m reflector into a feedhorn assembly. This signal gets converted to voltages and incorporated into the DMSP data stream. The reflector and feedhorns comprise the SSM/I antenna subsystem and rotate around the spacecraft vertical axis with a period of 1.899 seconds. Because of its rotation, the antenna, together with the sensor power supply, detectors, pre-amps, and digital signal processing electronics, is called the 'spun' section. The remaining portion of the sensor, called the "despun" section because it is fixed relative to the DMSP platform, contains two calibration reference targets (discussed below). Figure 3.2-1 illustrates the SSM/I sensor and its primary subsystems and components.

3.2 Calibration

Once each rotation, the path from the reflector to the feedhorn is interrupted by two reference targets used for calibration. One of these targets (called the "cold load") is a reflector to open space and thus has a temperature (to the sensor) of about 3 K (the cosmic background temperature). The other target, called the "hot load", has emission characteristics very close to an ideal blackbody, and is thermally connected to the sensor so that it has a temperature of approximately 300 K. Three precision thermistors measure the hot load temperature to within 0.1 K. As the spinning antenna passes each of the two targets, the corresponding detector voltages (in the form of "counts" from the A/D converters) are incorporated into the DMSP data stream. Later, during ground processing, the voltages obtained from Earth measurements are converted to temperatures, using the hot and cold load values as reference points in a simple linear calculation (see section 4.1 for more details).

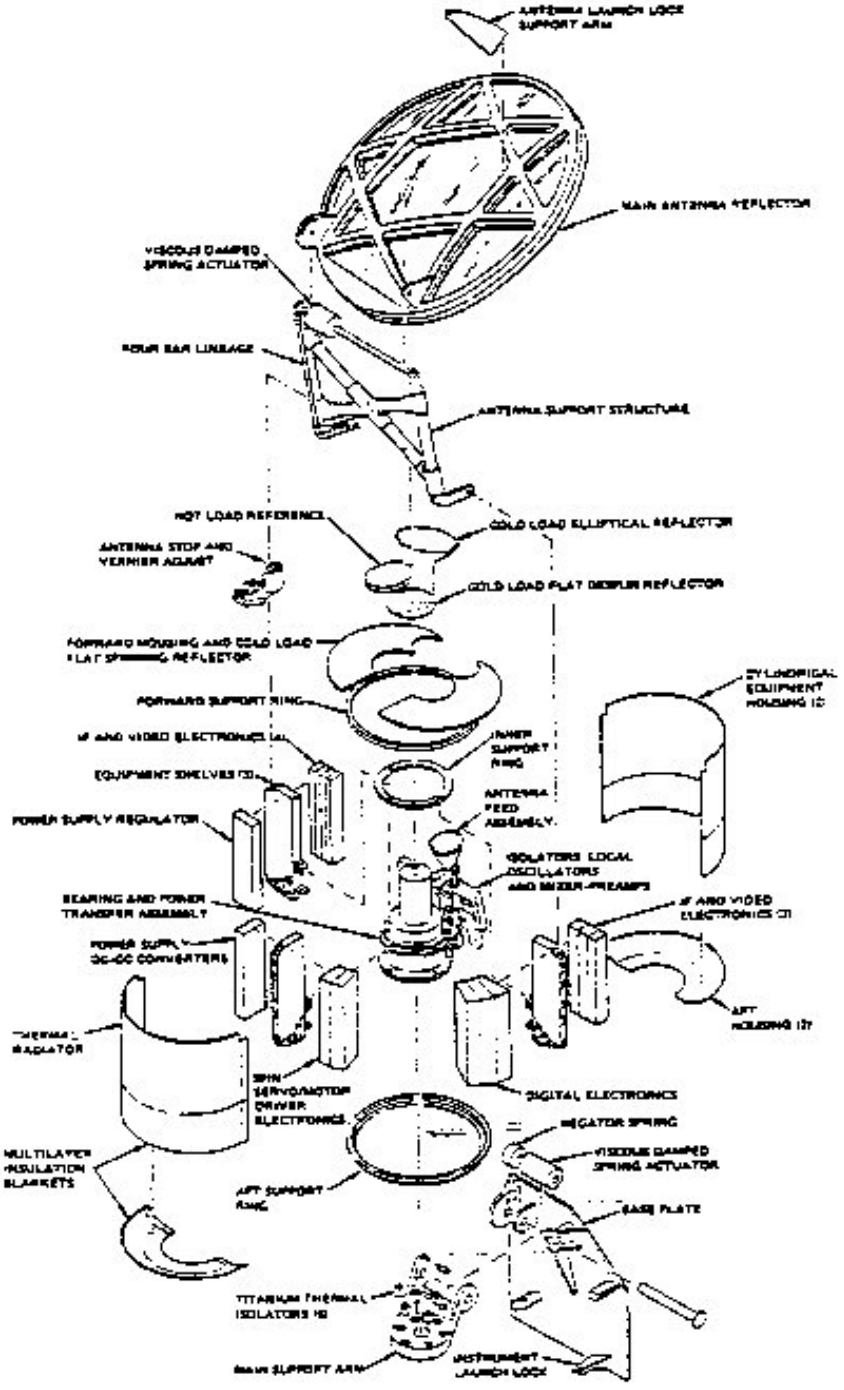

Figure 3.2-1. Exploded diagram of the SSM/I instrument.

3.3 Radiometric Characteristics

The radiometric characteristics of the seven SSM/I channels are listed in Table 3.3-1. These channels were selected to achieve specific objectives for measuring parameters. For example, a channel with a center frequency of 22.235 GHz was included in order to obtain estimates of atmospheric water vapor (described in 5.2.1). The 19 and 37 GHz channels were used to achieve the maximum transfer of scientific experience and algorithms from the ESMR and SMMR instruments. The 85.5 GHz channels were chosen in order to more effectively measure rain and cloud properties.

CHANNEL ABBREVIATION	CENTER FREQUENCY (GHz)	CENTER WAVELENGTH (cm)	BANDWIDTH (MHz)	POLARIZATION	INTEGRATION TIME (ms)
19V	19.35	1.549	240	Vertical	7.95
19H	19.35	1.549	240	Horizontal	7.95
22V	22.235	1.348	240	Vertical	7.95
37V	37.0	0.810	900	Vertical	7.95
37H	37.0	0.810	900	Horizontal	7.95
85V	85.5	0.351	1400	Vertical	3.89
85H	85.5	0.351	1400	Horizontal	3.89

Table 3.3-1. SSM/I channel characteristics.

Both of the 85 GHz channels aboard F8 failed (the 85V in February 1989, and the 85H in October 1990), most likely due to overheating of the RF electronics. For some time previous to complete failure, both of these channels had noise levels that gradually increased in an inconsistent manner until the signal from the Earth was completely submerged.

As discussed in 2.5, providing two channels at a frequency, to measure both horizontally and vertically polarized radiation, allows a determination of the amount of polarization. This capability has been incorporated into the 19, 37, and 85 GHz channels. The 22 GHz channel does not require a second polarization, since it is used primarily for measurement of water vapor, the signal of which comes from the atmosphere and is unpolarized..

Finally, the channel bandwidths were chosen as a compromise between spectral sensitivity (requiring the narrowest spectral intervals) and sensor noise. For broadband signals, the measurement uncertainty due to noise is inversely proportional to the square root of the bandwidth, so larger bandwidths generally result in more accurate measurements.

3.4 Scan Geometry

The reflector of the SSM/I is positioned at an angle of 45 degrees to the SSM/I spin axis. This angle is called the cone angle because the beam of the antenna sweeps out a 45 degree cone around the spacecraft. However, the SSM/I does not collect data through its entire rotation. As Figure 3.4-1 shows, the active portion of one revolution covers only 102.8 degrees. Thus the spot seen by the sensor sweeps across the Earth in curved arcs (Figure 3.4-2). Each of these arcs is called a scan. The rotation period of the SSM/I (1.899 s) was chosen to obtain a spacing of 12.5 km along the ground between each scan.

Due to the 45 degree cone angle and 102.8 degree active scan, the SSM/I swath width (length of each scan arc) is 1400 km (Figure 3.4-3), which is about half that of the OLS.

The nature of the SSM/I conical scan is such that the angle the beam makes with the local zenith (the incidence angle) is constant (about 53.1 degrees). This has important consequences for remote sensing, since the amount of polarization in a pixel depends strongly on the zenith angle. Lower incidence angles show much less difference between the horizontal and vertical polarizations of a channel than higher ones (Figure 3.4-4). At nadir, where the incidence angle is 0 degrees, the polarization difference disappears entirely.

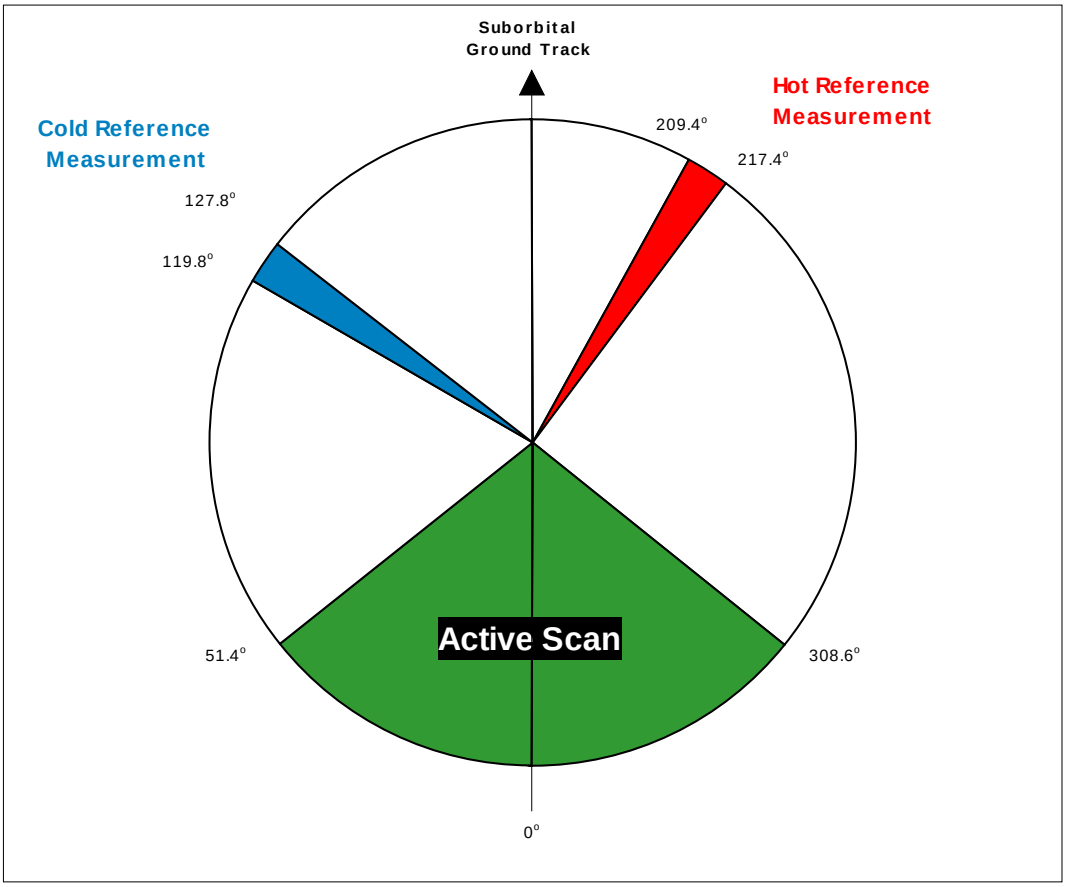

Figure 3.4-1. SSM/I scan sequence. Scan direction is clockwise. Rotation period is 1.899 seconds.

Another characteristic of the conical scan of the SSM/I is that the distance from the sensor to the point on the ground being observed is constant. This is in contrast to planar (cross-track) scanners like the OLS and AVHRR whose path length increases as the scan moves away from nadir. For this reason, the SSM/I does not require a correction for limb darkening (the effect of increased atmospheric attenuation as the path becomes longer). Yet one more aspect of the SSM/I conical scan is that it can be designed so that the plane

of polarization remains constant over the surface of the Earth as the antenna scans in azimuth. This is important for analyzing and imaging surface properties.

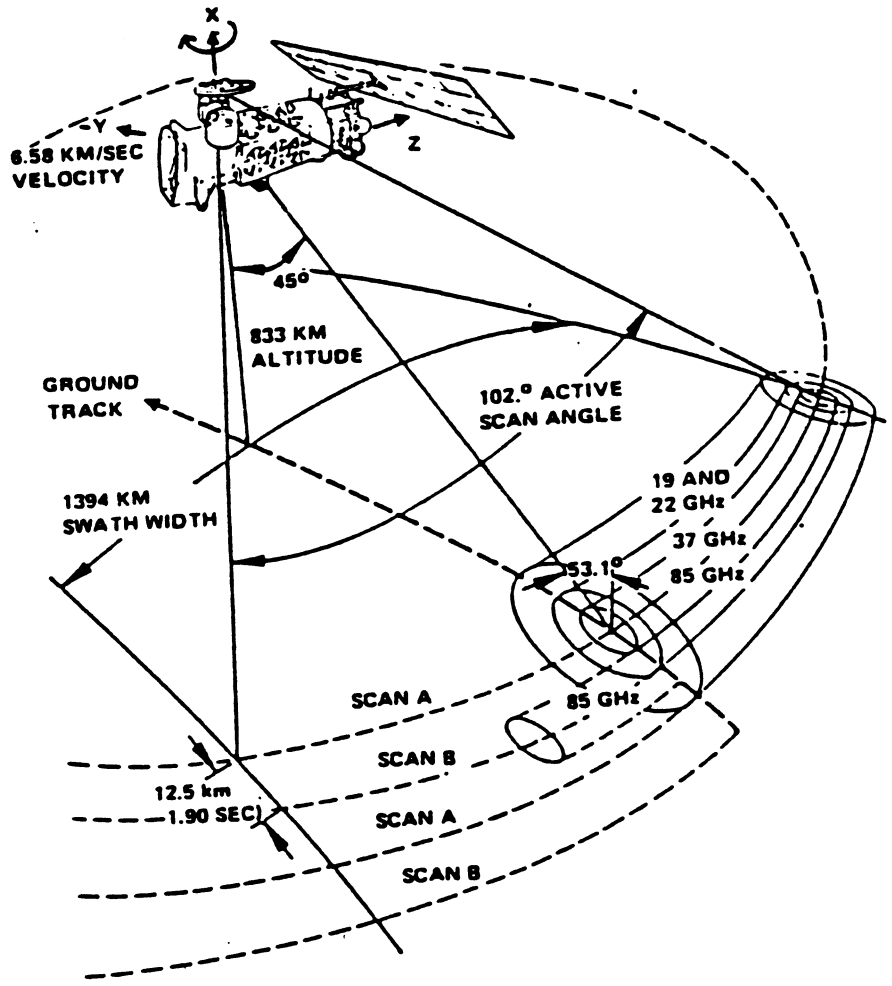

Figure 3.4-2. SSM/I scan geometry **(DMSP SSM/I Cal/Val Team, 1989)**.

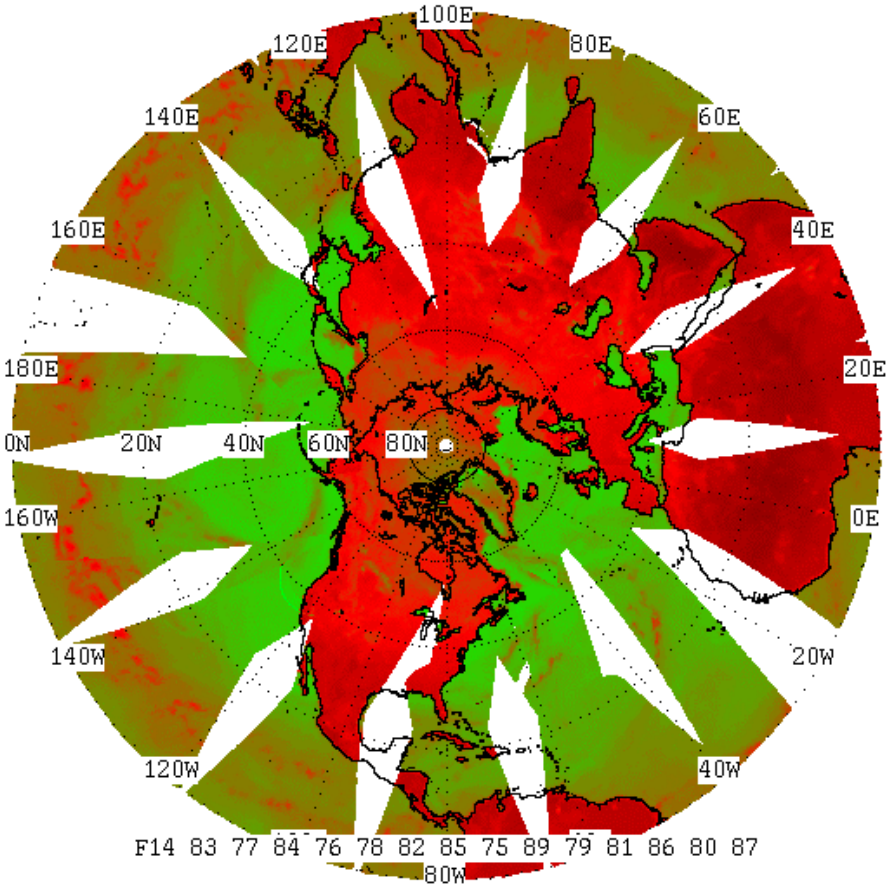

Figure 3.4-3. Example showing swath coverage and gaps at low latitudes. This represents one day of coverage by one satellite.

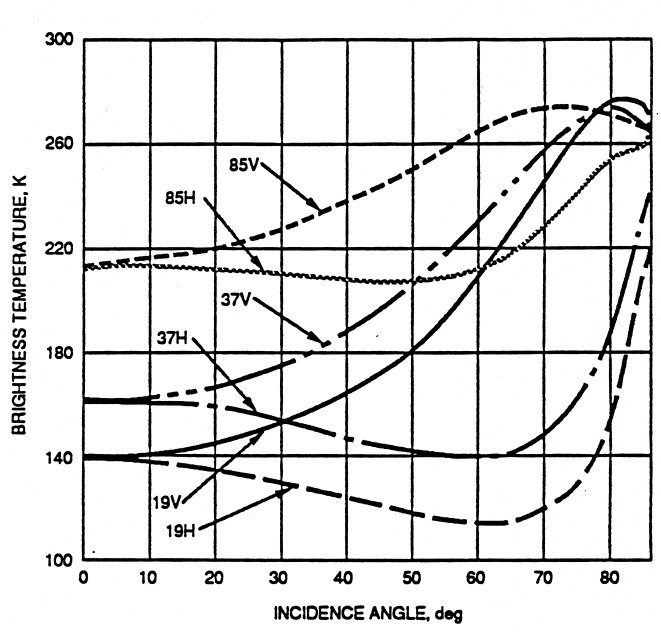

Figure 3.4-4. Polarization vs. incidence angle.

3.5 The SSM/I Scan Pattern

To talk about the "spot" seen by the SSM/I is somewhat misleading, because it is really the projection, on the ground, of the SSM/I beam pattern (Figure 3.5-1). The contour at which the energy of the beam falls off by a factor of 2 (3 dB) is called the "footprint" of the sensor. About half of the total energy received by the SSM/I comes from within this contour. The other half comes from outside, including from the antenna's sidelobes (local gain maxima).

Figure 3.5-2 shows the footprint sizes for each SSM/I frequency. These footprints are elliptical in shape since the SSM/I beam intersects the Earth at an angle. Since the beam pattern is fixed relative to the spinning antenna, the semi-major axis of each elliptical footprint lies along a line through the sub-satellite point. The direction of this line (perpendicular to the curved scan at every point) is known as "cross-scan", and is parallel to the satellite ground track only in the precise center of the SSM/I scan. The terms "cross-track" and "along-track" are used for more conventional planar scanners like the OLS, and are not applicable to the SSM/I conical scan.

In order for energy to be received at the sensor, the point from which the energy is radiated must remain in the sensor field of view for some finite time. The longer the spot remains in the beam, the more energy is received and the better the measurement. This process, by which the sensor averages the received radiation over a period of time, is called "integration". The amount of integration time is a compromise between accuracy (requiring more time) and resolution (requiring a smaller observation area).

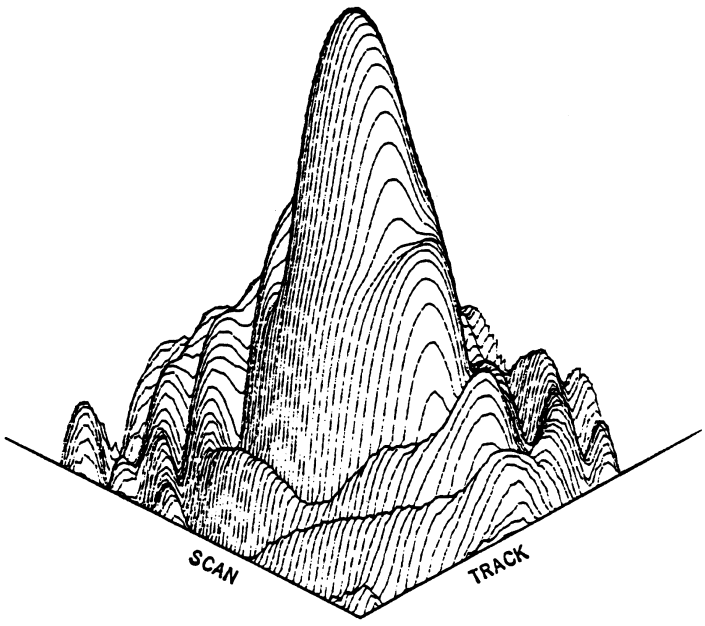

Figure 3.5-1. SSM/I beam pattern.

The 12.5 km spacing between SSM/I scans was chosen in order to meet a requirement for measurement of some environmental parameters (in particular, rain rate) at that resolution. For this reason, the 85 GHz channels are integrated for a period of about 4 ms, during which the center of the footprint will sweep 12.5 km on the ground. The resulting sample, which represents the area seen by the SSM/I for that channel, is called a scene station. All of the other SSM/I-derived environmental parameters are required to have a 25 km scene station spacing, so that the remaining channels are integrated aboard the sensor for a period of about 8 milliseconds (ms), resulting in an elongated sample. Figure 3.5-3 illustrates the SSM/I samples for all 4 frequencies.

Since the size of the footprint at the lower SSM/I frequencies is 25 km or greater in the cross-scan direction, observations need be taken only every other scan. So, the pattern of SSM/I scene stations consists of scan pairs, in which one contains alternating 85 GHz and all-channel scene stations (64 of each), and the next only 85 GHz scene stations (a total of 128). These scans are called the A and B scans, respectively, and are represented schematically (not to scale) in Figure 3.5-4.

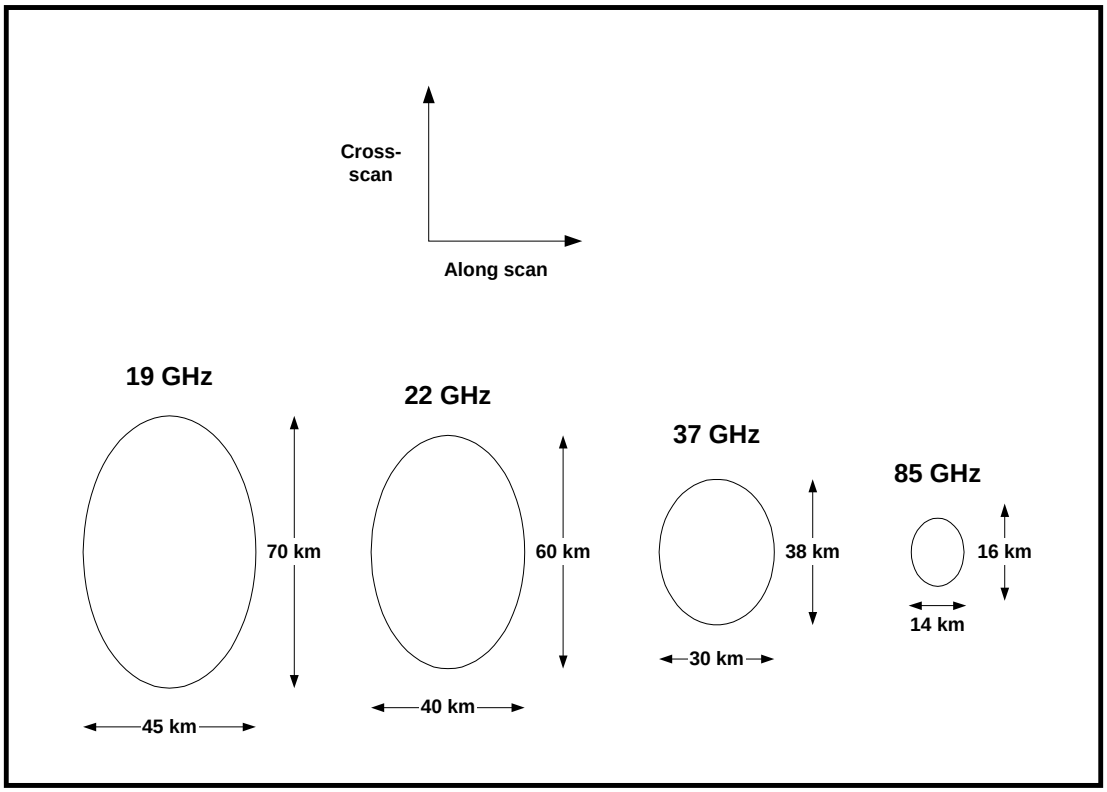

Figure 3.5-2. SSM/I footprint sizes (not to scale).

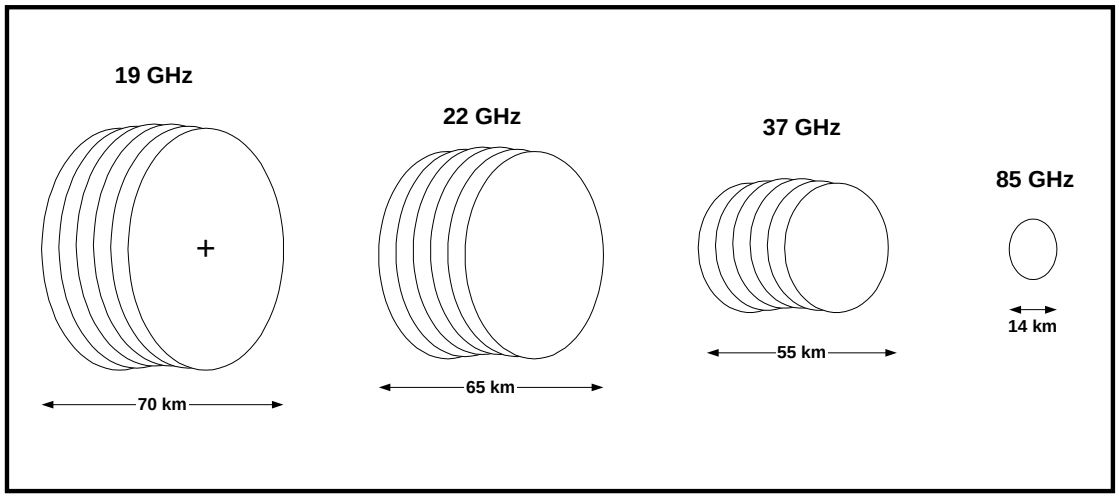

Figure 3.5-3. SSM/I sample sizes (not necessarily to scale). This illustrates the effect of integration as the channel footprints sweep over an area during the integration period of about 8 milliseconds.

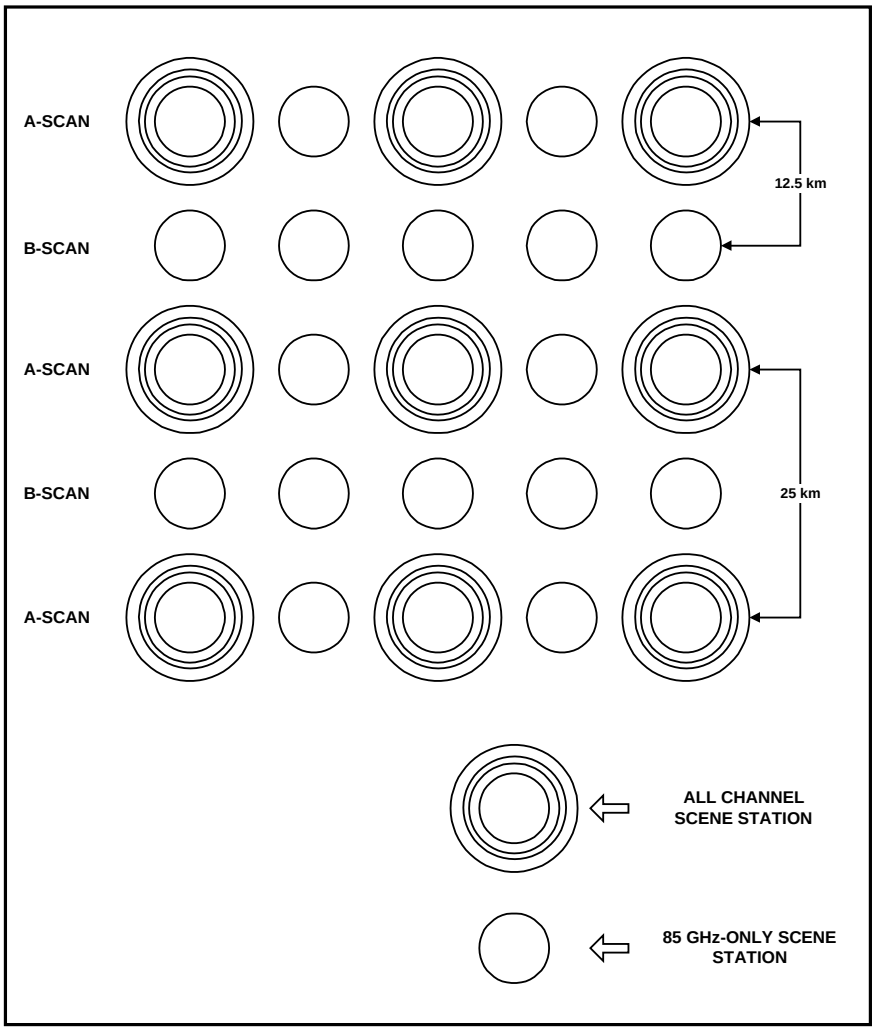

Figure 3.5-4. SSM/I scan pattern (not to scale).

4. SSM/I Data Processing

4.1 Processing overview.

SSM/I data processing involves acquiring raw data from the spacecraft and generating two products: Sensor Data Records (SDRs) and Environmental Data Records (EDRs). SDRs are calibrated, Earth-located, antenna pattern corrected brightness temperatures. They comprise the basic information the SSM/I is collecting from the Earth-atmosphere system. EDRs are derived from SDRs and contain environmental information in a form useful to the meteorologist or oceanographer. Parameters contained in the EDRs include cloud water content, rain rate, surface wind (over ocean), soil moisture, sea ice

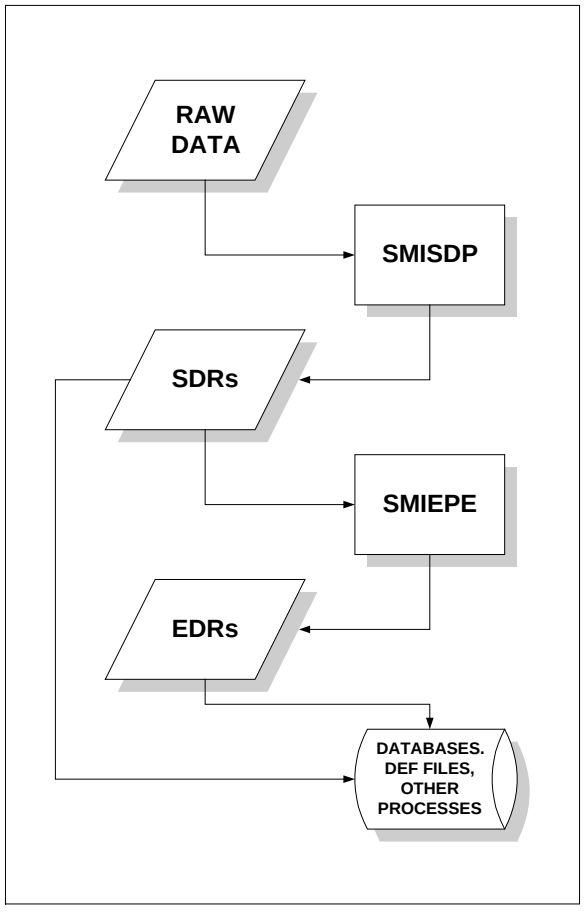

Figure 4.1-1. SSM/I data flow.

concentration and age, water vapor content, land surface types, snow depth, and rain and sea ice edge flags.

Data processing takes place at two central locations, the Fleet Numerical Oceanography Center (FNMOC) and the Air Force Weather Agency (AFWA). Processing at AFWA is accomplished on a large mainframe computer (UNISYS). Processing at FNMOC is performed on Sun UNIX workstations. The programs which create SDRs and EDRs are essentially the same at both locations. SDRs are created by a program called SSM/I Sensor Data Processing (SMISDP) and EDRs are created by a program called SSM/I Environmental Parameter Extraction (SMIEPE). The AFWA versions of SMISDP and SMIEPE contain additional code to interface with the AFWA databases. Figure 4.1-1 illustrates the data flow for SSM/I processing.

4.2 SDR Generation

SDR generation consists of four processes: raw data acquisition and unpacking, Earth location and tagging, calibration, and antenna pattern correction. Figure 4.2-1 shows schematically how these processes are related.

Processing of SSM/I data begins with raw data acquisition. This procedure can take two forms, depending upon where the processing is occurring. At the two centrals (FNMOC and AFWA), complete orbits are processed from the stored data stream. As the DMSP spacecraft orbits the Earth, the OLS and Special Sensor data is recorded onto an onboard tape recorder. When the spacecraft is visible from a DMSP ground station (which are located at Thule, Greenland, Fairchild, Washington, and Kaena Point, Hawaii), the data on the tape is transmitted as the tape is being rewound. This results in the data being acquired in reverse time order. Usually a single revolution is transmitted, but over some stretches of the Pacific up to three orbits are stored before they are played back. After the data stream has been received from the spacecraft, it is beamed to FNMOC and AFWA via a communications satellite.

At the tactical sites, only the real time data stream is available for processing. The DMSP spacecraft broadcasts the data it is acquiring in real time in addition to storing it on tape for eventual relay to the centrals. Any time the spacecraft is within a tactical site's readout circle, the site can pick up this real time broadcast. Since the data are being broadcast in real time, they are received in chronological order, unlike the reversed stored data. Also, since the data can be received only when the spacecraft is above the local horizon, tactical sites can process at most 17 minutes of a 101 minute orbit.

The raw data stream itself is packaged in one second blocks. Seven of these blocks are required for a complete set of Special Sensor information. Each group of seven blocks contains the SSM/I sensor voltage counts for two A/B scan pairs as well as the necessary calibration points and some sensor health information. SMISDP begins processing by gathering seven data blocks together, performing data quality and time continuity checks, and unpacking the blocks into the two A/B scan pairs, calibration data group, and sensor health group. All further SMISDP processing (Earth location, calibration, and antenna pattern correction) is performed before the next group of seven blocks are received. If any one of the seven blocks is missing or fails the data quality check, the entire group of seven is discarded. Processing for that group cannot be completed since some essential

data are missing. This shows up in the processed product as a four scan data dropout. Four scans are missing because the seven blocks contain two A/B scan pairs.

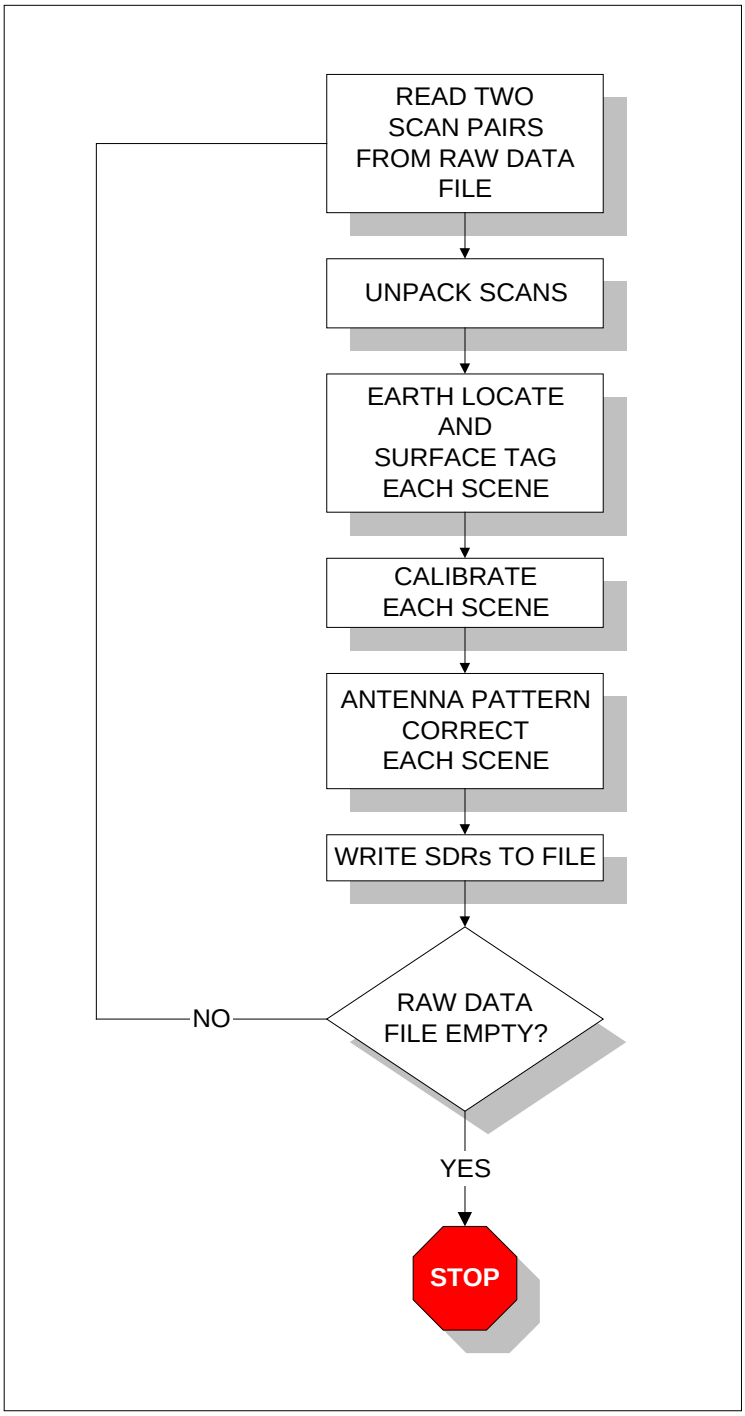

Figure 4.2-1. SDR generation process.

Once the four scans have been unpacked, each scene station is geolocated. In order to Earth locate the SSM/I data, SMISDP requires knowledge of the spacecraft position.

This positional information consists of the latitude, longitude, and altitude of the spacecraft at a specific time and is known as a position vector. The predicted ephemeris file contains position vectors at one minute intervals, while on-board ephemeris files contain position vectors at 2 to 2.5 second intervals. Earth location is accomplished by finding position vectors which bracket the B scan start time. Each scene station within the two scan pairs is then located into precise geodetic latitude/longitude coordinates relative to the satellite subpoint interpolated between the position vectors.

The ephemeris file itself is generated in one of two ways. At the centrals, the onboard ephemeris is extracted from the OLS data stream and formatted for use by SMISDP. At the tactical sites, orbital elements are extracted from the Direct Mode Data Message (DMDM) and are used to generate a predicted ephemeris. The centrals also have an option of using a predicted ephemeris. The onboard ephemeris is considered more accurate since it is updated more frequently, but for day-of-year determination, the coarser predicted ephemeris is required, since the onboard ephemeris lacks this information. After each scene station is Earth located, it is assigned a surface type from a fixed database. The fixed surface types are land, coast, ocean, ice, and possible ice.

Calibration of each SSM/I channel involves converting the sensor voltages into antenna temperatures incident on the antenna feedhorn. The hot and cold load voltage counts, as well as the hot load thermistor readings, are unpacked from the raw data stream. Using the Rayleigh-Jeans linear approximation, an equation for converting voltages to antenna temperatures is derived for each of the channels using the known hot and cold load temperatures and voltages. Each channel in each scene station in the four scans is then evaluated using these equations, converting the voltage counts into antenna temperatures.

Once the raw antenna temperatures are calculated they must be antenna pattern corrected to produce the brightness temperatures given in the SDRs. As energy from a particular scene station is sampled by the sensor, additional energy is measured due to the antenna side lobe pattern. To remove the effect of the sidelobes, an antenna pattern correction (APC) is performed on each sample. To correct a particular channel at a given scene station, the adjacent along scan scene stations and the cross polarization term at the current scene station are used to remove the energy contributed by the sidelobes. As an example, to correct the 37 GHz vertically polarized sample at scene station 40, the 37 GHz vertical samples at scenes 39 and 41 and the 37 GHz horizontal sample at scene 40 are used. The exact coefficients used to obtain the corrected brightness temperatures are found in the Sensor Calibration File.

Once the two A/B scan pairs have been Earth located, calibrated, and antenna pattern corrected, they are written out to the SDR file. SMISDP then repeats the process with the next seven data blocks until the entire raw data file has been read. At this point SDR processing terminates and the EDR generation program, SMIEPE, is initiated.

4.3 EDR Generation

Environmental Data Records are produced from the SDRs generated by SMISDP. SDRs are read in as a scan pair, and each scene station within the scan pair is processed individually.

The processing path for each scene station is determined by its surface type. A fixed surface type was assigned by SMISDP to each scene based upon its latitude and longitude. Three paths are possible: ocean parameters, land parameters, and ice parameters. Table 4.3-1 shows which parameters are calculated for each surface type. Scenes tagged as coast are not processed, since mixed land/water footprints are difficult to interpret. Figure 4.3-1 illustrates how the surface typing drives the processing sequence. Based upon surface type and latitude, one set of parameters (ocean, land, or ice) is calculated for each scene station.

SURFACE TYPE	EDRs TO CALCULATE
OCEAN	RAIN RATE CLOUD WATER CONTENT SURFACE WIND WATER VAPOR RAIN FLAG
ICE	ICE CONCENTRATION ICE AGE ICE EDGE
RAIN OVER SOIL	RAIN RATE
RAIN OVER VEGETATION	RAIN RATE
WATER/LAND MIX	NONE
GLACIER	NONE
VEGETATION	SURFACE TEMPERATURE
MOIST SOILS	SURFACE TEMPERATURE SOIL MOISTURE
AGRICULTURAL AND RANGE	SURFACE TEMPERATURE
DRY SOIL, DESERT	SURFACE TEMPERATURE
COAST	NONE

Table 4.3-1. Parameters calculated for each surface type.

Most EDRs are generated through a regression technique. The value of a particular EDR is calculated as a linear combination of specific channels. However, two EDRs, rain rate and water vapor over ocean, use nonlinear combinations of SSM/I channels. Once an EDR is calculated, its value is checked against out-of-limit boundaries and then quantized into the proper units. If it fails the boundary checks, an indicator of a bad value is incremented. This allows the user to determine, through experience, if a particular

parameter is unreliable. A good example of this is ice concentration during the spring melt. Pools of water lying on top of ice floes will result in a greater than normal count of bad (out of range) ice concentrations.

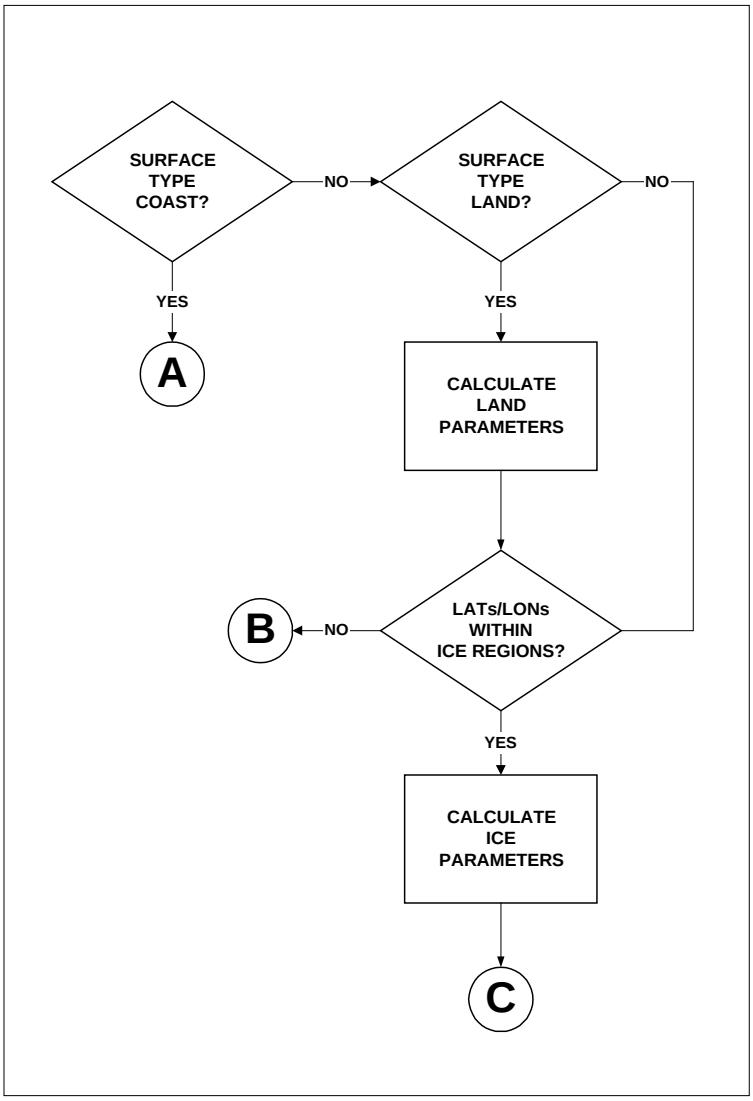

Figure 4.3-1. EDR generation process.

The only parameters which are not calculated as a combination of SDR channels are surface characteristic and rain flag. These EDRs are determined through a series of IF-THEN-ELSE statements comparing various channels to each other and to fixed values

As each SDR is processed into environmental parameters, the EDRs are written to the EDR file. When the SDR file is exhausted, SMIEPE processing is terminated.

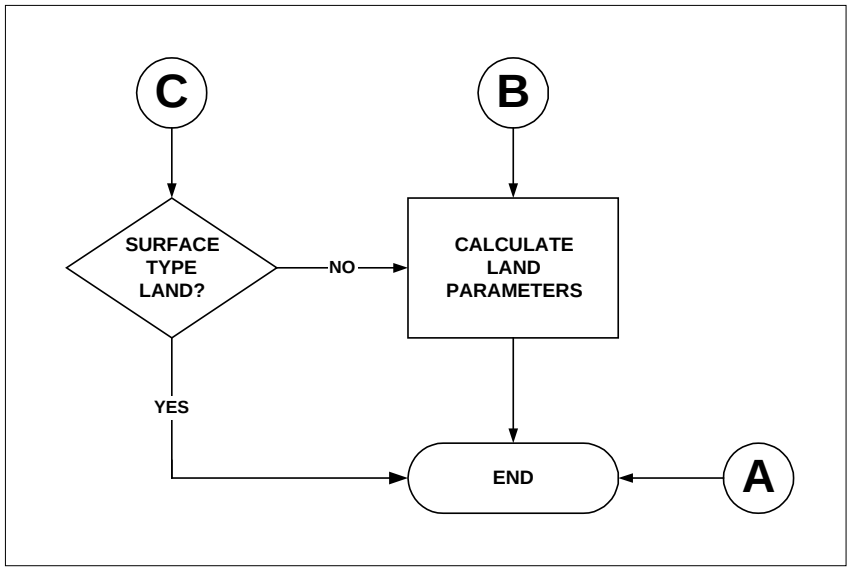

Figure 4.3-2. EDR generation process (continued).

4.4 Other Processing

Processing beyond the EDR generation stage varies greatly between locations. In general, SDRs and EDRs are prepared for display on a variety of devices. The following sections summarize the post-EDR processing at each site.

4.4.1 FNMOC

FNMOC is the prime archival site for SSM/I data. As such, two additional processes are performed on each orbit. The first, sensor health monitoring, provides the user with statistical information on the performance of the sensor in the form of Quality Data Records (QDRs). The second, DEF data reformatting, writes the SDRs, EDRs, QDRs, and Temperature Data Records (TDRs) into the Data Exchange Format (DEF). TDRs are SDRs without APC applied. They are important because they are directly reversible into antenna counts. Subsequent processing steps are nonlinear; they cannot be reversed. The DEF files, as well as the sensor calibration and parameter extraction files, are shipped to Naval Research Laboratory and subsequently NOAA/NESDIS for long term archival. FNMOC uses the SDRs and EDRs in forecast models.

4.4.2 AFWA

AFWA grids SDRs and EDRs directly into a polar stereographic eighth mesh[3] data base (Figure 4.4-1). This database can then be accessed by the Satellite Data Handling System (SDHS). In addition, full resolution SDRs are stored in a circular file (first in-first out), containing up to 20 previous readouts, where they can be accessed by other AFWA applications.

[3] In figure 4.4-1 there are 64 hemispheric "neph" boxes. There are 8X8 "whole mesh" boxes within each of these neph boxes. Each whole mesh box consists of an array of 8X8 "eighth mesh" boxes. The nominal resolution of each eighth mesh box (true at 60^{o} latitude) is 47.625 km. The next finer mesh level is sixty-fourth mesh, with a resolution of 5.953 km (Hamill, *et al*, 1992).

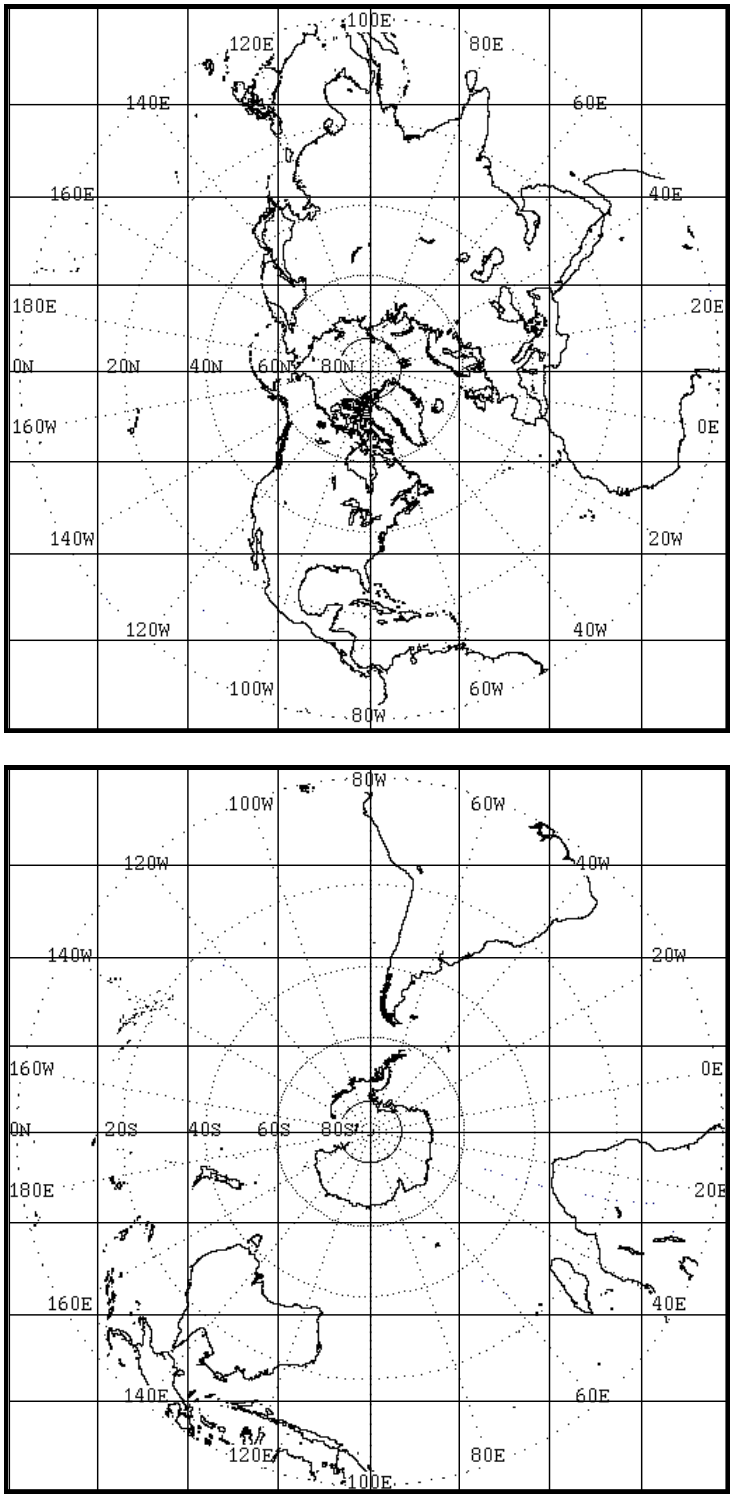

Figure 4.4-1. Format of AFWA polar stereographic eighth mesh databases.

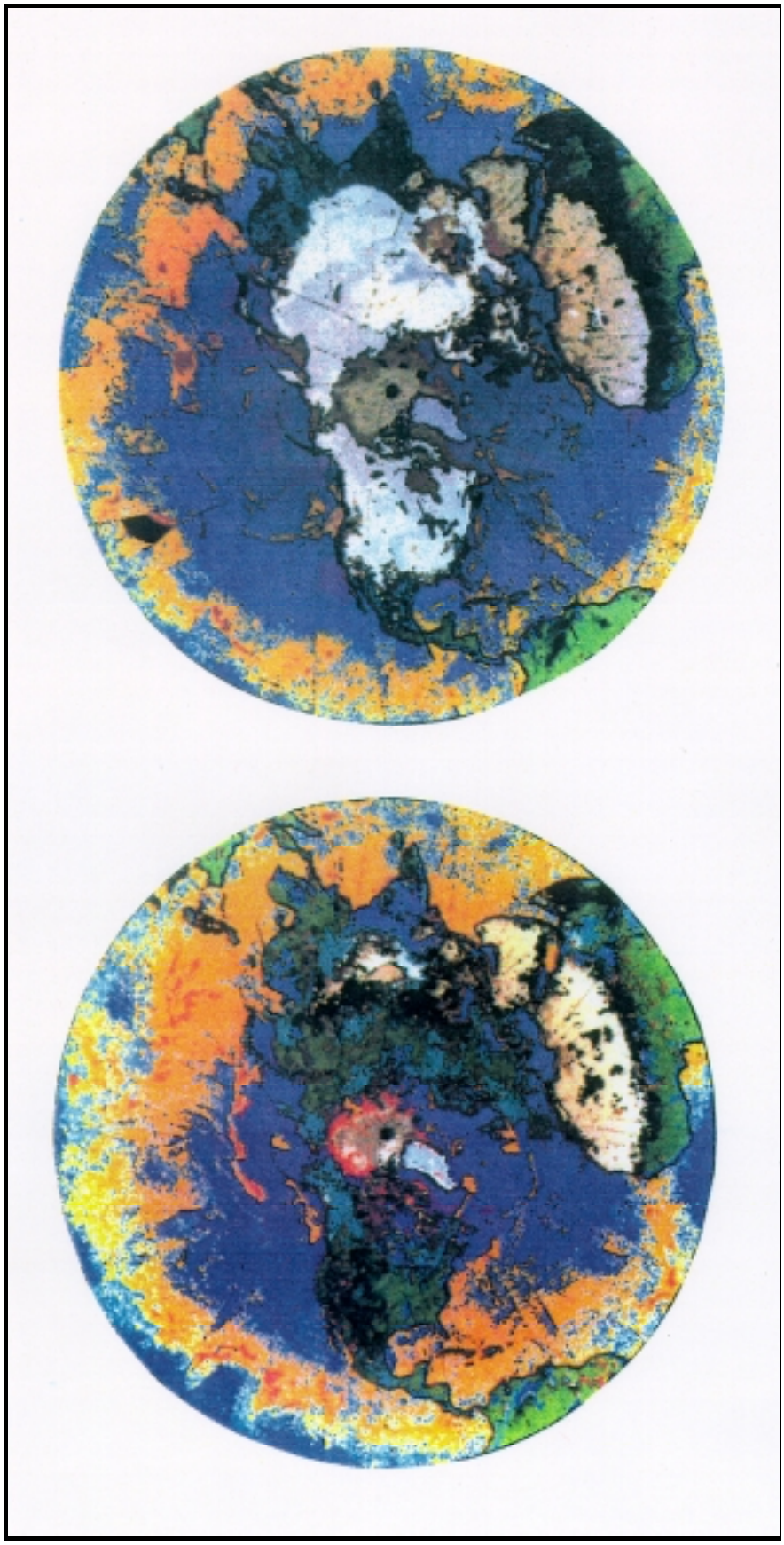

Figure 4.4-2. Surface type of each eighth-mesh grid point in the Northern Hemisphere in winter (top) and summer (bottom), as determined by the Seasonal Surface Type Database (SSTDB) classification algorithm. In the winter image, snow (white and grey) covers much of Asia, Europe, and North America. The North Polar ice cap is near its maximum extent, with the Bering Strait and Hudson Bay frozen over. Multiyear sea ice is shown in light brown, with first year ice in dark brown. Open ocean is shown in blue, and the yellowish and orange areas are ocean areas with large amounts of water vapor or clouds (seen in the belt around the equator, corresponding to the ITCZ or Inter-Tropical Convergence Zone). The summer image is quite different. Snow has almost completely vanished, except for Greenland and the Tibetan Plateau. The ice cap is near minimum, and the red fringe around it is melting ice. Note that the areas identified in winter as multiyear ice now show up as first year. This is because of the pools of meltwater often found on top of the ice during polar summer. Vegetation now covers most of the land areas (green areas in SE US and SE Asia. The ITCZ has expanded with moist air masses extending much farther to the north.

4.4.2.1 Seasonal Surface Type Database (SSTDB)

Another operational application for SSM/I data at AFWA creates and updates a record of changes in the Earth's surface. This record consists of an eighth-mesh polar stereographic grid file on the AFWA UNISYS called the Seasonal Surface Type Data Base (SSTDB). A Raytheon-developed software package, the SSM/I Relational Channel History (SMIRCH), is run once per day to scan the eighth-mesh SSM/I SDR database, classify each point into one of 23 different categories (Table 4.4-1), and update the SSTDB at all those points where the surface has changed significantly. The SSTDB contains information for the most recent and four previous states at each grid point.

Data from the SSTDB can be retrieved using AFWA software. The information retrieved consists of the surface type, three discriminators (used for classification), and a confidence factor, which is a misclassification probability.

Land Categories	**Ocean Categories**	**Other Categories**
Snow	Dry air over calm ocean	Coast
Deep snow	Dry air over ocean	Unknown
Glacial snow	Fronts, thick clouds over ocean	
Bare soil	Moist air over ocean	
Dry desert	Rain over ocean	
Flooded land/land-water mix	First year sea ice	
Cold vegetation	Multiyear sea ice	
Dense vegetation		
Sparse vegetation		
Moderate vegetation		
Rain over land		
Wet desert		

Table 4.4-1. SSTDB surface types.

The interpretation of SSTDB data is relatively straightforward, particularly if looking at images of surface type. An appropriate color table is used with natural appearing colors for each type (green for vegetation, tan for desert, various shades of blue for the ocean types, etc.). Figure 4.4-2 shows winter and summer SSTDB composites over the Northern Hemisphere displayed in this way.

Microwave signals for some surface states are similar enough to cause ambiguities in some categories (snow/wet desert, bare ground/melting snow, and desert/flooded soil).

Usually, examination of the previous history of the grid point (as stored in the SSTDB) will resolve the situation.

4.4.2.2 RTNEPH (IR Background Temperature)

Another way the SSM/I is used operationally is for improving cloud detection, as part of the (Real-Time Nephanalysis (RTNEPH) cloud analysis system at AFWA. The RTNEPH estimates cloud amount, among other parameters, on an eighth-mesh basis, using sixty-fourth mesh OLS IR and visible data.

Modifications have been made to the RTNEPH system to use the SSM/I data in the following way: if the SSM/I and OLS data for any point were taken within a 20 minute interval, the SSM/I data is used to obtain an estimate of the IR temperature that would be seen if no clouds were present. This value is called the IR background brightness temperature, or clear-air brightness temperature. The IR background brightness temperature thus obtained is used in place of that determined using modal analysis of the IR data alone or by reference to a surface temperature history. Since surface observations, from which the surface temperatures are obtained, are abundant only in certain areas (i.e. U.S., Canada, Western Europe), using the SSM/I data in this way improves the cloud analysis when performed over other areas where data may be more important operationally but not so readily available.

The accuracy of the background IR estimation equations depends on the surface below (vegetation being the best at about 2K RMS error and snow and ice the worst at 4K and above). The only exceptions to this are very thick convective clouds, which may attenuate the microwave radiation enough to prevent the estimate from being accurate. However, in these cases, the pixel in question is almost always completely overcast, making the detailed cloud analysis unnecessary.

4.4.3 Tactical Sites

Tactical sites acquire raw data in real time through Mark 3 or TMQ-29 ground stations, and STTS (Small Tactical Terminal Station). Processing is performed by the STTS.

4.5 SSM/I Data Display Systems and Software

Numerous systems exist for displaying and manipulating SSM/I images. Historically, these systems include HEODS (Hughes Early Orbit Display System), MISTID (Microwave Surface Type Display), TOTO (Tropical Oceanic Technique Optimizer), HuMID (Hughes Microwave Image Display), HuSLID (Hughes Scan Line Image Display). The MSTVUE system was written as a second generation tool for general purpose DMSP image display on a Sun workstation. Specter was the third generation imaging system. Specter is obsolete and unused at the centrals. The current generation of software for displaying SSM/I data is the DMSP Image Generation System (DIGS).

4.5.1 Specter

As a historical overview, the Specter system, in addition to display, handled system management and control, mission management, and data processing for a variety of satellites and sensors. Of interest in this document are the processing and display capabilities for DMSP, and more specifically, SSM/I data. Through its system controls functions, Specter can automate the processing of data from specified satellites and sensors, including ingest, Earth location, calibration, and derived parameter calculation. The processed data is then archived in the form of location (.loc) and data file (.dat) sets which are ready for display and manipulation by the Specter display module. Raytheon's Sun workstation-based DMSP data processing software outputs data in the same format output by the Specter processing stream, so the Specter Display module may use data from either system as input.

Once SSM/I data has been processed by the appropriate system, it is ready for display and manipulation via the Specter Display module. Specter Display is an interactive tool based on a graphical user interface, which allows users to display satellite data (including SSM/I data) in various configurations.

Specter allows the user to define areas of interest (AOIs) using the following criteria: projection, spacecraft, sensor, revolution number, data channel (either sensor data or derived parameters), and image center location. Once these criteria have been selected, Specter extracts and projects the selected data, making it available for manipulation and enhancement.

Specter Display supports a variety of image enhancements including filling, smoothing, equalization, and edge detection. It also allows data from two sources to be combined into a single image plane with user-defined filters applied to each data source. Multiple images may also be placed in a single image plane adjacent to one another so that different parameters may be easily compared.

In addition to data manipulation options, Specter Display also allows users to add any number of overlays to displayed images. Supported overlays include latitude/longitude grid, geopolitical boundaries and features, contour lines, and text or graphic labels.

Finally, Specter display supports several statistical analysis capabilities. For example, the mean, variance, minimum, maximum and mode values may be computed over any user-defined area.

4.5.2 DMSP Image Generation System (DIGS)

The DMSP Image Generation System (DIGS) is a fully automated image generation system for DMSP data which outputs images in either TIFF or Specter image formats. DIGS supports most of the capabilities available in Specter Display, but with DIGS,

image generation is automatic, whereas Specter Display depends on user interaction to generate each image. Also, while DIGS generates image files, it does not support display

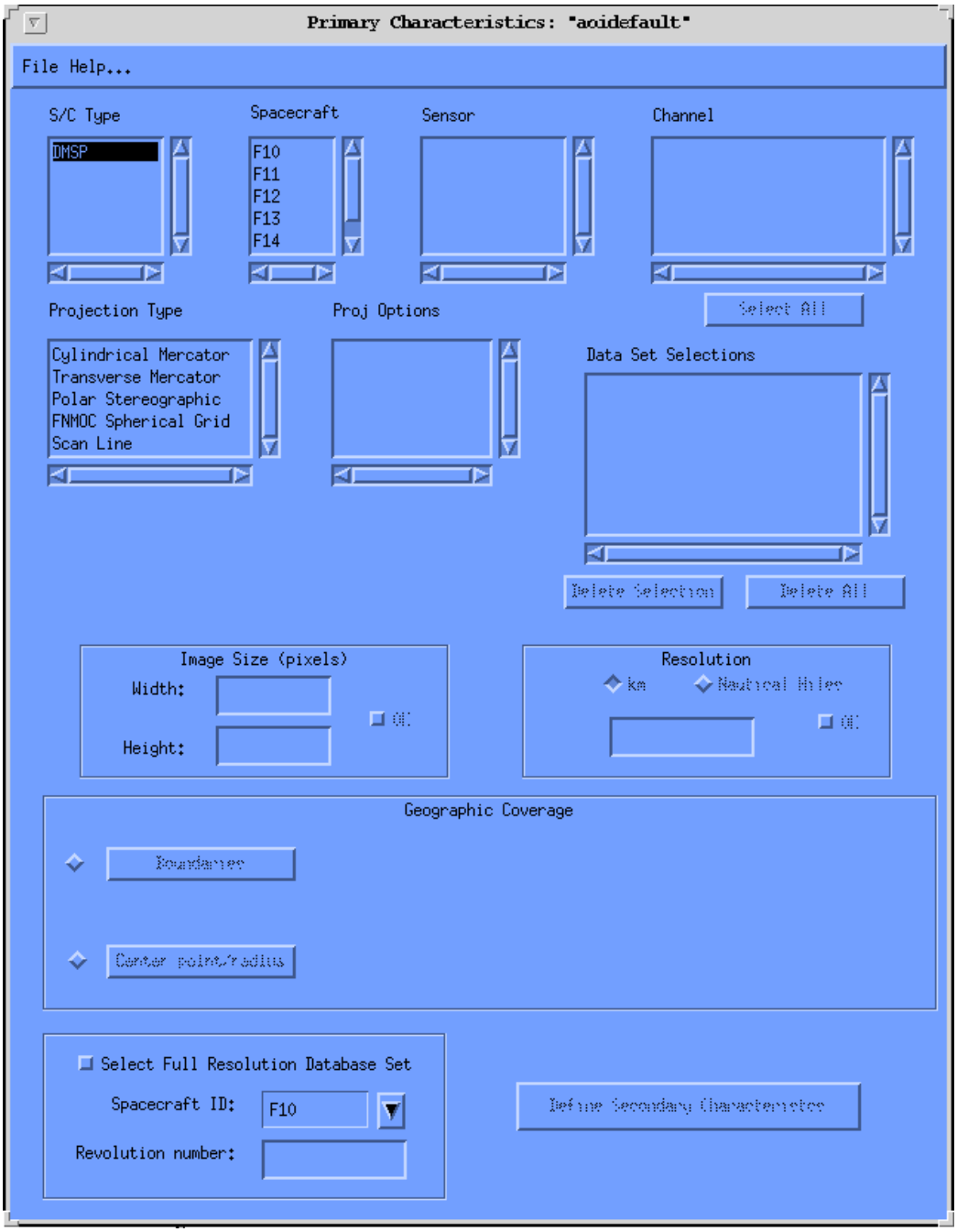

Figure 4.5-1. DIGS graphical user interface.

capabilities; display is facilitated via Specter for Specter format images or other commercially available or custom display programs for TIFF image files. DIGS accepts as input location and data files in the same format as those produced and used by Specter or Hughes' Sun Workstation DMSP data processing software. Rather than requiring the user to define each image in an interactive session, as Specter does, DIGS allows users to pre-define any number of geographical areas of interest (AOIs) which are automatically populated with data as it becomes available. All DIGS image characteristics are defined in an ASCII configuration file. DIGS provides a graphical user interface (the AOI GUI or AG) which facilitates easy generation of these files (Figure 4.5-1). A command line interface is also available. Once these files are generated and placed in the appropriate directory, DIGS automatically generates images with the characteristics specified in the configuration files.

Like Specter , DIGS allows users to perform a multitude of data manipulations and image enhancements. DIGS also allows the user to specify image shipment criteria; that is, the user may specify that images be output after each orbit, at specific times, or only when data covers a specified portion of an AOI. DIGS also supports the capability to include only data from within a certain time or age range within any given AOI. For example, the user may specify that a certain AOI should contain only data from the past 10 hours, and images will be output only if data covers at least 50% of the AOI. DIGS also supports a variety of data manipulation and enhancement functions, including filling, smoothing (Figure 4.5-2), contrast adjustment, and data range limits. The user may specify a multitude of overlays in the AOI configuration file, including geopolitical features, latitude/longitude grid, orbit information, data time information, and user-defined text to be added to each image.

A separate image viewer (such as XV) is necessary to view DIGS TIFF images, while the Specter software is necessary to view Specter format images created by DIGS.

a)

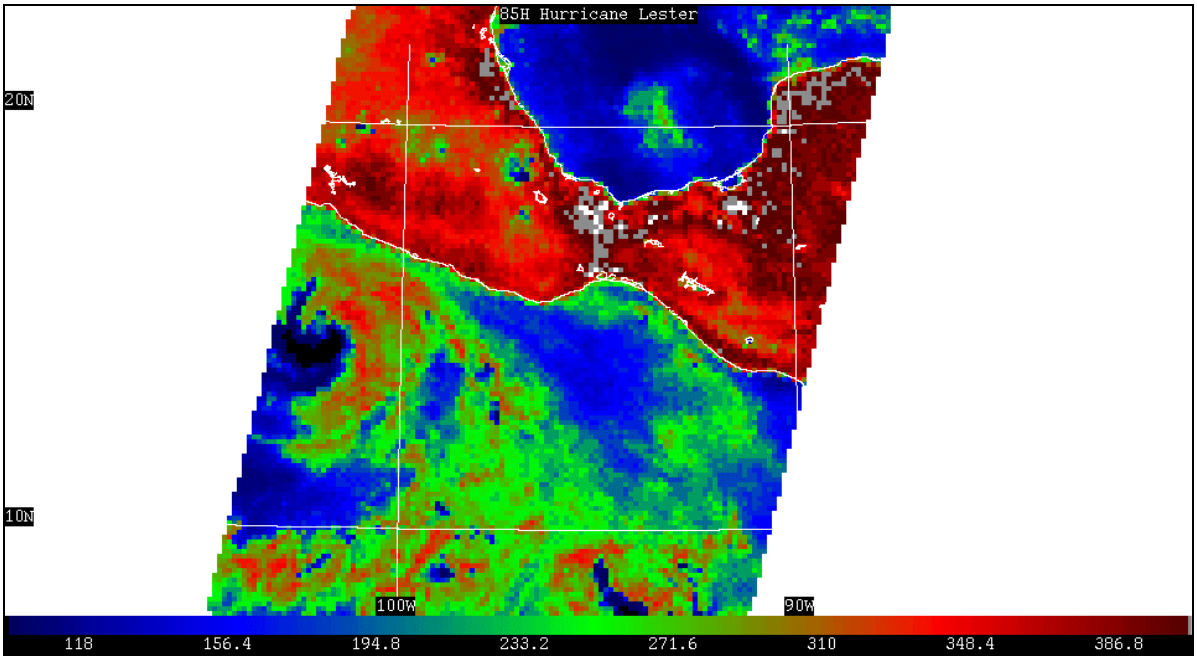

b)

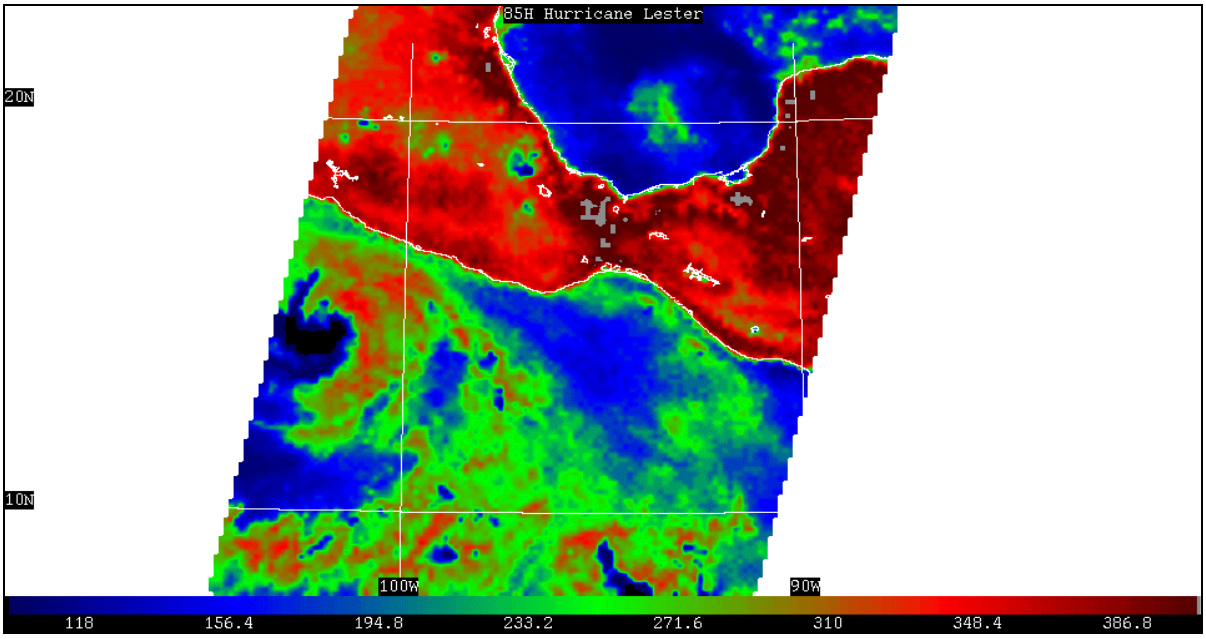

Figure 4.5-2. a) (top) 85 GHz Horizontal polarization channel (85H); b) (bottom) The same image after the SMOOTH and FILL functions have been applied. The FILL function will interpolate into missing pixels, while the SMOOTH function will average each pixel with the surrounding pixels.

5. SDR INTERPRETATION

The most primitive forms of SSM/I data likely to be encountered by operational personnel are Sensor Data Records (SDRs). SDRs are basically brightness temperatures that have been calibrated, geolocated, and antenna pattern corrected. This section discusses how to interpret SDR images and specifically covers those surface and atmospheric phenomena that can be analyzed with the use of SSM/I SDRs.

In order to illustrate the appearance of various phenomena in the SDR images, as well as the relationships between the channels, most of the figures in this section are made up of images from multiple SSM/I channels.

5.1 Surface phenomena

5.1.1 Land

5.1.1.1 Bare soil

During the day, the land surfaces of the Earth, because of their relatively low albedo (fraction of solar radiation reflected back to space), receive a great deal of energy from solar radiation. This energy is turned into heat and is re-radiated at lower frequencies (infrared and microwave).

Normal, dry soil has an emissivity of 0.90 - 0.95 at microwave frequencies. This means that its apparent temperature to the SSM/I is fairly close to the true (thermometric) temperature. Furthermore, the emissivity of dry soil is nearly constant with frequency, so that, ignoring atmospheric effects, all SSM/I channels would record a similar brightness temperature. In practice, however, water vapor absorption at 22 GHz and cloud and rain effects at 85 GHz limit the use of these frequencies for observing the surface. Finally, the emission from dry soil is fairly highly polarized (the amount of vertically polarized energy received is more than the amount of horizontally polarized radiation). At the SSM/I incidence angle, the polarization difference can exceed 50 K.

Adding water to dry soil dramatically changes its radiative characteristics and appearance in SSM/I imagery. Thoroughly dampened soil has an emissivity of 0.6 or less, and thus significantly lower brightness temperatures than the same soil in a dry condition.

Another characteristic of wet soil is that its emissivity increases with frequency, so that it would appear cooler at 19 GHz than 37 GHz. This means that the variation of brightness temperature with soil moisture (and hence the sensitivity of the SSM/I to it) is greater at 19 GHz than 37 GHz. As soil moisture increases, the polarization difference increases as well, from about 50 K for dry ground to 70 - 80 K for thoroughly soaked soil. Since the brightness temperatures for those channels that receive vertically polarized radiation are significantly higher than for those that receive horizontally polarized radiation, the 19H and 37H channels are most sensitive to soil moisture.

The radiative characteristics of soil arise from the properties of top layers. The depth from which the energy comes decreases rapidly with increasing frequency. This property can be exploited to distinguish different soil types (for example, desert and arable land)

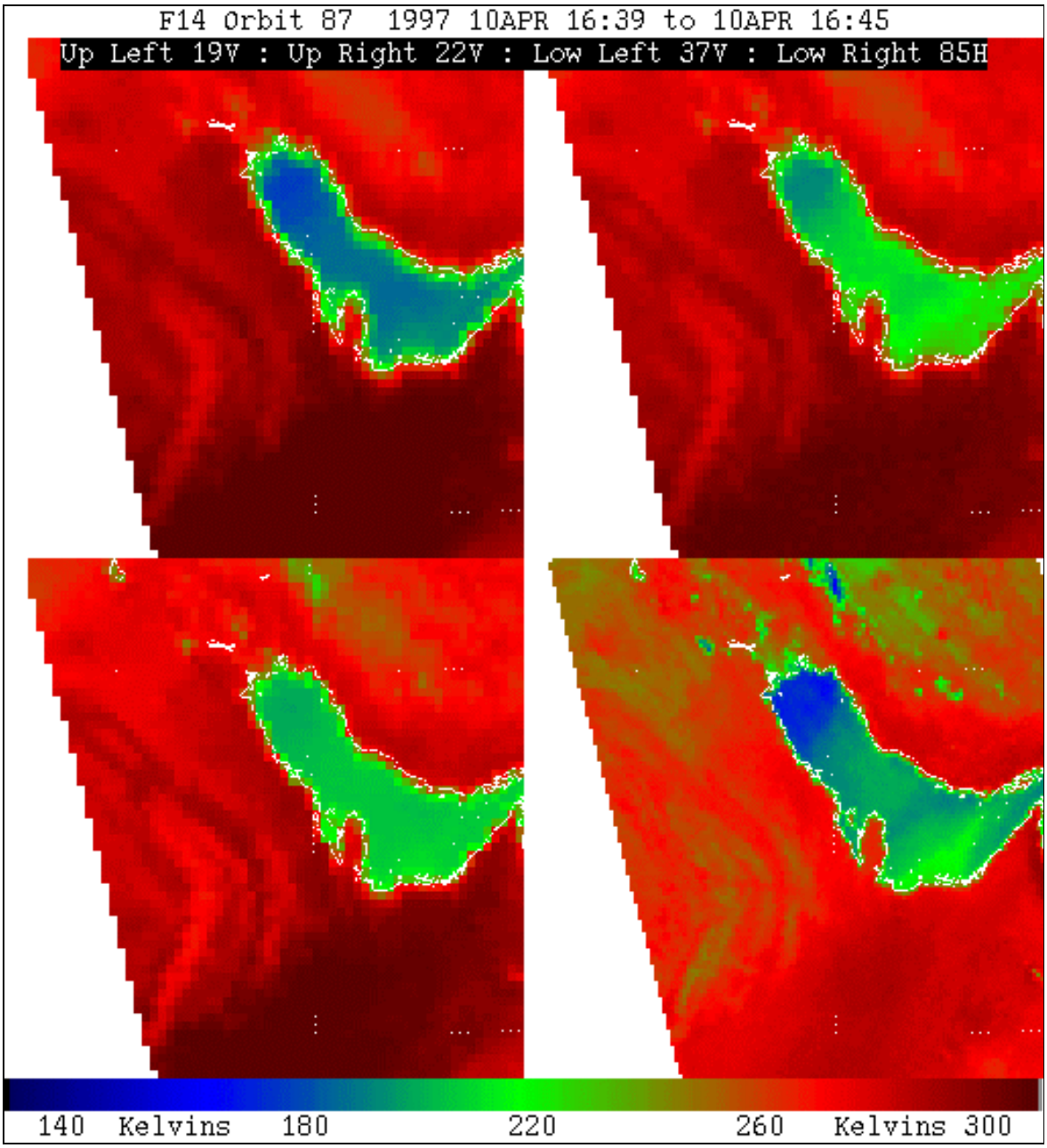

Figure 5.1-1. Portion of the Middle East in 4 SSM/I channels (clockwise from upper left are 19V, 22V, 85H, and 37V). The body of water in the center is the Persian Gulf

that retain water differently, particularly if observations of an area are available from different times in the diurnal cycle. For desert soil, moisture near the surface evaporates rapidly during the morning. An adjoining tract of plowed soil might appear similar to the SSM/I at night, but would lose its moisture much more slowly early the next day and appear significantly cooler.

Another effect to be considered in observing soil with microwaves is the roughness of the surface. It has been observed that the emissivity of rough soil is slightly higher than that of smooth ground. A freshly plowed tract, for example, should appear slightly brighter in 19 GHz imagery than prior to plowing. This increase in emissivity with roughness, however, reduces the range of variation due to soil moisture, and thus the SSM/I sensitivity to it.

Figure 5.1-1 shows a large portion of the Middle East during spring in 4 SSM/I channels. There is some cloud cover in this image. The first thing to notice is the great contrast between the water in the Persian Gulf (T_{19V} between 195K and 215K) and the radiometrically much warmer land surrounding it (T_{19V} between 250K and 300K). This difference is greatest at 19V.

Next, note how much cooler the Tigris/Euphrates basin (located just off the northwestern tip of the Persian Gulf), which is extensively irrigated, is than the adjoining desert (240K vs. 300K at 19V). This is due to the effect of increased soil moisture reducing the emissivity of the soil.

The effect of different terrain elevations and soil types can be seen as well. The linear feature seen in central Saudi Arabia (bottom center of the images), which looks rather like a comma, is an elevated line of hills, and is cooler because of both its altitude and soil condition. The same applies to the top center of the image, which is the semi-arid mountainous terrain in western Iran. This soil not only holds moisture better than the desert sand, but often has a sparse vegetation cover. Both of these effects tend to reduce brightness temperatures, so these areas are noticeably cooler.

5.1.1.2 Vegetation

The appearance of vegetation in SSM/I imagery is a combination of modified radiation from the underlying soil and emissions from the vegetation canopy itself. Both of these processes depend on the optical thickness of the vegetation at SSM/I frequencies, which in turn depends on the biomass (amount of biologically active material) present.

At a simple level, plants can be described as a collection of small (approximately cell-sized) aggregates of liquid water retained in fibrous structures (leaves, stems, branches, trunks, etc.). The water in the plants' cells both absorbs and, because of its dispersion into small particles, scatters radiation from the soil below. Also, plants are very good emitters of thermal radiation, having a relatively high emissivity (0.8- 0.9).

As described in section 5.1.1.1, adding moisture to soil substantially decreases its emissivity (from around 0.8 to around 0.6). This is significant because, generally, soil on which enough biomass is present to affect radiation at SSM/I frequencies is moist. Since they are physically close together, the vegetation and soil are at or near the same thermometric temperature (the soil may actually be cooler due to shading by the canopy), so that the higher emissivity of vegetation yields higher brightness temperatures. The result is that vegetation appears warmer than the surrounding ground, particularly at 19 and 37 GHz.

Another property of the radiation emitted by vegetation is that it is unpolarized. To the extent that scattering and absorption block the signal from the ground, the signal from the soil/vegetation composite will have a lower polarization difference, which goes almost to zero for lush rainforest.

Research has shown that a lack of water in the plant (and hence the stress on it) has a significant effect on its emissions. As plant moisture decreases, the emission, absorption, and scattering also decrease, and the effects on radiation from the soil are reduced. In the most extreme case, when the vegetation is dead, the radiometric effect is similar to increased soil roughness. The polarization of the radiation is generally higher for unhealthy plants, as the polarized signal from the ground is less affected. This property has been used to calculate a Microwave Polarization Index (MPI), which can serve as an indicator of plant health.

Figure 5.1-2, a composite of three successive orbits, is a 19V image of portions of South America (note that gaps are visible in the data; multiple days worth of data are required to fill the gaps). This image shows clear contrasts in brightness temperature, due to the presence and nature of the vegetation cover, between different areas in South America. The dark red areas are lush rainforest, in Brazil, Bolivia, and elsewhere in the Amazon drainage basin, which appears very warm (~280K) to the SSM/I. The Amazon river itself and its floodplain, because of the cooling effect of high soil moisture levels, appears lighter (red to green). The coolest land brightness temperatures (~250K) in the image occur in the Andes Mountains, which are not only thermometrically colder than lower terrain, but may have snow cover. The cool spots in the center if the image are Lakes Poopó and Titicaca (partly off in the gap).

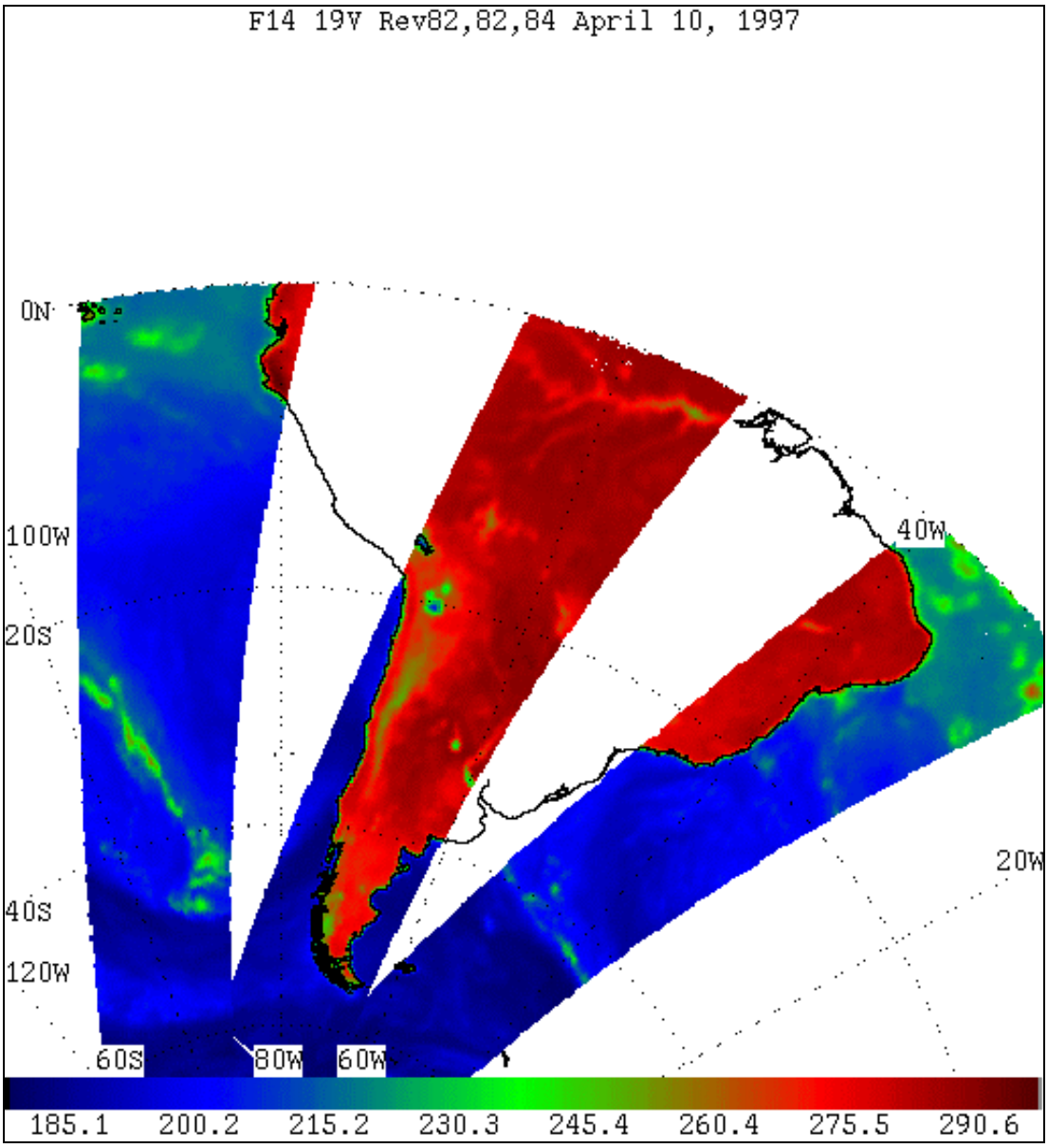

Figure 5.1-2. Channel 19V image of portions of South America from three successive orbits in April, 1997.

5.1.1.3 Snow

The primary effect of a cover of dry snow at frequencies above 20 GHz is to scatter the radiation from the ground below, since the snow particles are close in size to the wavelengths. This scattering asymptotically approaches a maximum value as depth increases. The effect is that snow is much colder than bare soil, and, up to a limit, gets even colder as more snow is added. This is seen more at 37 GHz than 19 GHz, which has a greater penetration depth and receives more emitted energy from the soil. As with other surface phenomena, the 85 GHz channels are affected too much by clouds and rain to be useful.

In addition to lowering the brightness temperatures at 19 and 37 GHz, a snow cover substantially reduces the polarization difference of the soil. This situation changes dramatically when the snow becomes wet. Even the thinnest layer of liquid water in a snowpack will completely block the signal from the soil. In addition, the water acts, in comparison to snow, as a good emitter. The result is that wet snow appears warmer than dry snow, as well as having a higher polarization difference (due to the greater discontinuity between water and air). The difference between dry and wet snow is greatest at 37 GHz, again because 19 GHz penetrates too far, while 85 GHz often cannot see the surface.

As a snowpack melts and re-freezes repeatedly, the size of the snow grains increases, making them better at scattering radiation. For this reason, an old snowpack will appear colder than a fresh one.

Finally, the appearance of snow undergoing significant melting is very difficult to distinguish from extremely wet soil. The only reliable way to separate the two is with a multi-temporal approach, examining the history of an area and noting the transition from dry snow to melting.

Figures 5.1-3 and 5.1-4 are composites of one day's worth (filling the gaps would require multiple days) of 37V and 37H passes over the Northern Hemisphere. The greenish areas over land (37V brightness temperatures between 240K and 265K) are points with a snow cover. Snow is clearly visible in the northern Soviet Union (Siberia), and northern Canada. Along the snow edge, the mixed green and red pixels can represent either melting snow or very wet soil. Note how similar the brightness temperatures of the snow-covered areas are in both polarizations at 37GHz, in contrast to the other, more polarized, land areas. Warmer non-polarized areas are most likely vegetation.

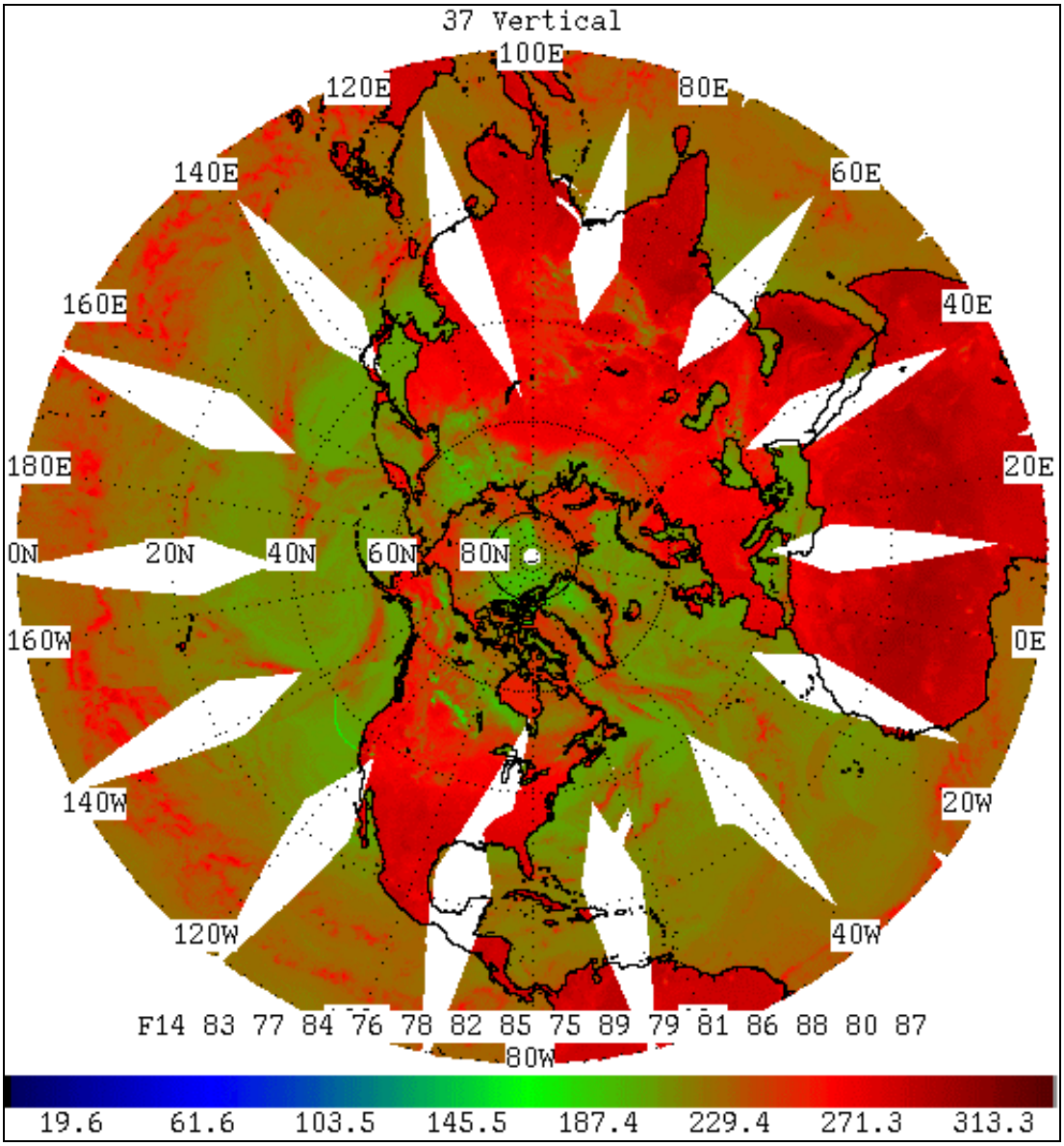

Figure 5.1-3. Channel 37V composite of one day's worth of orbits during April, 1997. Greenish areas over land indicate areas with snow cover.

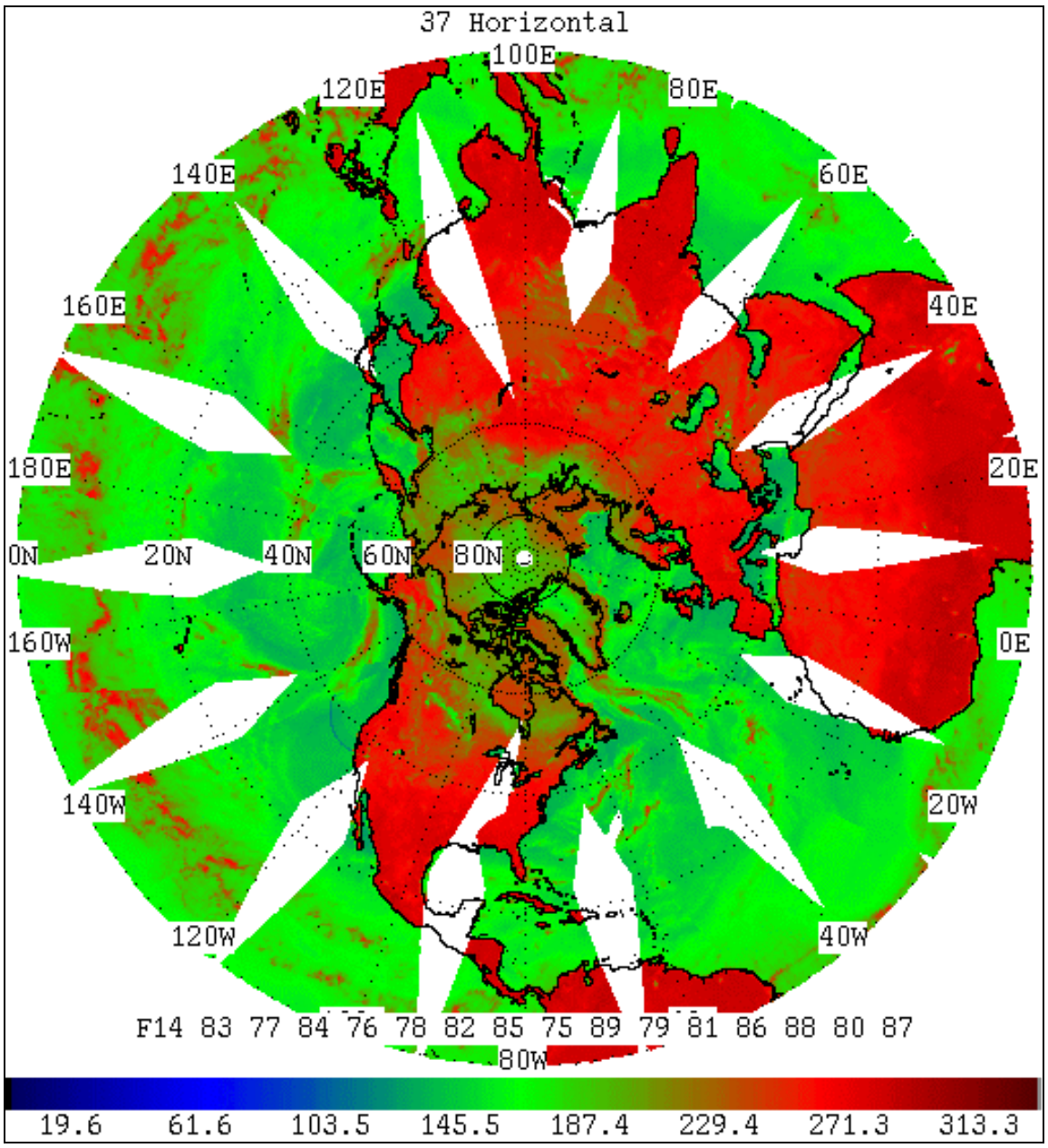

Figure 5.1-4. Channel 37H composite of one day's worth of orbits during April, 1997. These orbits are coincident with those in the previous image (Figure 5.1-). Greenish areas over land indicate areas with likely snow cover.

5.1.2 Ocean

5.1.2.1 Open Water

The emissivity of open calm seawater is relatively low and increases with frequency, ranging from about 0.4 at 19 GHz to about 0.6 at 85 GHz. The sea surface temperature varies from about 270 K to about 310 K, resulting in brightness temperatures that range from 150 K at 19 GHz to 240 K at 85 GHz (vertical polarizations). Since the water surface is so smooth, it is highly polarized, with the horizontally polarized channels having brightness temperatures 50 to 70 K lower. Furthermore, the polarization difference is greater at 19 GHz than 37 GHz.

Because open water has an emissivity generally much lower than that of land its brightness temperatures will be lower. This difference is most pronounced at the lower SSM/I frequencies (particularly at 19 GHz, where the ocean brightness temperature can be 50 to 70 K below that of the land), making it possible to unambiguously distinguish between land and ocean.

Since the effect of water salinity on emissivity is negligible above 4 GHz, fresh and salt water bodies at the same temperature will appear much the same. Furthermore, even the 19 GHz channels of the SSM/I do not show great sensitivity to sea surface temperature.

The result of all these properties is that calm open ocean appears to the SSM/I at the lowest frequencies as a cool, homogeneous, polarized background. The presence of clouds, rain, water vapor, wind, or surface roughness changes the ocean signal substantially, which, as we will see in later sections, allows accurate measurements to be made of these phenomena.

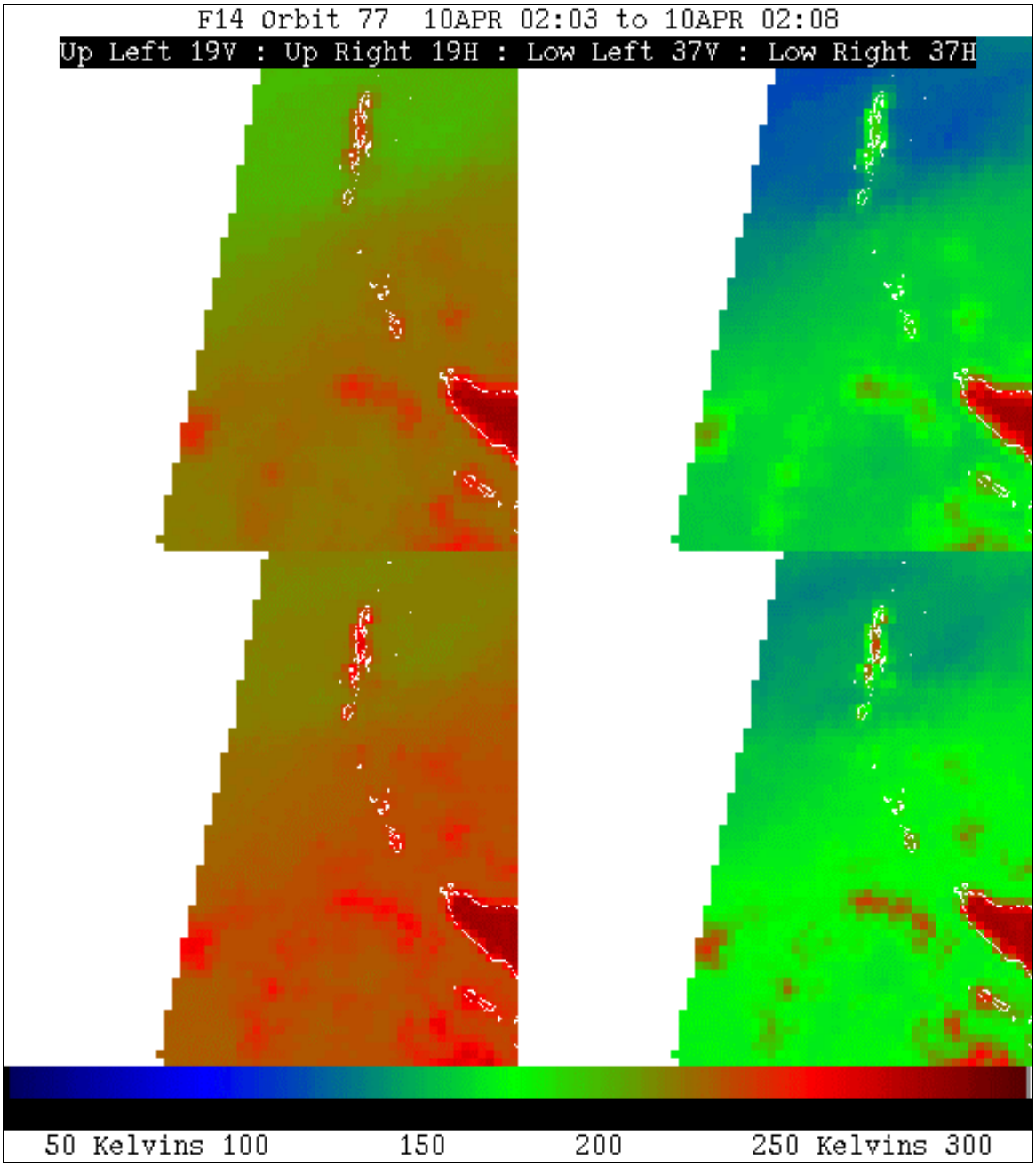

Figure 5.1-5. Clockwise from top left are the 19V, 19H, 37H, and 37V channels over Sumatra (Indonesia), Malaysia, the Bay of Bengal (upper left), and Indian Ocean (bottom left)

In Figure 5.1-5, the first thing to note is the difference between the Indian Ocean as seen in the 19 GHz channels. This polarization difference (~50K) is typical of ocean areas. Note how smooth (spatially homogenous) the area appears in all channels.

5.1.2.2 Sea Ice

From a radiometric viewpoint, sea ice falls into three categories: newly formed ice (thickness up to 30 cm), first year (FY) ice (thicknesses between 30 cm and 1 m**),** which has yet to go through the annual process in which the upper layers melt and refreeze, and multi-year (MY) ice (thickness greater than 1 m**),** which has undergone at least one melt cycle.

Except for the thinnest newly formed ice the radiation from an ice-covered area is due to thermal emission from the ice and not the ocean below. This is because sea ice is a very effective scattering medium for microwaves.

Both new and FY ice have high emissivities (0.9 - 0.95), which are constant with frequency, while the emissivity of open water is around 0.5. The difference in thermometric temperature between ice and open water is overwhelmed by this difference in emissivity, so that ice looks significantly warmer (by 20 - 30 K) than the surrounding ocean. Because of volume scattering by the ice, the polarization difference is much less than that of water. However, during the polar summers, when a thin layer of meltwater can be found on the ice, the amount of polarization increases.

The emissivity of MY ice is slightly lower (0.8 - 0.9) than that of FY ice, and varies slightly with frequency. The result is that MY ice is radiometrically cooler than FY ice, particularly at 19 GHz (where the difference can be as much as 30 - 40 K). Because MY ice has a large number of trapped air bubbles, the amount of volume scattering taking place is greater than for FY ice, so that the signal is even more depolarized.

Finally, the presence of a snow cover over the ice increases the ice emissivity slightly, since the interface from ice to the air becomes less discontinuous. The effect of this is that areas where snow overlies the ice are warmer than ice alone. Furthermore, the presence of a snow layer insulates the ice, producing higher thermometric temperatures and, in turn, higher brightness temperatures.

In Figure 5.1-6, sea ice shows up as red or reddish-green over the polar oceans (over land, the green-tinted areas represent snow or very moist soil). Note the contrast between the open polar ocean and the ice (brightness temperature differences of 30-40 K). The areas with the darkest green tint (for example, the polar ice cap) indicate multiyear ice, while the dark red indicates first year ice. Reddish spots within green areas indicate an increase in emissivity due to snow cover.

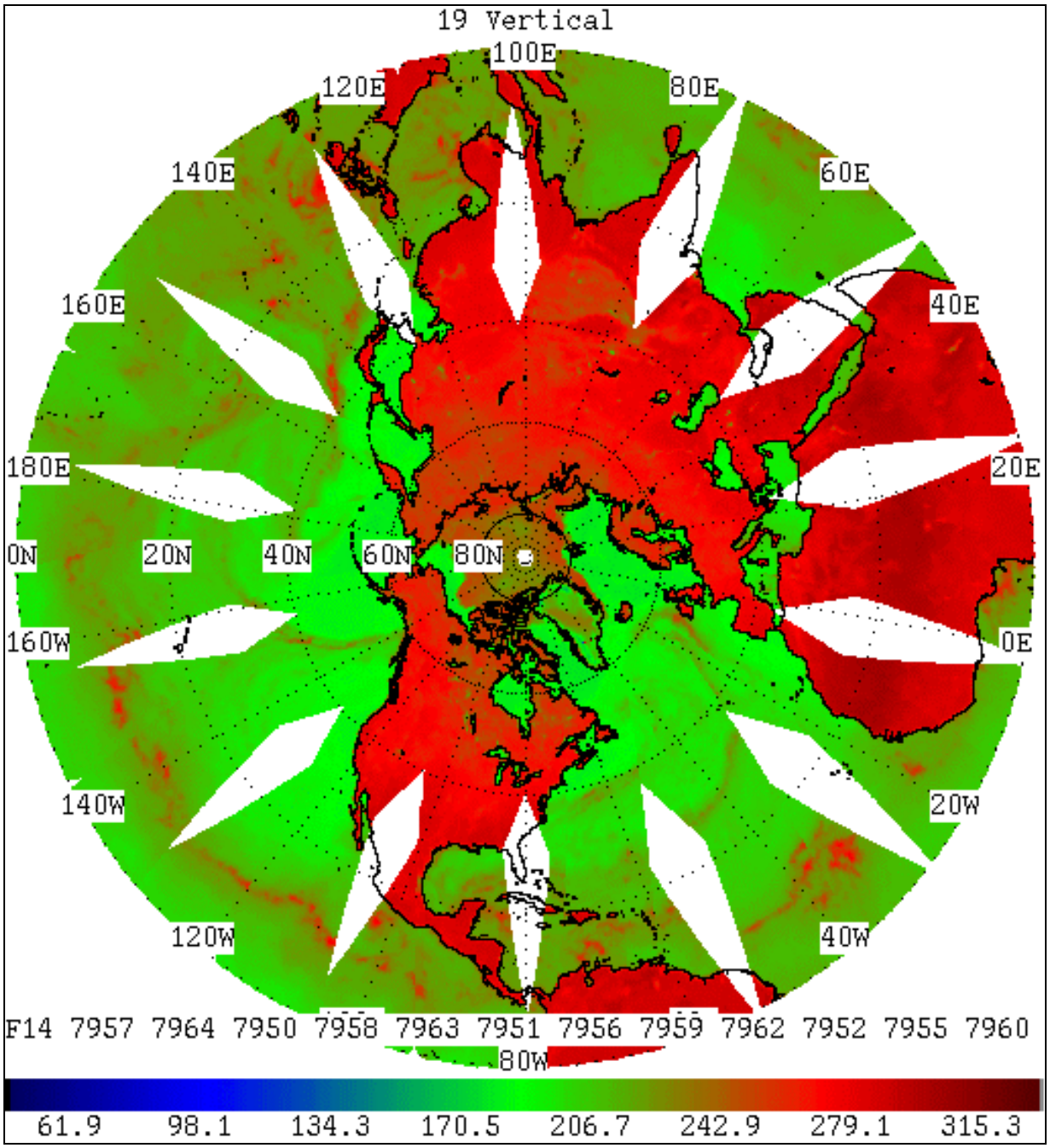

Figure 5.1-6. Composite of one day's worth of 19V passes over the Northern Hemisphere.

5.2 Atmospheric phenomena

5.2.1 Water Vapor

Measurement of atmospheric water vapor (WV) by the SSM/I relies on the 22.235 GHz channel. As mentioned earlier (Section 3.3), this frequency is the center of a water vapor absorption/emission line. The 19 GHz channels are less affected by WV, and differ so little in frequency from 22 GHz that the slow rise in atmospheric absorption and emission with frequency is insignificant. Thus differences between the 19V and 22V channels are primarily due to the presence of WV in the column of air from the sensor to the ground. The WV is a good emitter, making it warmer at 22V than the ocean background, while 19V does not show a corresponding increase. As will be seen later, this difference is related in a predictable way to the integrated columnar amount of WV.

Because of its spatial homogeneity, and the larger amounts of WV present, the ocean forms a much better background than land for identifying WV concentrations. Variations in 19V due to soil moisture, vegetation, and other land surface phenomena easily swamp the differences due to WV. Furthermore, even over ocean, the presence of rain or large amounts of liquid cloud water will dominate the signal.

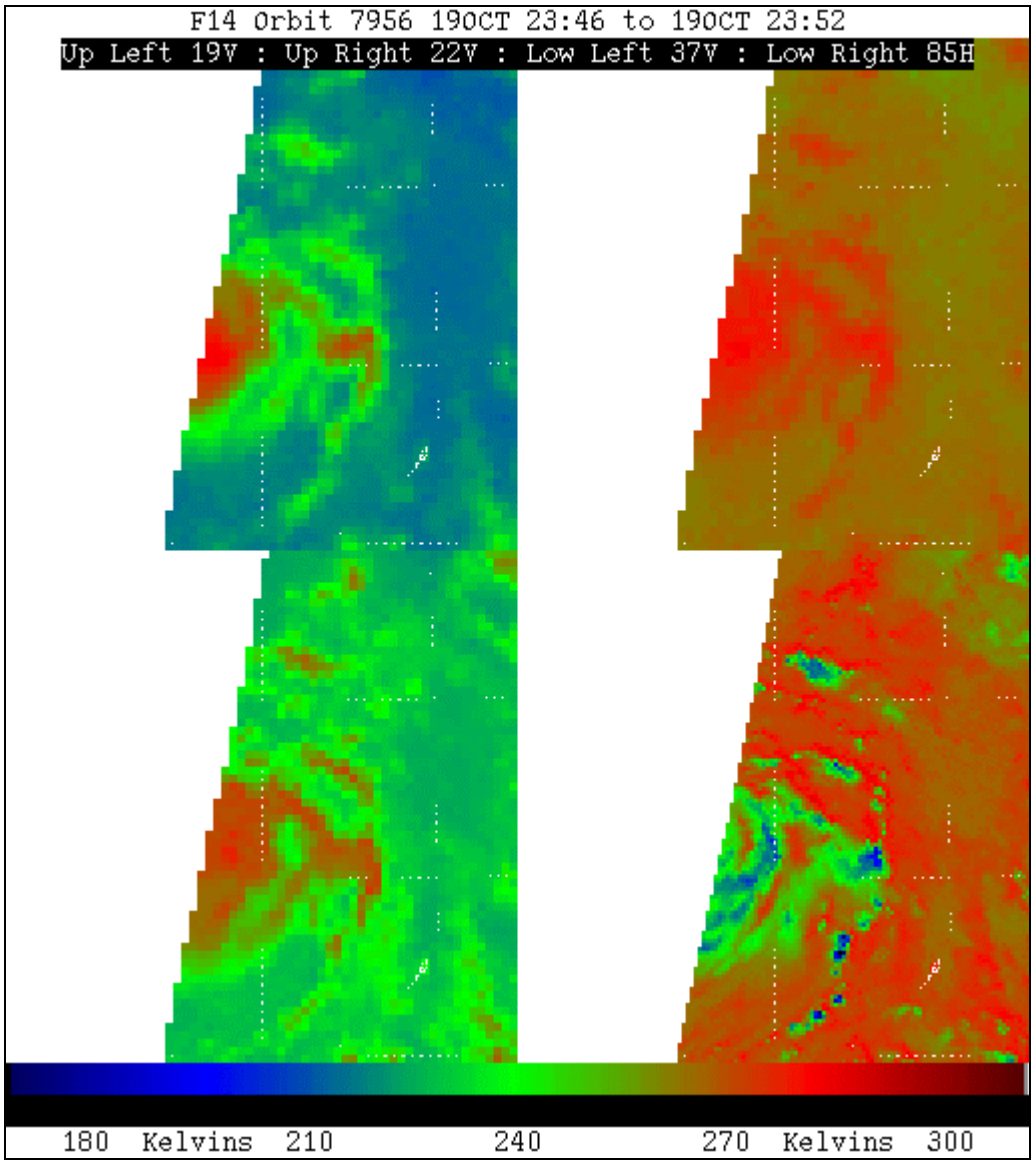

Figure 5.2-1. Typhoon Babs, 19 Oct 1998. The 85V image clearly shows the spiraling cyclonic structure of the system. Notice that in the 22V image, the vapor being drawn into the system is warmer than the background.

5.2.2 Clouds

The appearance of clouds in SSM/I imagery is the result of a complex combination of both primary radiative processes (emission/absorption and scattering). From the point of view of the SSM/I, clouds can be divided into two broad categories by altitude and composition.

The first category contains high-altitude clouds made of small ice crystals (i.e., cirrus). These are optically very thin at SSM/I frequencies, so are virtually invisible. This can be a significant advantage when studying storm systems, which often have a cirrus shield

that prevents the use of IR and visible data for analyzing the underlying structure of the system. The SSM/I does not see the shield, so that the location of cumulonimbus and other thick clouds can be determined. Other ice species that can be found in clouds (hail, graupel, etc.) appear somewhat like rain to the SSM/I, but scatter even more radiation (see section 5.2.3 for more information on the effect of rain).

The second category contains low- and mid-altitude clouds (cumulus, stratus, etc.) that are composed primarily of spherical or near-spherical water droplets. The total amount of extinction (combination of absorption and scattering) of the land/ocean surface emission caused by these droplets increases with the thickness and water content of the cloud. The thickest clouds can block virtually all of the radiation from the surface, while others leave it almost unchanged. This blocking effect is seen at its peak in the 85 GHz channels, since both absorption and scattering increase with frequency. In addition to affecting the radiation from below, clouds are fairly good emitters. Like extinction, the emissivity of a cloud depends on its thickness and water content, but is often high (0.9 - 1.0). So, for denser clouds, not only is the signal from the surface masked, but replaced. Furthermore, the energy from the cloud is emitted by the atmosphere, so it is unpolarized. To the extent that the cloud has enough water, the polarization differences (particularly at 37 and 85 GHz) of the surface can be substantially reduced.

It is important to note that the SSM/I responds to the amount of liquid water within the cloud, not to its thickness. Each cloud type has a different liquid water density and, if the type is known, some estimate of the thickness may be possible.

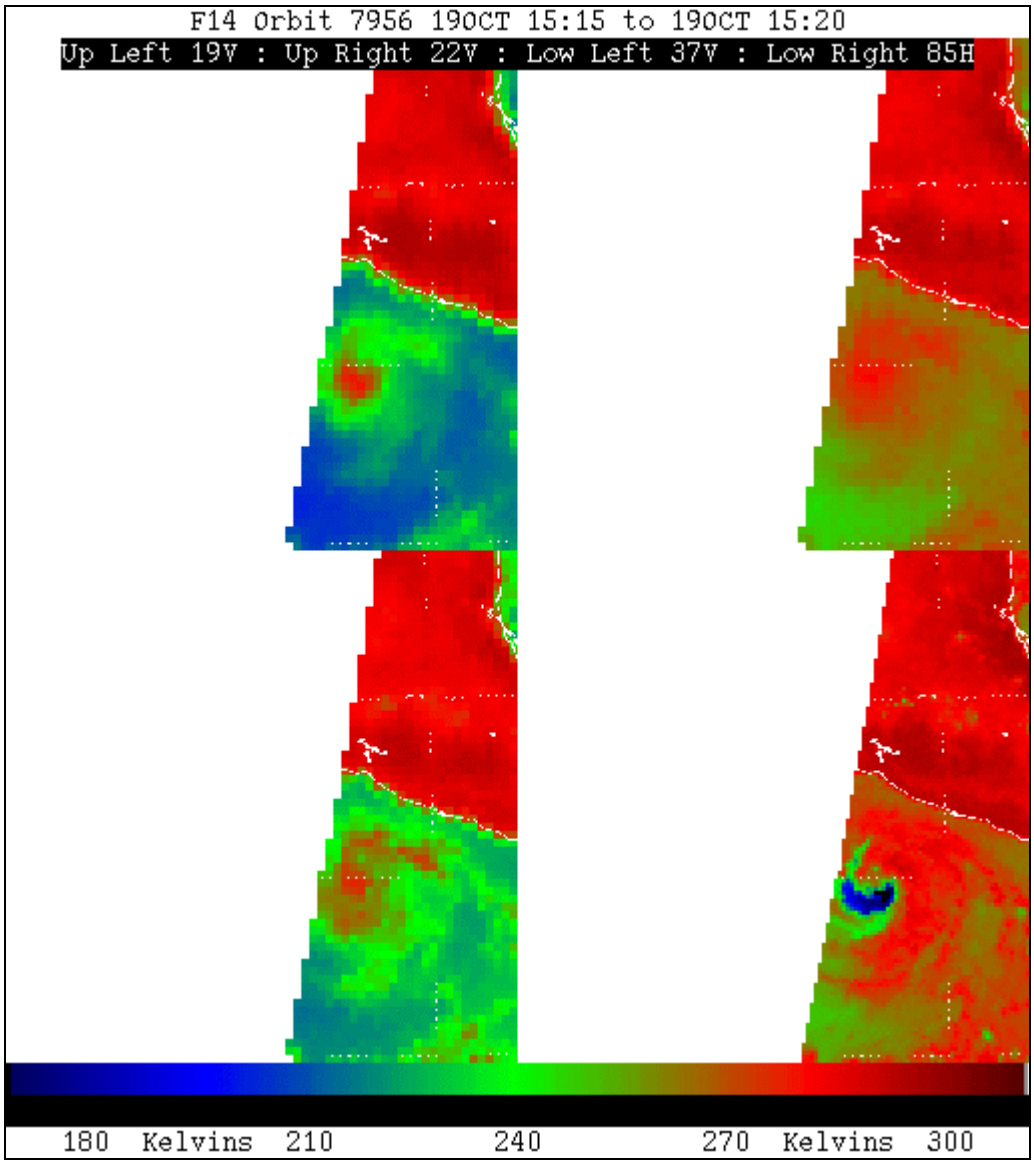

Figure 5.2-2. Hurricane Lester, 19 Oct 1998.

The effect of these processes is that over ocean, where the emissivities range from 0.4 to 0.6, most low and medium altitude clouds appear significantly warmer than the background. The thermometric temperature difference between the surface and the height of the cloud is overwhelmed by the difference in emissivities. The relation between cloud water content and the increase in brightness temperature is predictable enough to be used as the basis for a liquid water estimation algorithm (see Section 6.7 for additional details).

Over land, the situation is quite different. Despite variations due to soil moisture and vegetation cover, land emissivities are generally high, approximating that of relatively dense clouds. Therefore, the determining factor for the brightness temperatures is the

thermometric temperature gradient due to altitude, which means that the signature of clouds can be very difficult to detect, particularly for low-altitude or less dense cloud layers. Layers with high levels of liquid water or areas in which vertical development is extensive will appear much cooler than the underlying land.

The presence of snow covering the surface beneath the clouds can be confusing, particularly if the snow depth is not great and only slightly scatters the energy from the ground below. The result is a brightness temperature not markedly different from that of clouds. Over deeper snow, however, the background is cold enough that the clouds can appear significantly warmer, particularly at 85 GHz.

5.2.3 Rain

The behavior of microwaves in the presence of rain particles is influenced primarily by three factors: the background surface type, the extinction from rain and clouds (absorption, emission, and scattering), and the presence of ice in the upper cloud regions. Consequently, the major factors influencing rain detection are ocean versus land backgrounds, and small nonconvective versus large convective storms. Convective storms are defined as storms with sufficient vertical development to produce ice particles in their upper regions.

The interaction of microwaves with hydrometeors can be summarized by two factors: the size of the particle and its state (liquid or solid). This gives rise to the following four conditions:

- Large liquid particles (rain) - Absorption, emission, and scattering are all present. The scattering by the raindrops is compensated by their emission, resulting in little net loss to the signal from scattering.
- Small liquid particles (cloud drops) - Absorption and emission are the only mechanisms at work.
- Large solid particles (ice) - Scattering is the only mechanism applicable to ice particles. Attenuation of the upwelling radiation is severe, particularly at higher frequencies.
- Small solid particles (cirrus ice) - These particles have no effect on microwaves, and are thus undetectable.

As stated above, the background surface type has an important effect on rain detection. The following is a discussion of the influence of ocean and land backgrounds.

5.2.3.1 Influence of ocean background on rain detection.

The emissivity of the ocean is very low, although it does increase with increasing frequency. Clouds in the atmosphere are radiometrically warmer than the ocean surface; they emit more radiation than the ocean. Cloud drops and rain drops are generally the

largest contributors to upwelling radiation over ocean areas. If the rainfall is light and the storm is only mildly convective (so that ice particles are not found in the cloud tops), the brightness temperatures will increase with increasing rain rate. However, in convective storms where ice is found in the upper regions, scattering plays a major role. Ice particles scatter the higher frequencies more readily than the lower frequencies since ice particles are closer in size to the 85 GHz wavelength. Large storms with a high degree of vertical development not only generate high rain rates, but have large numbers of ice particles in their tops. The larger the vertical development of the storm, the higher the rain rate and the number of ice particles in the upper atmosphere. The ice particles will scatter the upwelling 85 GHz radiation out of the field of view of the sensor. In addition, the cosmic background radiation (which has a temperature of 3 K) will be scattered by the ice into the sensor field of view. Ice particles act like mirrors reflecting cold space to the sensor (see Figure 5.2-3). Thus, in convective storms, the higher the rain rate, the lower the brightness temperature of the 85 GHz channel. Scattering in fact plays a role at all frequencies. As rain rates increase, the brightness temperatures of all frequencies will decrease, although this decrease is much more rapid at 85 GHz. Another problem in detecting rain, particularly in non-convective storms, is the difficulty in distinguishing rain drop emission from cloud drop emission at a given frequency. This can be overcome by using several frequencies, since the emission characteristics of each species are different at different frequencies.

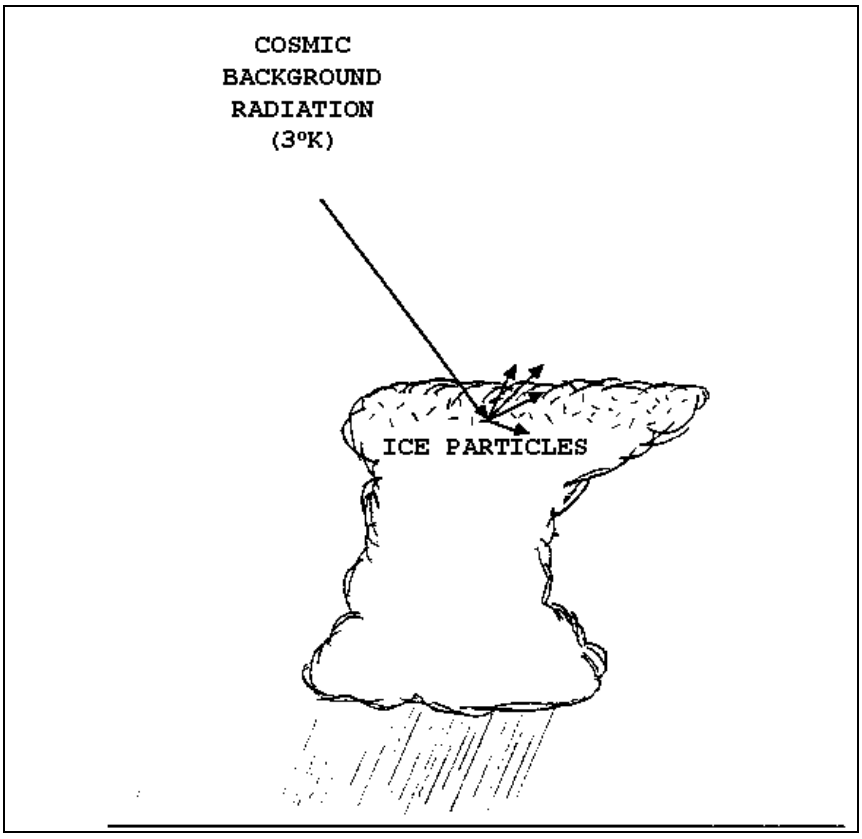

Figure 5.2-3. Cosmic background scattering from ice.

5.2.3.2 Influence of land background on rain detection.

Rain detection over land is more difficult than over ocean areas. Unlike the ocean, the emissivity of land is fairly high, so the background brightness is quite high. Over vegetated land, the emissivity is constant with frequency. Vegetation can be thought of as a suspension of water particles, much like a cloud. Therefore, it is very difficult to distinguish between the emission from vegetation and the emission from non-convective rain clouds. Large convective storms, however, give rise to scattering ice particles in the upper storm layers. As is the case with oceanic convective storms, scattering from ice decreases the brightness temperatures of all frequencies. Thus, increasing rain rate results in decreasing brightness temperatures. This effect is most pronounced at the higher frequencies.

5.2.4 Wind

Wind affects water surfaces in two ways that are important to microwave remote sensing. A perfectly calm body of water has an emissivity from approximately 0.4 (at 19 GHz) to 0.6 (at 85 GHz). As the wind blows across the water, it roughens the surface and produces foam; both of these effects increase sea surface emissivities. Sea foam, in particular, has a very high emissivity.

The manner in which wind roughens the surface is important. Small waves, known as capillary waves, cause the greatest changes in microwave emissivity since they are approximately the same size as the microwave wavelengths. Fortunately, capillary waves are also very responsive to changes in wind speed. Small gusts will create these waves quickly. They dissipate equally rapidly in calm winds. Larger waves require long duration winds to build. The sensitivity of the SSM/I to wind at low speeds is due primarily to the effect of capillary waves on microwave emissivity.

As wind speeds increase, the production of sea foam becomes important. The effect from capillary waves saturates at 12 - 15 m/s. Above these speeds, the effect of sea foam is dominant. Sea foam acts as an impedance matching device, permitting more energy from the sea to pass the air/water interface than in the case of a calm sea. Foam depth and the mixture of air to water affect the specific emissivity of sea foam which, under the right conditions, can approach 1.0. For wind speeds greater than 15 m/s, the majority of the energy due to wind speed detected from the orbiting SSM/I may be due to foam.

Horizontally polarized channels are more sensitive to the wind speed signal than vertically polarized channels, particularly at the SSM/I angle of incidence. Since surface roughness increases brightness temperatures, any phenomenon that roughens the surface could result in erroneous wind speeds. Rain is the most common culprit. Wind speed is not accurate in areas of heavy rain, and even light rain will degrade the signal. The degree to which wind speed estimates are degraded by rain is indicated by the rain flag, whose values correspond to different wind speed accuracies. Virga and cloud water can

also lead to erroneous wind speed calculations, even though they do not roughen the surface of the ocean. The polarization difference at 37 GHz (37V-37H, the so-called "D37" calculation) can be useful in determining whether the wind speed signal has been degraded by any of these phenomena.

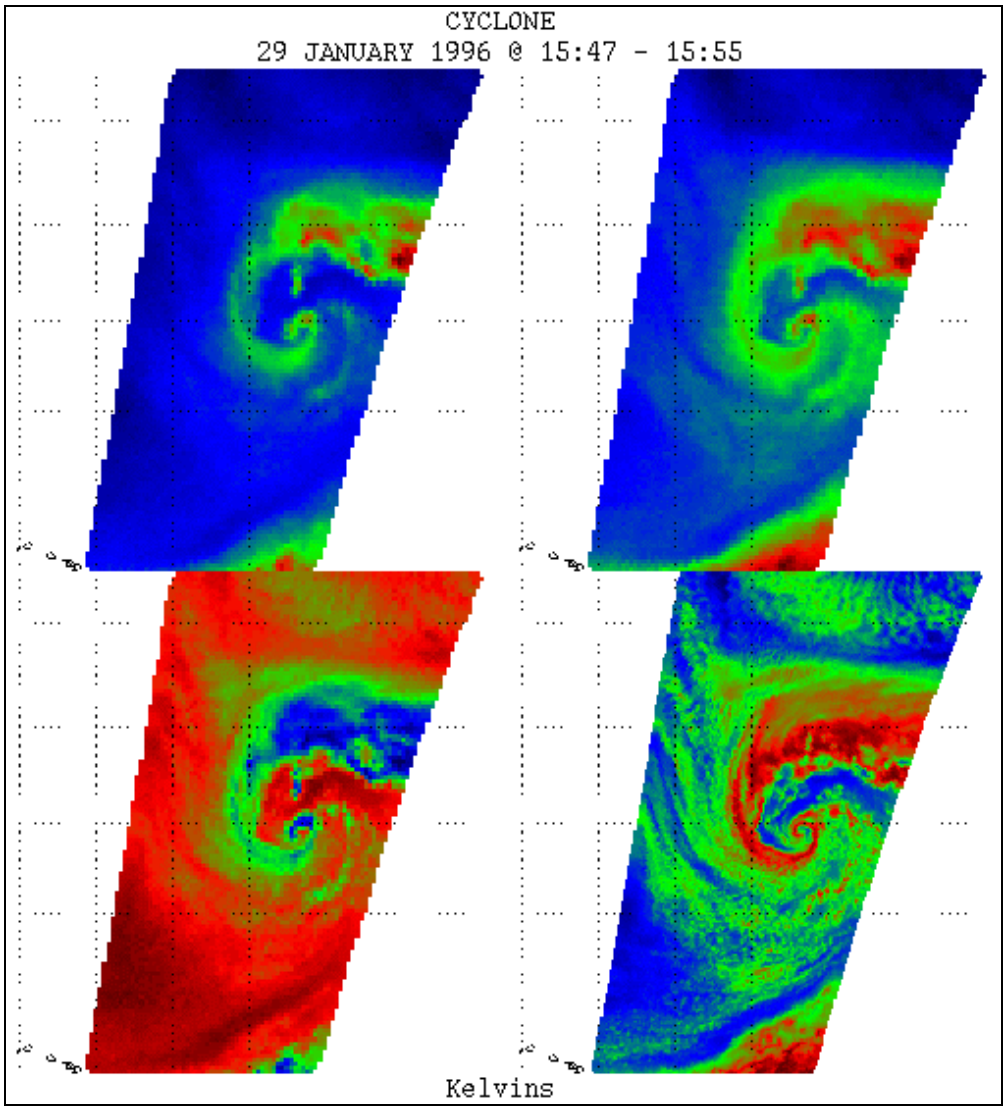

	Blue	Green	Red
19V (upper left)	183.5 – 199.2 K	199.3 – 223.0 K	223.1 – 238.8 K
22V (upper right)	193.0 – 211.5 K	211.6 – 239.5 K	239.6 – 258.0 K
D37 (lower left)	9 - 25 K	26 – 50 K	51 – 66 K
85H (lower right)	187.9 – 210.8 K	210.9 – 245.2 K	245.3 – 268.1 K

Figure 5.2-4. A fledgling cyclone in the Pacific Ocean (note Hawaiian Islands at lower left). Clockwise from upper left are the 19V, 22V, 85H, and D37 images. The 19V image shows warm regions associated with emission from clouds and rain, and increased emissivity from the effect of the wind (seen in red). The 85H image shows markedly colder regions in the rain bands. The D37 image shows large areas below 25 Kelvins. These are rain-contaminated areas where the wind signature is masked.

6. EDR INTERPRETATION

This section discusses each of the SSM/I-derived environmental products in detail, including:

- The basic phenomenology involved, expanding upon topics covered in Section 5,
- The nature of the current algorithm used to produce each product,
- Indications of the performance of the algorithms derived from operational experience,
- Aspects of the processing or phenomenology which are necessary to properly interpret the product or know where it is valid, and
- Examples of products illustrating the above.

Algorithms are documented in Hollinger (1990), except where noted.

6.1 Water Vapor over Ocean (WVO)

This EDR, which is also called Oceanic Total Precipitable Water, is a measurement of the amount of water vapor in a column extending from the surface to the top of the atmosphere. WVO is calculated in kg/m^2 and ranges from 0 to 80 kg/m^2, quantized in levels of 0.5 kg/m^2

The current WVO algorithm was developed by John C. Alishouse of NOAA/NESDIS, and then modified by Grant Petty of Purdue University (Petty, 1993):

```
A = 232.89393 - (0.148596) *T(19V)  -  (1.829125)* T(22V)
          +  (0.006193) *T(22V)**2 -  (0.36954)*T(37V)

WVO =  -3.75  +  (1.507)*A  -  (0.01933)*A**2  +  (0.0002191)*A**3
```

WVO is calculated only over points classified as water.

In general, WVO values are reliable. However, precipitation may partially or fully contaminate a scene station and, because of the squared 22V term in the calculation, dramatically increase WVO error.

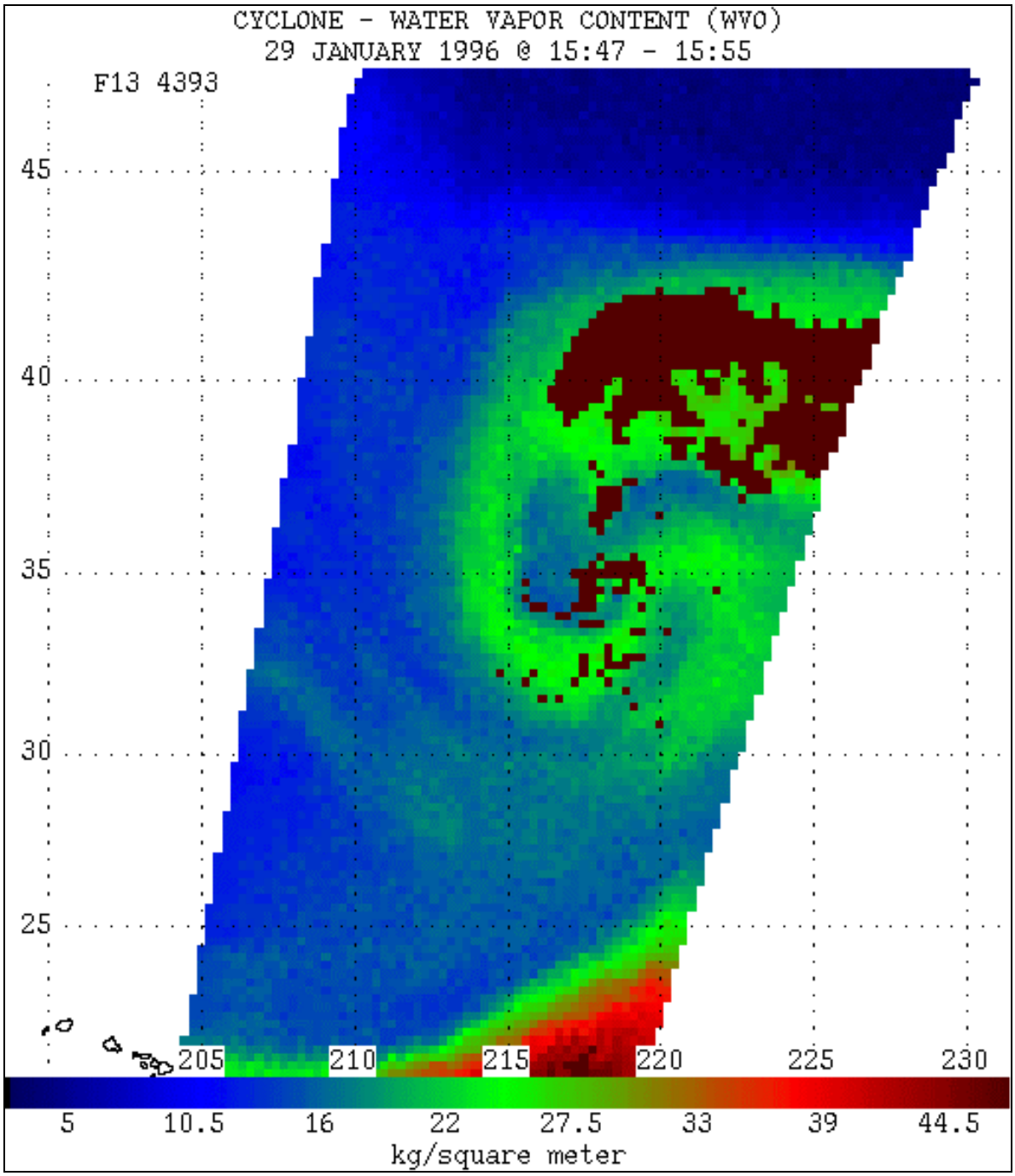

Figure 6.1-1. Image of the vicinity of a fledgling cyclone in the Pacific Ocean made from Water Vapor Content EDR values. The red pixels represent the highest values of water vapor content (33 to 44.5 kg/m^2), followed by green (16 to 33 kg/m^2), and blue (5 to 16 kg/m^2). The cyclone appears to be circulating in a counterclockwise motion with water vapor entering from the south, southwest.

6.2 Sea Ice Concentration (IC) and Ice Age (IA)

Ice concentration is defined as the fraction of an ocean area that is covered by ice. The SSM/I IC EDR provides this value in percent, ranging from 0% to 100% with a quantization of 5%.

The current IC algorithm was developed by James Hollinger of NRL and Rene Ramseier at York University in Canada, and consists of a series of tests and calculations using the 19V, 19H, 37V, and 37H channels (Figures 6.2-1 through 6.2-4). IC is not calculated unless a fixed surface type file indicates ice or possible ice for a particular scene station.

Operational experience has demonstrated that when actual IC values are low, the calculated IC values are biased too high. As a result, one can readily identify the ice edge, but specific concentrations near the edge are potentially unreliable.

The ice age EDR is a flag having two values: first year (FY) and multi-year (MY). If a scene station is determined to have an ice concentration greater than 25%, IA is determined with reference to the 19V brightness temperature by calculating an intermediate value, TBI, as follows:

$$TBI = [T(19V) - TC - (1.0 - IC) * 180] / IC$$

where TC is determined by the season (TC = 6.8 for Autumn/Winter or 14.0 for Spring/Summer) and IC is the calculated ice concentration, ranging from 0.00 to 1.00. If TBI is less than 238.0, the scene station is considered predominantly MY ice, and predominantly FY ice otherwise. Thus far, distinctions made between the two ice types have been generally reliable.

The logic used to determine both IC and IA can be found in Figures 6.2-1 through 6.2-4. Figures 6.2-5 and 6.2-6 show examples of the IC and IA EDRs, respectively.

EQUATIONS

A. TOTICE = CWF(1) * T(37V) + CWF(2) * T(19V) + CWF(3)

B. TOTICE = CSS(1) * T(37V) + CSS(2) * T(19V) + CSS(3)

C. D = 1.0 - 0.0513 * (T(37V) - T(19V))

D. TOTICE = [T(37V) + (0.5 * T(37H)) - 265.0] * 0.01

E. TBI = [T(19V) - TC - (1.0 - TOTICE) * 180] / TOTICE

F. TC = 14.0

G. TC = 6.8

H. WCUT = 6.0

I. WCUT = 8.5

FALL / WINTER COEFFICIENTS	SPRING / SUMMER COEFFICIENTS
CWF(1) = -0.013656219	CSS(1) = - 0.015231617
CWF(2) = 0.024412842	CSS(2) = 0.025911011
CWF(3) = -1.677645	CSS(3) = - 1.656920

TESTS

1.	T(19V) $\leq$ 151.0	OR	T(19H) $\leq$ 92.0	OR
	T(37V) $\leq$ 171.0	OR	T(37H) $\leq$ 125.0	OR
	T(19V) - T(19H) $\geq$ 80.0	OR	T(37V - T(37H) $\geq$ 80	OR
	T(19H) > T(19V)	OR	T(37H) > T(37V)	
2.	TOTICE $\leq$ 0.7	AND	D $\leq$ 0.7	
3.	D $\leq$ 0.3	AND	(T(37V) * 1.5) - T(19V) > 120.0	
4.	T(37V) $\leq$ 215.0			
5.	D $\leq$ 0.15	OR	T(37H) - (2 * T(37V)) + 270 $\geq$ WCUT	
6.	TOTICE $\leq$ 0.5	AND	D $\geq$ 0.15	

Figure 6.2-1. Tests and equations for the Sea Ice Concentration EDR

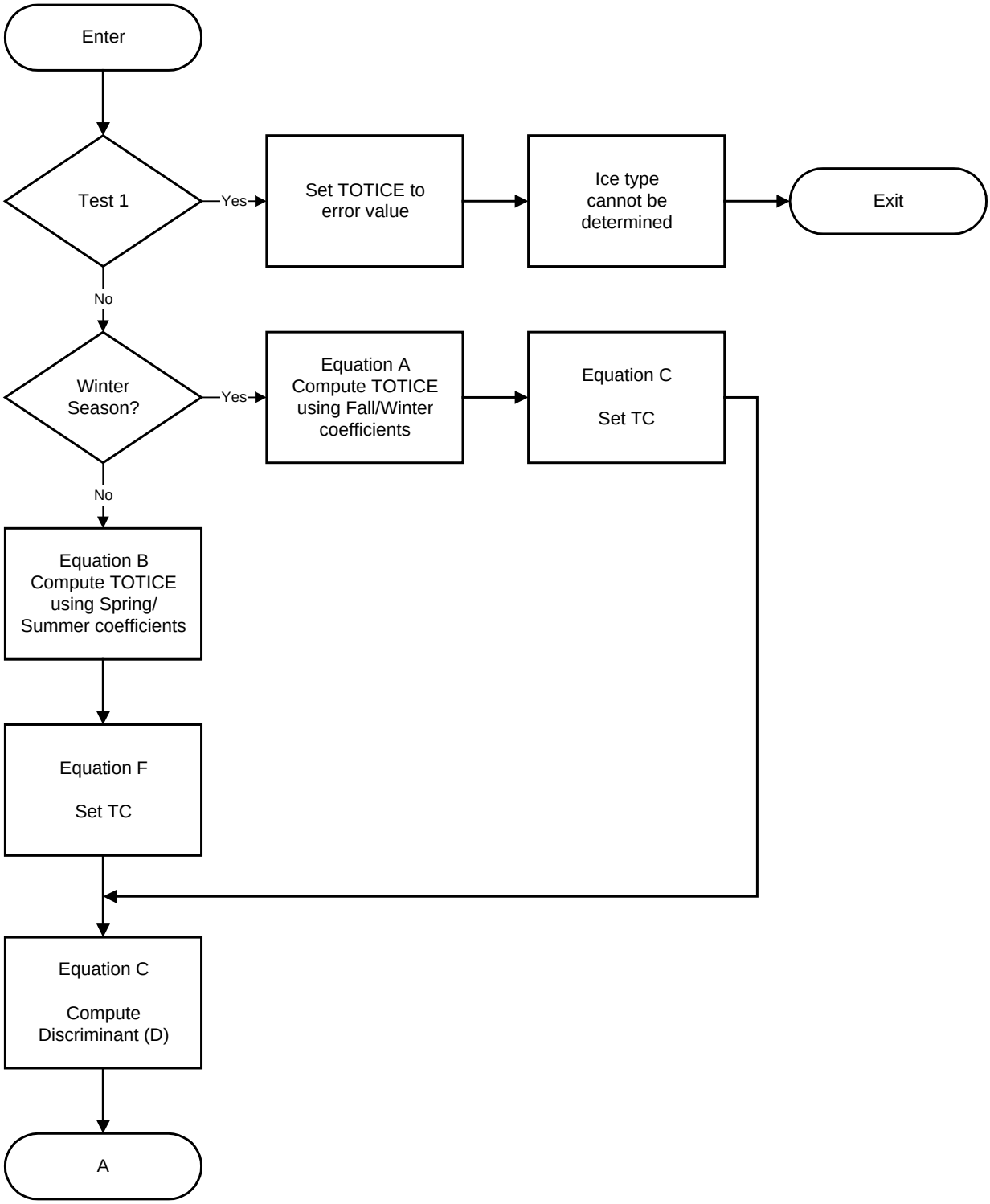

Figure 6.2-2. Sea Ice Parameter Logic Flow (Part 1)

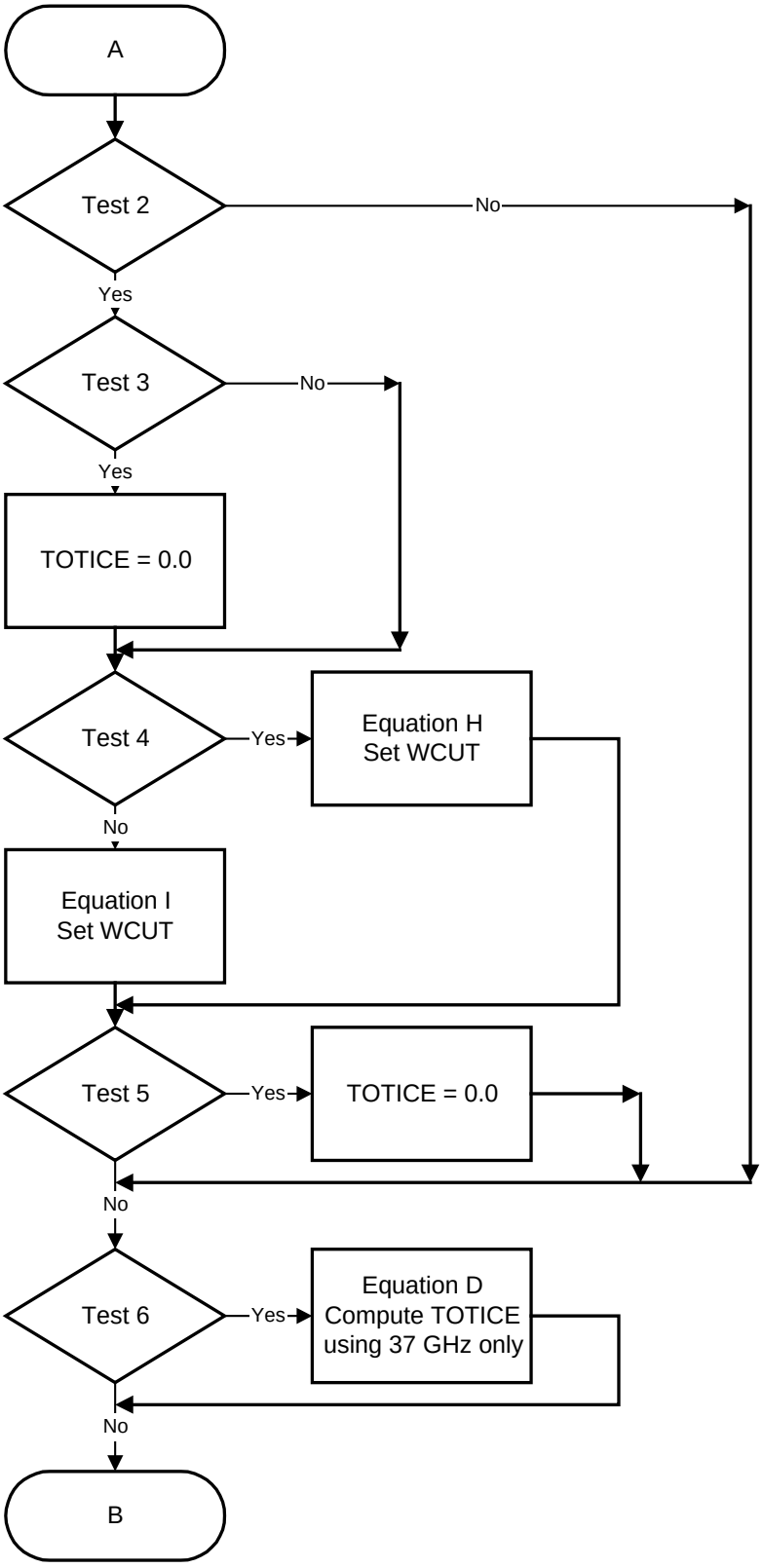

Figure 6.2-3. Sea Ice Parameter Logic Flow (Part 2)

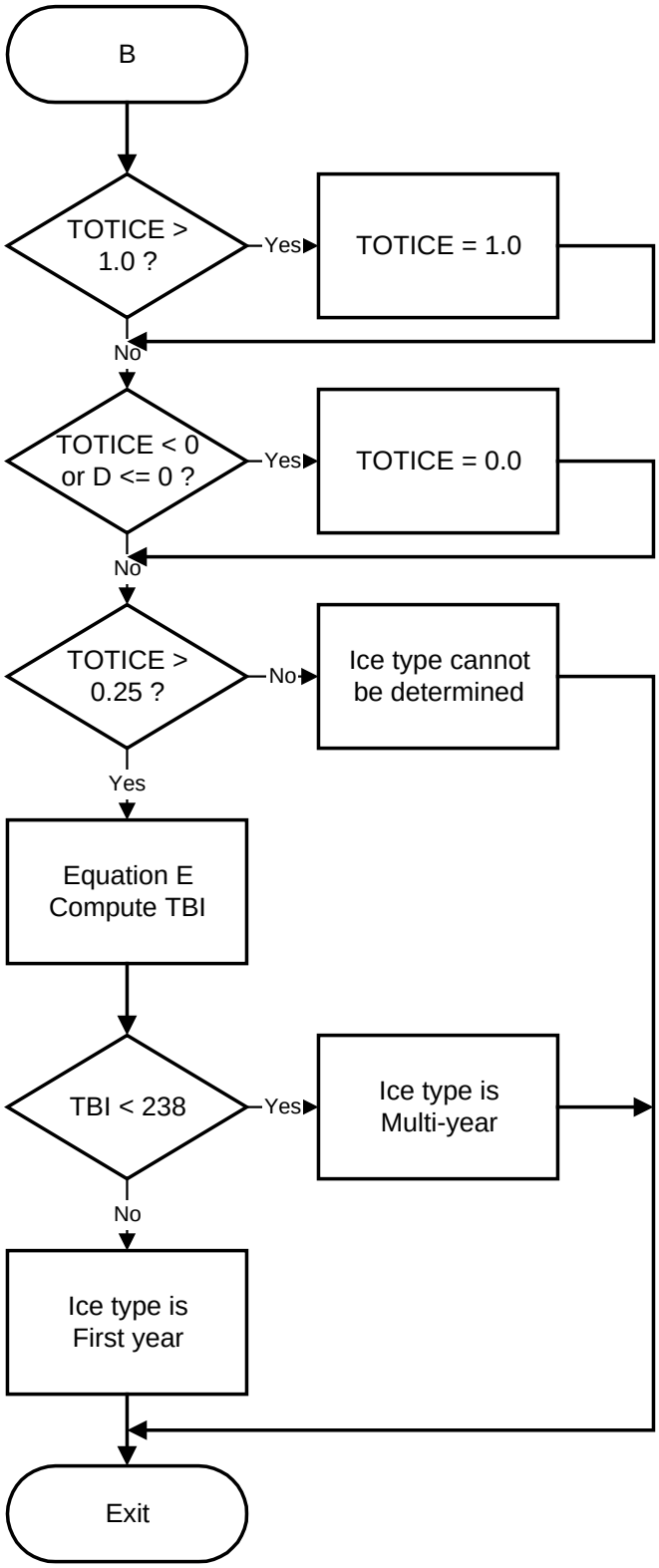

Figure 6.2-4. Sea Ice Parameter Logic Flow (Part 3)

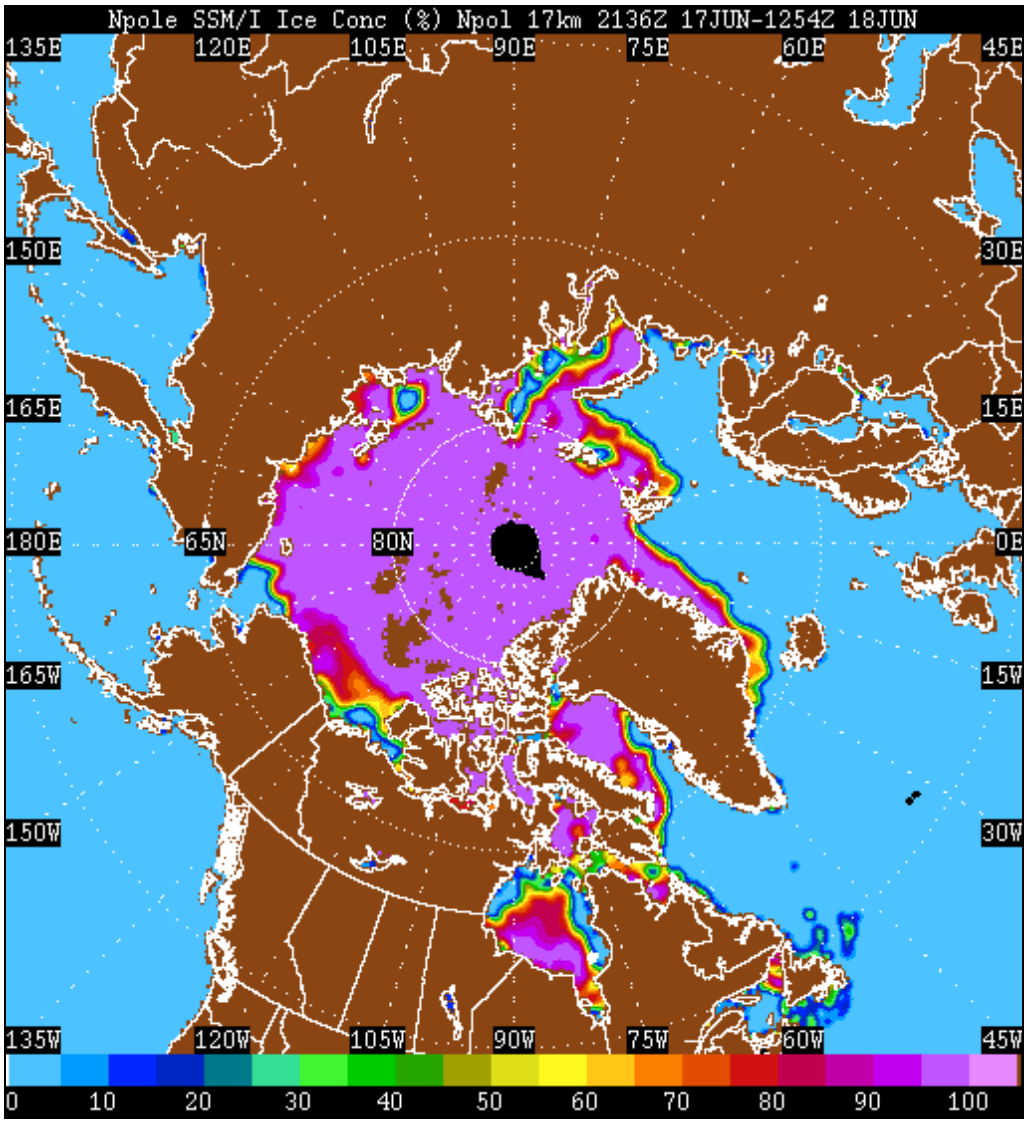

Figure 6.2-5. Composite image of Ice Concentration (IC) EDR values taken from several passes over the north polar region on 17-18 June 1997. At this time of the year, the ice cap is decreasing toward its minimum extent, which typically occurs in August.

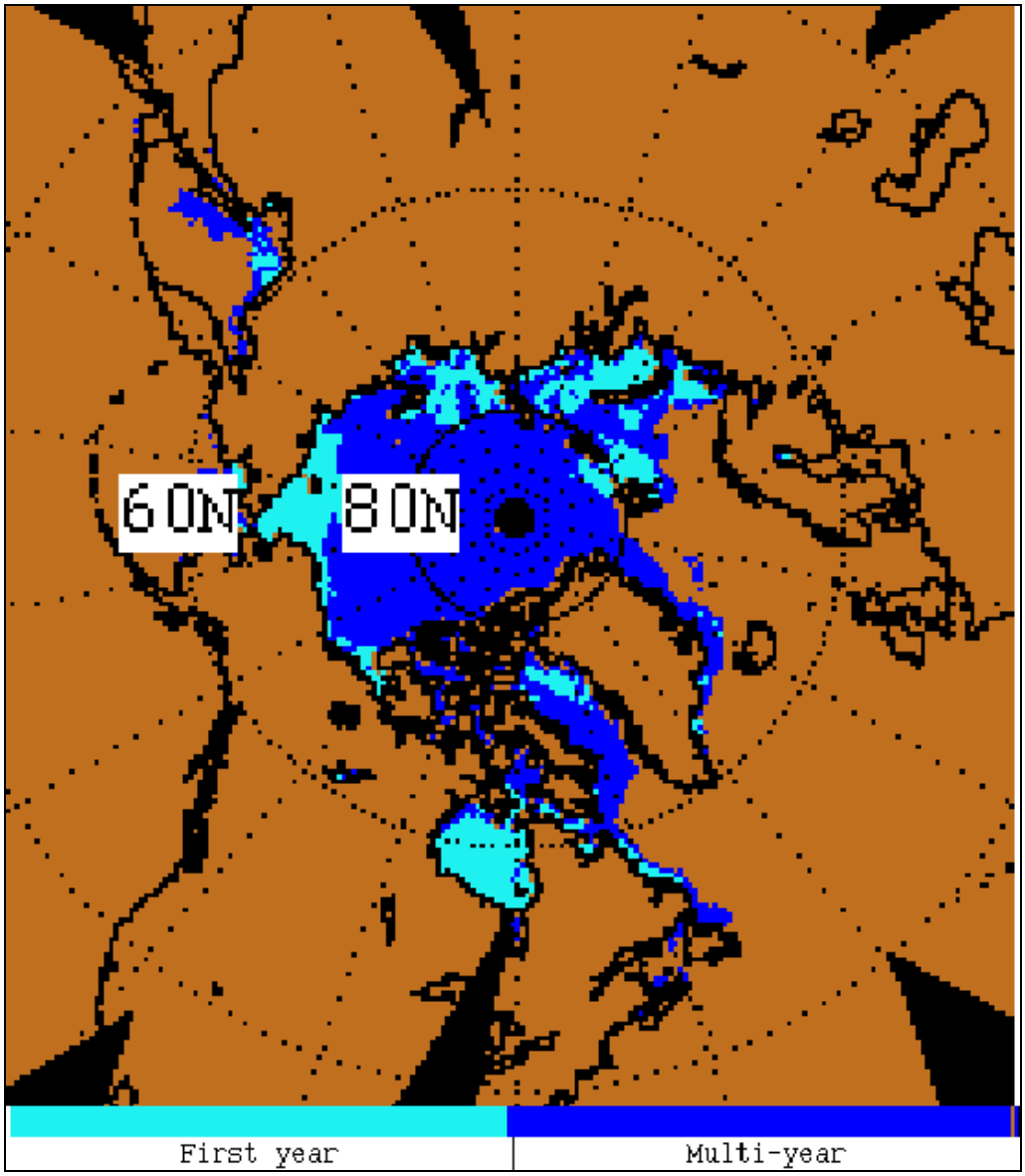

Figure 6.2-6. In this ice age (IA) EDR image, taken from a day's worth of orbits on 09-10 April 1998, first year ice appears in light blue. These areas correspond to locations that normally freeze over and melt annually (for example, Hudson Bay).

6.3 Surface Type (TYPE)

Most of the land EDRs require a determination of surface type to be made as a prerequisite for calculation of the parameter. In other cases (i.e. surface temperature), the choice of which estimation equation to use is made on the basis of the surface type.

The current algorithm for surface type, developed by Marshall J. MacFarland of Texas A&M and Christopher M. Neale of Utah State, recognizes fifteen distinct surface types. Grody and Basist (1996) developed an extension to subclassify snow *types*. The process of determining to which category a scene station belongs involves applying a series of tests, using combinations of brightness temperatures as discriminators. Table 6.3-1 lists the various surface types and the tests used to classify individual points. Alternate algorithms, for use only if the 85V channel or both 85 GHz channels are disabled, are also available, but not discussed here.

Operational experience with this classifier has been somewhat limited, but the following anomalies have been noted:

- Snow appearing over desert where no snow exists
- High terrain erroneously classified as wet soil
- High terrain erroneously classified as rain over vegetation
- Snow appearing where none exists over high plateaus
- Sea ice over inland seas (i.e. Caspian) is not detected

In general, the discrimination between ocean, land, and sea ice works well. Over land, identification of desert areas is reasonably accurate, while no results have yet been reported for vegetation.

To determine if the surface type is precipitation over soil, the rain rate over land algorithm is first used to determine that precipitation over land is detected. If precipitation is detected, then the algorithm used in Table 6.3-1 is used to determine if the surface type is precipitation over vegetation. If a scene station is classified as precipitation over land but it is NOT precipitation over vegetation, then the station is classified as precipitation over soil.

To determine if the surface type is glacial, dry snow, wet snow, or refrozen snow, the following algorithm is used:

```
SC37 = T(19V) - T(37V) - 3.0
SCAT = T(22V) - T(85V) - 3.0
SCX  = T(37V) - T(85V) -1.0
IF (SC37 > SCAT) THEN SCAT = SC37

IF(SCAT > 5.0) THEN

        SNOW IS TRUE
        TT = 169.0 + (0.5)*T(85V)
        PD19 = T(19V) - T(19H)
        SCX = T(37V) - T(85V)

        Remove rain
```

```
        IF  (   (T(22V) >= 261.0)  AND  (SCAT <= 6.0)   ) THEN
                SNOW IS FALSE
        ELSE    IF (   (T(22V) >= 265.0)  OR  (T(22V) >= TT)   ) THEN
                SNOW IS FALSE

        Remove cold desert

        IF (   (PD19 >= 18.0)   AND   (SC37 <= 14.0)   AND   (SCX <= 11.0)  ) THEN
                SNOW IS FALSE

        Remove frozen ground

        IF (   (SCAT <= 10.0)   AND   (PD19 >= 8.0)   ) THEN
                SNOW IS FALSE

        Check for snow over glacial ice

        IF (   (T(22V) < 216.0)   OR   ( T(22V) <= 235.0)    AND
                ((T(19V) - T(19H)) >= 23.0)  ) THEN
                SNOW IS TRUE
                TYPE IS GLACIAL

ELSE SNOW IS FALSE
```

If a scene station is classified as snow, but not glacial, then the algorithms in Table 6.3-1 are used to determine if the surface type is dry snow or wet snow. If a scene station is classified as snow, but not classified as glacial, dry snow, or wet snow, then it is classified as refrozen snow.

Actual values for the Surface Type EDR and their corresponding surface types are as follows:

EDR Value	**Surface Type**
0	Land
1	Unused
2	Near Coast
3	Ice
4	Possible Ice
5	Ocean
6	Coast
7	Flooded Soil
8	Dense vegetation
9	Range land
10	Dry arable soil
11	Moist soil
12	Semi-arid
13	Desert

EDR Value	Surface Type
14	Precipitation over vegetation
15	Precipitation over soil
16	Composite soil and water
17	Wet soil
18	Dry snow
19	Wet snow
20	Refrozen snow
21	Glacial

Table 6.3-1. Summary of surface type classification rules.

	Brightness Temperature Combination Threshold Values (K)							
LAND TYPE	[a]	[b]	[c]	[d]	[e]	[f]	[g]	[h]
Flooded	> 4							
Dense Vegetation	≤ 4	≤ 1.9		≥ –1	< 4.5	> 262		
Dense Agricultural/ Range Vegetation	≤ 4	≤ 4 > 1.9		≥ –1	< 4.5	> 262		
Dry arable	≤ 4	> 4 ≤ 9.8	≥ 6.5	< 0.5 ≥ –5	< 4.2			
Moist soil	≤ 4	> 4 < 19.7	≥ –6.5	≥ 0.5 < 4	< 4.2			
Semi-arid	≤ 4	> 9.8 < 19.7		< 0.5	< 6			< –1.8
Desert	≤ 2	≥ 19.7			> –1	> 268		
Precip over vegetation	≤ 4	≤ 4		< –1		> 268		
Precip over soil	≤ 4	> 4	< –3	< –5	< –4.1	> 268		
Vegetation and water	≤ 4	< 6.4		≥ –1	> 4.5		> 257	
Wet soil	≤ 4	≥ 6.4	≥ –6.5	≥ 0.5	> 4.2			
Dry snow*	≤ 4	> 4	< –6.5				> 225 ≤ 257	
Wet snow	≤ 4	> 9.8	≤ –0.8 ≥ –6.5	< 0.5			≤ 268 > 253	≥ –1.8 ≤ 6.5
Glacial	(IF (T(22V) < 216) OR ((T(22V) ≤ 235) AND (T(19V) - T(19H) ≥ 23))							
Refrozen snow	≤ 4	> 4	< –6.5	< 0	< 0		≤ 225	< 0

[a] T(22V) - T(19V)
[b] T(19V) + T(37V)/2 - (T(19H) + T(37H))/2
[c] T(37V) - T(19V)
[d] T(85V) - T(37V)
[e] T(85H) - T(37H)
[f] T(19V)
[g] T(37V)
[h] T(37H) - T(19H)

*Additional conditions: T(19V) - T(19H) ≥ 5

Surface Type Example

Figure 6.3-1 shows the results of the surface characteristic algorithm as applied to land points in the Quebec and Ontario Provinces. The bright red to dark red pixels represent points identified as various states of snow (dry snow, wet snow, refrozen snow, and glacial) and they compare well with average permafrost and snowfall data for the region. The bright red pixels that represent points identified as dry snow compare well with the snow depth data (refer to Figure 6.9-1). The dark brownish red pixels represent points identified as wet ground and the brownish red pixels represent points identified as mixture of soil and water. These compare well with elevated soil moisture counts (Figure 6.4-1). The dark green and green pixels represent points identified as dry arable land and moist arable land respectively and they compare well with average vegetation data for the region. Finally, the blue pixels represent points identified as coastal, which can be easily verified from the image (see along Hudson Bay and Atlantic coast).

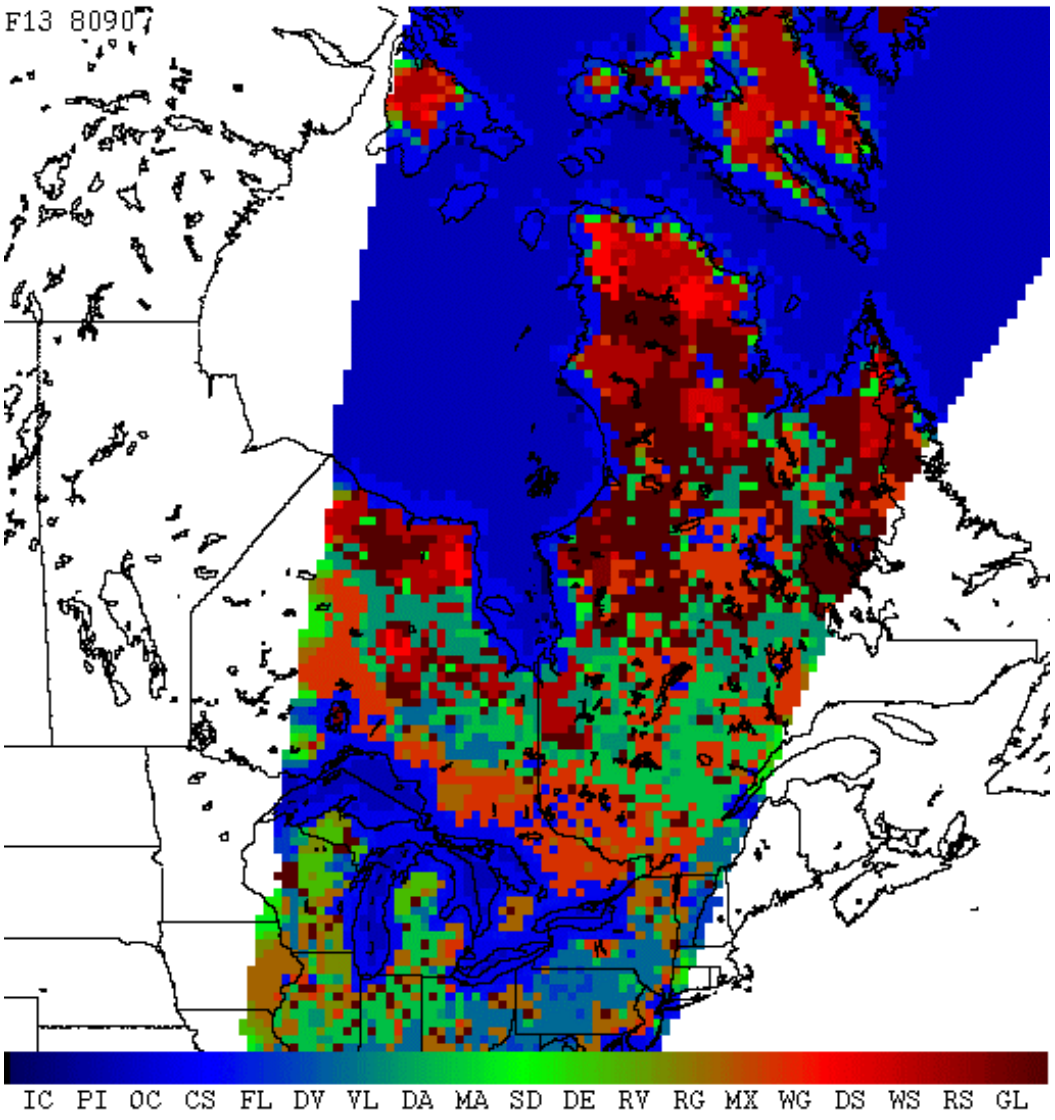

IC	Ice	DE	Desert
PI	Possible Ice	RV	Rain over Vegetation
OC	Ocean	RG	Rain over Ground
CS	Coast	MX	Mixture (composite) of Soil and Water
FL	Flooded Land (Flooded Soil)	WG	Wet Ground (Wet Soil)
DV	Dense Vegetation	DS	Dry Snow
VL	Vegetative Land (Range Land)	WS	Wet Snow
DA	Dry Arable Soil	RS	Refrozen Snow
MA	Moist Arable Soil (Moist Soil)	GL	Glacial
SD	Semi-Desert (Semi-Arid)		

Figure 6.3-1. Surface classification (land type) EDR for the Quebec and Ontario Provinces, 17 October 1996, F13.

6.4 Soil Moisture (SM)

The soil moisture EDR is more accurately an Antecedent Precipitation Index (API), and measures the approximate amount of recently deposited precipitation in the soil. The SM EDR has units of mm, ranges from 0 to 70 mm, and is quantized in increments of 1.0 mm.

Estimation of soil moisture is subject to a number of difficulties. The presence of vegetation or the roughness of the soil can easily confuse the signal, as can clouds with high liquid water content. Furthermore, the penetration depth of even the lowest SSM/I frequency (19 GHz) is only a few millimeters. Depending on the soil type, the amount of moisture in this thin layer may have little correlation with that in the soil beneath.

The current SM algorithm was developed by Marshall J. MacFarland of Texas A&M and Christopher M. Neale of Utah State, and utilizes a normalized brightness temperature ratio (T_{19H}/T_{37V}) and a series of tests to determine vegetation density class. The normalized temperature ratio will increase slowly over a particular area in phase with the increase in plant growth over a growing season. If the vegetation is not so dense as to significantly degrade the signal, a precipitation event will cause the normalized temperature ratio to drop rapidly. Eventually, as the soil dries out, the ratio will return to its original value, assuming the additional moisture did not result in a greater vegetation density than before the event. This points up the need for careful interpretation of the values generated by this algorithm. It should work best in sparsely vegetated regions (desert, semi-desert, or open areas not in the growing season), and is subject to slow variations over the course of a season. At this time, no definitive results of the algorithm are available for review.

The algorithm is

$$SM = A1 + [\, B1 * T(19H)/T(37V) \,]$$

where A1 and B1 are determined by a test of vegetation density as follows:

$$\text{Test value (TV)} = (T(19V) + T(37V)) / 2 - (T(19H) + T(37H)) / 2$$

TEST	Vegetation Density Class	A1	B1
TV > 8 K	Low Density Vegetation	659.35	- 675.22
6 < TV ≤ 8 K	Medium Density Vegetation	1126.58	-1145.48
4 < TV ≤ 6 K	High Density vegetation	1707.24	-1724.14

Soil Moisture Example

Figure 6.4-1 shows the soil moisture as determined for scene stations in the Quebec and Ontario Provinces region. The data shows soil moistures ranging from 4 to 67 mm. As always, it is difficult to assess the accuracy of these calculations without ground truth.

The values do seem to match well with anecdotal evidence, however. On the day of the pass, rain did fall in the area to account for the blue and green pixels.

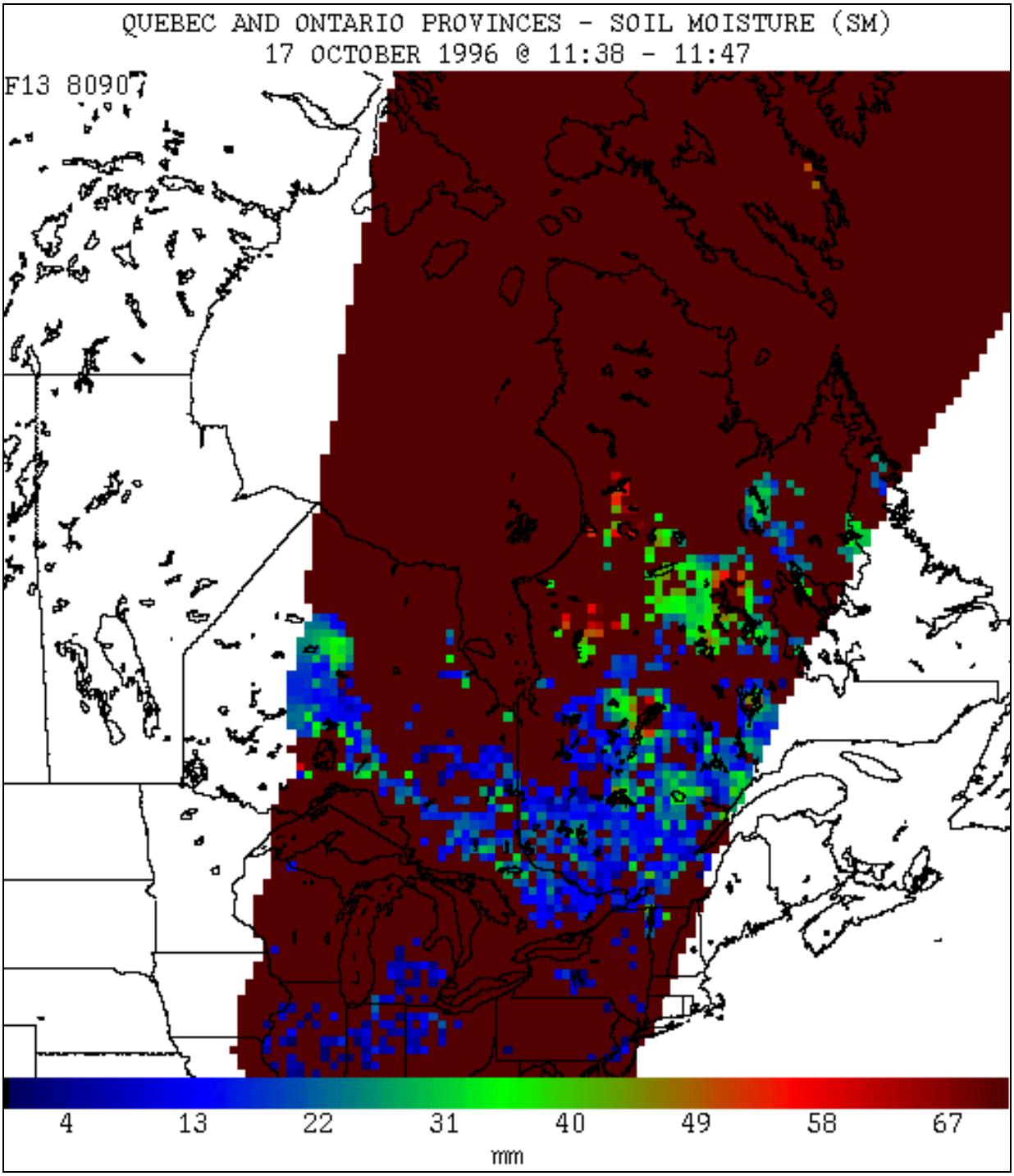

Figure 6.4-1. Soil moisture (SM) EDR for the Quebec and Ontario Provinces, 17 October 1996, F13.

6.5 Rain Rate[4]

The current rain rate algorithms were developed by Ralph Ferraro and Norm Grody of NOAA/NESDIS (Ferraro, 1997).

6.5.1 Rain Rate over Land (RL)

```
IF (100 <= T(19V) <= 300)  AND  (80 <= T(85V) <= 300) THEN

        SI85  =     451.9  -  (0.44) *T(19V) -  (1.775)* T(22V)
                          + (0.00574) *T(22V)**2 - T(85V)

        IF  (SI85 >= 10.0) THEN

                RL = (0.00513)* (SI85)**1.9468

                TT = 175.0 + (0.49)* T(85V)

                PD19 = T(19V) - T(19H)

                Check for snow cover:

                IF ((T(22V) < 264.0) AND (T(22V) < TT) ) THEN RL = 0

                Check for desert:

                ELSE IF (PD19 > 20.0) THEN RL = 0

                Check for semi-desert:

                ELSE IF ( (T(85V) > 253.0) AND (PD19 > 7.0)  ) THEN RL = 0

        ELSE RR  =  0

        IF (RL > 35.0) RL = 35.0
ELSE
        RL cannot be determined
END IF
```

[4] Previously, alternate algorithms were used for rain rate in the absence of the 85 GHz channels. They were developed by William Olsen of the University of Wisconsin. While, no longer deemed operational, they are included here for reference and historical purposes.

```
RL =  exp(-17.76849 - (0.09612)* T(37V) + (0.15678)* T(19V)) - 1.0

RO = exp(5.10196 - (0.05378)* T(37V) + (0.02766)* T(37H) + (0.01373)*T(19V)) -  2.0
```

These alternative algorithms do not perform well over land. Some spot checks have revealed rain rates being calculated in cloud-free areas. In addition, rain rates in tropical storms of only 5 mm/hr have been observed. This is due to the large size of SSM/I footprints relative to the rain cell.

6.5.2 Rain Rate over Ocean (RO)

```
IF (100 <= T(19V) <= 300)  AND  (80 <= T(85V) <= 300) THEN
        SI85    = -174.4 + (0.715)*T(19V) + (2.439) *T(22V)
                          - (0.00504)*T(22V)**2 - T(85V)
        IF (SI85 > 10.0) THEN
                RO = (0.00188) (SI85)**2.034
                TT = 44.0 + (0.85)*T(19V)

                Check for sea ice

                IF (POSSIBLE ICE) THEN
                        IF  (T(22V) <= TT) THEN RR = 0.0
                        IF  ( (T(22V) > 264.0) AND ((T(22V) - T(19V)) < 2.0) )RO = 0.0
                END IF

        ELSE

                Q19 = 0.0
                Q37 = 0.0

                IF ( (T(19V) < 285) AND (T(22V) < 285) ) THEN
                        Q19 = (-2.70)*(ALOG(290 - T(19V)) + (-2.84)
                                + (-0.40)*ALOG(290 - T(22V)))
                END IF

                IF (Q19 >= 0.60) THEN
                        RO = (0.001707)*(Q19 * 100)**(1.7359)
                ELSE

                        IF ((T(37V) < 285) AND (T(22V) < 285)) THEN
                        Q37 = (-1.15)*(ALOG(290 - T(37V)) + (-2.99)
                                        +(-0.32)*ALOG(290 - T(22V)))
                        END IF

                        IF (Q37 >= 0.20) THEN
                                RO = (0.001707)*(Q37*100)**(1.7359)
                        END IF

                END IF
        END IF

        IF (RO > 35.0) RO = 35.0
ELSE
        RO cannot be determined
END IF
```

Incorrectly located data may give false rain rates near coastlines. If the algorithm believes a pixel is a land pixel and the data was actually gathered over ocean, a false rain rate will be seen. A similar situation may arise if ice is falsely typed as open ocean.

Rain Rate Example

Figure 6.5-1 shows the rain rate EDR from a Pacific cyclone. Values range from 3 to 55 mm/hr. The general shape of the rain area corresponds to the shape of the other EDRs shown from this pass: Water Vapor Content (Figure 6.1-1), Surface Wind Speed (Figure 6.6-1), D37 (Figure 6.6-2), and Rain Flag (Figure 6.6-3).

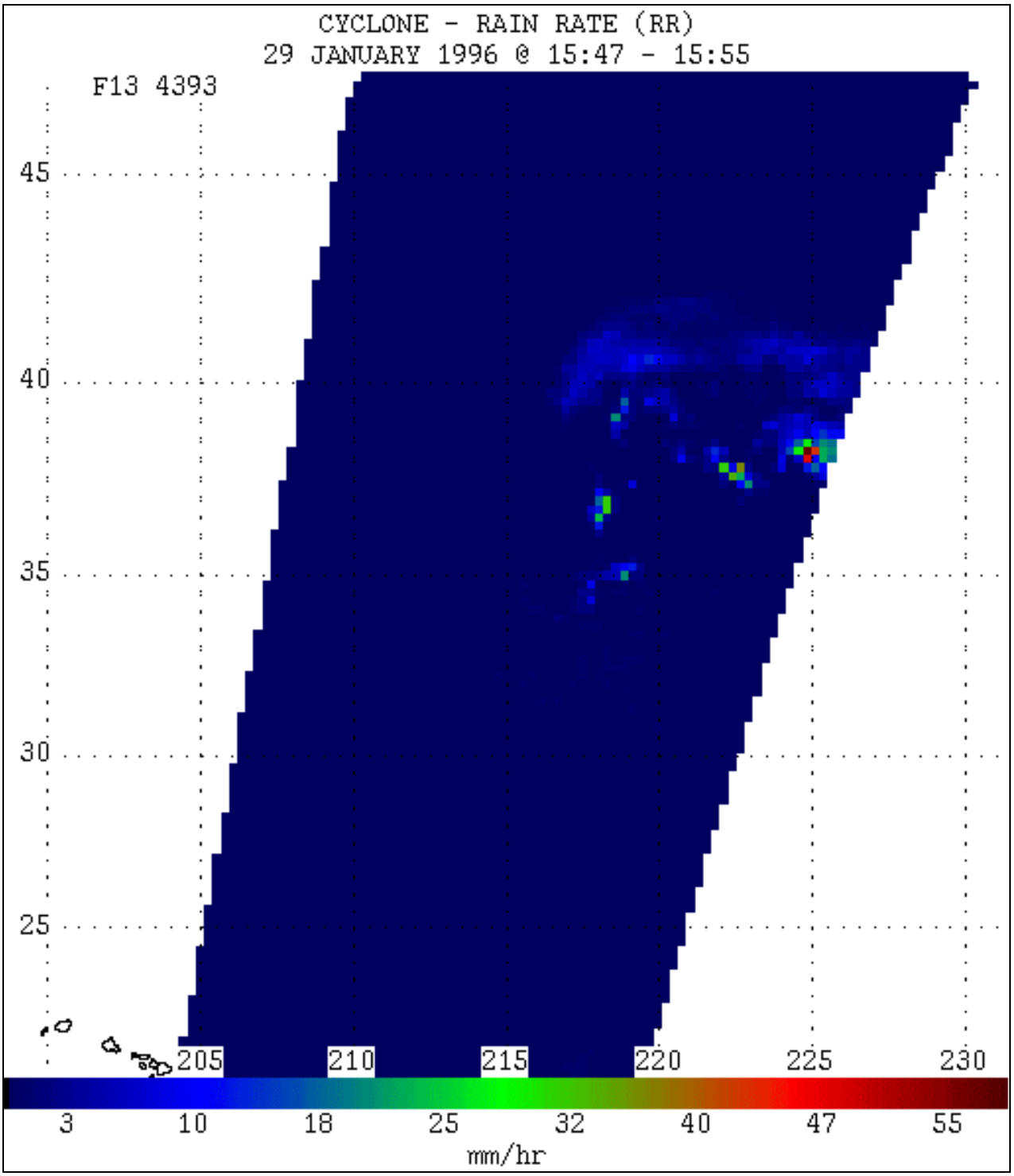

Figure 6.5-1. Rain rate over eastern Pacific Ocean from F13 on 29 Jan 1996.

6.6 Ocean Surface Wind Speed (SW) and Rain Flag (RF)

Wind speed is calculated only over the ocean and is measured in units of meters/second. Values range from 0 to 25.3 m/s, quantized in levels of 0.1 m/s. The rain flag is dimensionless and varies from 0 to 3. The rain flag denotes the accuracy of the wind speed measurement as follows:

Rain Flag	Wind Speed Accuracy
0	< 2 m/s
1	2 - 5 m/s
2	5 - 10 m/s
3	> 10 m/s

The current wind speed algorithm was developed Mark Goodberlet of the University of Massachusetts, and subsequently corrected by Grant Petty of Purdue (Petty, 1993). Wind speed (SW) is calculated as a linear combination of SSM/I channels; the current wind speed algorithm is as follows:

```
IF (Rain Present) THEN RF cannot be determined

/* Standard Goodberlet Wind Speed Algorithm */
U = (147.90) + (1.0969)*T(19V) + (-0.4555)*T(22V) + (-1.76)*T(37V) + (0.7860)*T(37H)

/* Correction Based on Amount of Precipitable Water Present */
WV = (0.1741E+3) + (0.4638E+1)*ALOG(300.0 - T(19V)) +
       (-0.6176E+2)*ALOG(300.0 - T(22V)) + (0.1958E+2)*ALOG(300.0 - T(37H))

UCOR = (-2.130) + (0.2198)*WV + (-0.4008E-2)*WV*WV

SW = U + UCOR
```

The rain flag is calculated as follows:

```
IF (      (T(37V) - T(37H)) > 50.0 AND (T(19H) < 165.0) ) THEN RF = 0
          ( < 2 m/s accuracy)
ELSE   IF ((T(37V) - T(37H)) <37.0) THEN RF= 2
          (5 to 10 m/s accuracy)
ELSE   IF ((T(37V) - T(37H)) < 30.0) THEN RF = 3
          (> 10 m/s accuracy)
ELSE RF = 1
          (2 to 5 m/s accuracy)
```

As related earlier, the wind speed calculation can be degraded by other environmental phenomena. Raindrop impact on the sea surface roughens the surface and causes higher brightness temperatures, which results in the calculation of erroneous wind speeds. Large amounts of cloud water can alter the wind signal. The presence of rain or cloud water results in wind speed values higher than the actual value. When using the wind speed EDR, one should be aware that the accuracy of individual measurements changes because of local weather effects. For example, a wind speed reading of 5 m/s sampled in a dry

atmosphere is much more reliable than a wind speed reading of 5 m/s sampled in the middle of a rain storm. It is the analyst's job to ascertain the reliability of the wind speed reading and to factor this into any forecast. The rain flag value translates directly into a wind speed accuracy; it does not, however, take into account excess cloud water. The 37 GHz differential (D37) is affected by both rain and cloud water, so it is especially useful for determining the reliability of the wind speed calculation. The 37 GHz differential is a measure of the polarization of the 37 GHz signal (D37 = 37V - 37H). Since emission from the atmosphere is unpolarized and emission from the sea surface is highly polarized, a measure of the polarization of the 37 GHz channel at the sensor will indicate how much of the signal is due to atmospheric effects (bad for wind speed calculations) and how much is due to surface effects (good for wind speed calculations)

Surface Wind Speed Example

Figure 6.6-1 is a surface wind speed image of a fledgling cyclone in the Pacific Ocean. Surface wind speeds range from 4.6 to 24.1 m/s. One could cross check this EDR with the D37 (Figure 6.6-2), Rain Rate (Figure 6.5-1), Rain Flag (6.6-3), and Water Vapor Content (Figure 6.1-1) EDRs.

Figure 6.6-2 is the D37 image of the cyclone; i.e. the difference between the vertical and horizontal polarization at 37 GHz. The surface wind speed calculation should be very accurate in the red regions (50 K to 66 K). The analyst should be cautious of the surface wind speed values in the green areas (34 K to 42 K). Finally, the blue areas (9 to 26) are areas where wind speeds should NOT be used. Compare these areas with Figure 6.6-3, the Rain Flag EDR. The red areas indicate the surface wind speeds are no more accurate than 10 m/s. The green areas indicate the surface wind speeds are no more accurate than 2-10 m/s. The blue areas indicate the surface wind speeds are accurate to less than 2 m/s.

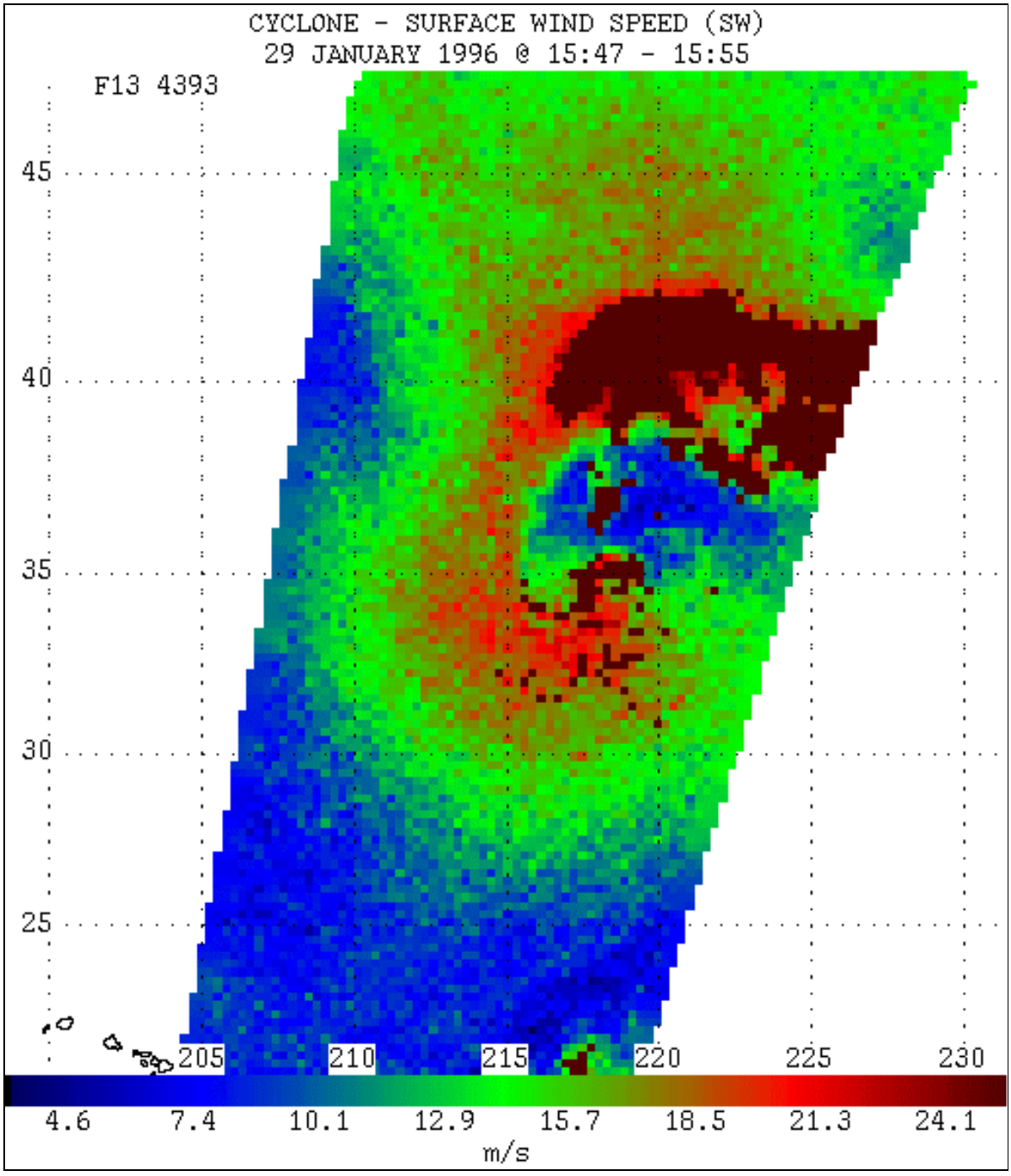

Figure 6.6-1. Surface wind speed EDR output for a cyclone over the eastern Pacific on 29 January 1996 (F13).

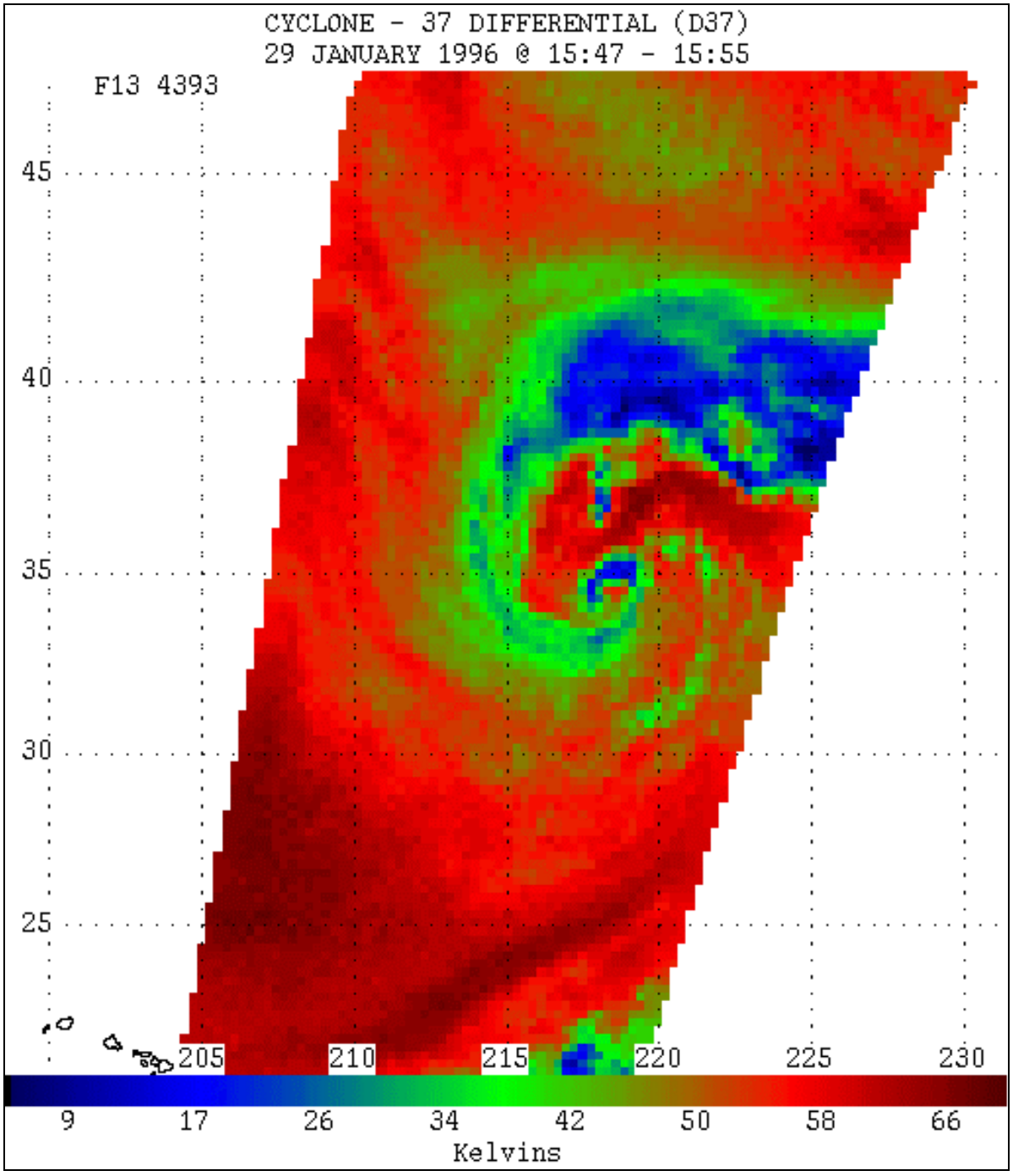

Figure 6.6-2. 37 GHz differential (D37) for the same data as in Figure 6.6-1.

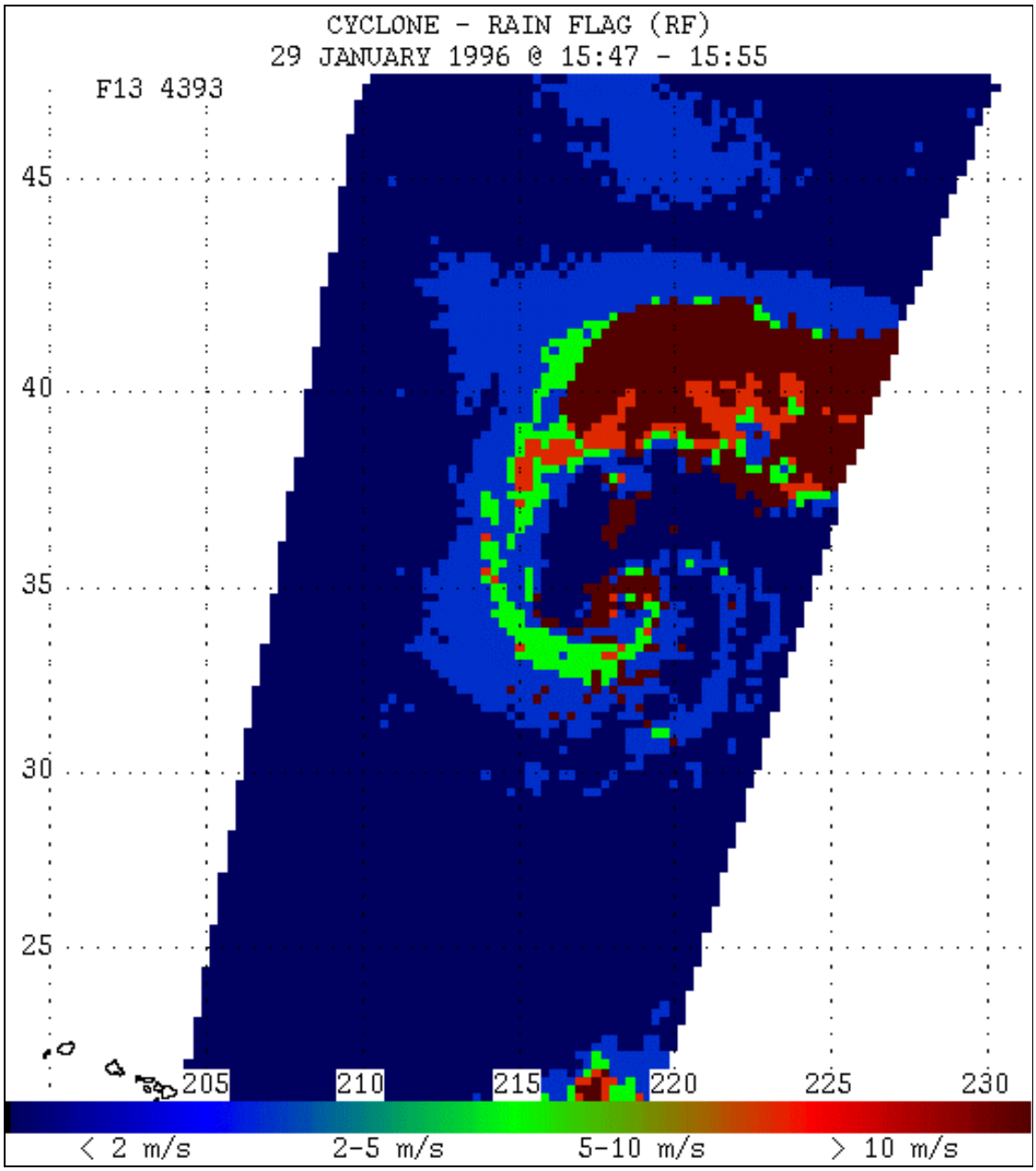

Figure 6.6-3. Rain Flag EDR display for the same data as in the previous two figures. Colors relate to accuracy wind speeds yielded by the surface wind EDR.

6.7 Cloud Water Content (CWO)

The cloud water content EDR (Weng, *et al.*, 1997) measures the integrated total cloud water in a footprint in units of kg/m^2. It is a linear combination of SSM/I channels as follows:

$$CWO = -3.14559 + (0.0060257)*T(19H) - (0.0048803)*T(22V) + (0.019595)*T(37V) - (0.0030107)*T(85H)$$

An alternative algorithm may be used in the absence of the 85H channel:

$$CWO = -2.838179 + (0.0084333)*T(19H) - (0.0075959)*T(22V) + (0.0201310)*T(37V) - (0.0053066)*T(37H)$$

Values range from 0 to 12.6 kg/m^2 and are quantized in levels of 0.05 kg/m^2

Cloud Water Content Example

Figure 6.7-1 is a cloud water content image of the Pacific Ocean, centered at 10 degrees north latitude and 225 degrees east longitude. The cloud water content ranges from 0.1 to 0.95 kg/m^2. The blue areas indicate a relatively small amount of cloud water content; whereas the red areas indicate a relatively large amount of cloud water content, with the green areas indicating a medium amount.

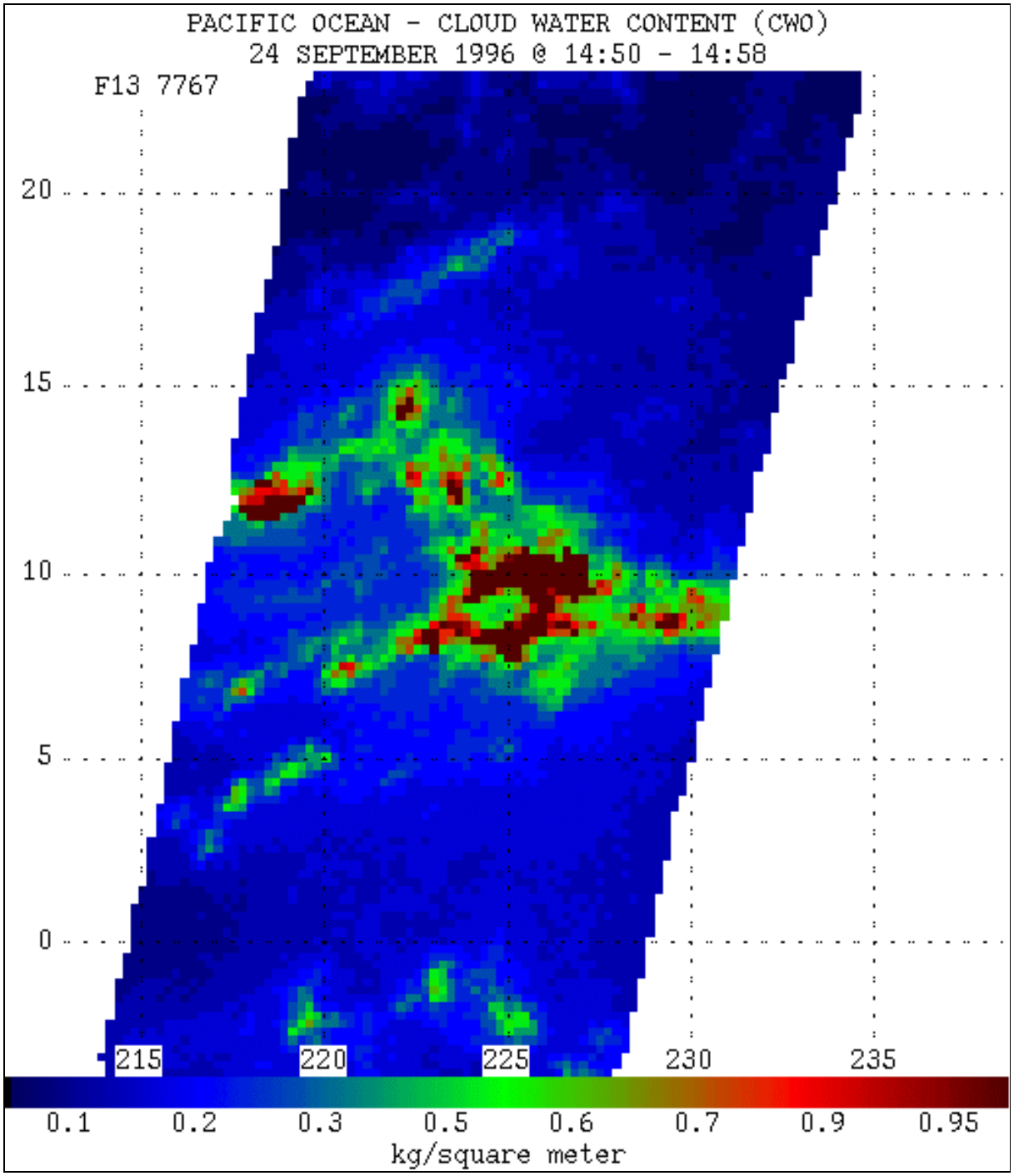

Figure 6.7-1. Output of the cloud water over ocean (CWO) EDR for 24 September 1996, F13.

6.8 Land Surface Temperature (ST)

The land surface temperature EDR is an estimate of the actual ground temperature, and is provided in Kelvins, with a range of 240 K to 340 K and quantization levels of 1 K.

The current method for determining ST was developed by Marshall J. MacFarland of Texas A&M and Christopher H. Neale of Utah State. Four different algorithms are used, depending on the determined surface characteristic:

VEGETATION: ST = 24.94 - (1.2784)*T(19H) + (0.8800)*T(22V) +(0.5933)*T(37V) + (0.7299)*T(85V)

MOIST SOILS: ST = 23.16 - (0.1873)*T(19H) + (0.5221)*T(22V) - (0.6271)*T(37V) + (1.232)*T(85V)

AG AND RANGE: ST = 6.97 - (0.6266)*T(19H) + (0.2716)*T(22V) - (0.1297)*T(37V) + (1.482)*T(85V)

DRY SOILS: ST = 72.68 - (0.4598)*T(19H) + (0.5984)*T(22V) + (0.8828)*T(37V) - (0.2623)*T(85V)

Insufficient experience has been gained operationally with this algorithm to evaluate its performance, although preliminary indications are that temperatures over desert areas are biased high (by as much as 12 K over the Saudi Arabian desert).

An alternative set of equations was developed to compensate for the failure of the 85 GHz channels on F8:

ALL: ST = 83.7 - (0.49)*T(19V) - (0.02)*T(19V) + (1.58)*T(22V) - (0.34)*T(37H)

MOIST SOIL: ST = 89.6 - (0.47)*T(19V) + (0.01)*T(19H) + (1.49)*T(22V) - (0.32)*T(37H)

CROPS/RANGE: ST = 32.4 + (0.31)*T(19V) - (0.26)*T(19H) + (0.82)*T(22V) + (0.04)*T(37H)

DRY SOIL: ST = 76.7 - (0.39)*T(19V) + (0.31)*T(19H) + (1.24)*T(22V) - (0.42)*(T37H)

Example of the Land Surface Temperature EDR

Figure 6.8-1 is calculated from the same pass as the Soil Moisture, Surface Type, and Snow Depth EDRs, and compares well with those images. The dark brownish red areas are snow/water covered, and surface temperature is not calculated there. The lowest temperatures (blue areas), corresponding to 253 K to 263 K are in the snow regions and higher elevations. The middle temperatures (green areas), corresponding to 263 K to 279 K are in the arable regions and lower elevations. The highest temperatures (red areas), corresponding to 279 K to 289 K are in the foothills separating Canada with the United

States and also the United States. In addition, this image corresponds well with the actual temperatures for that day.

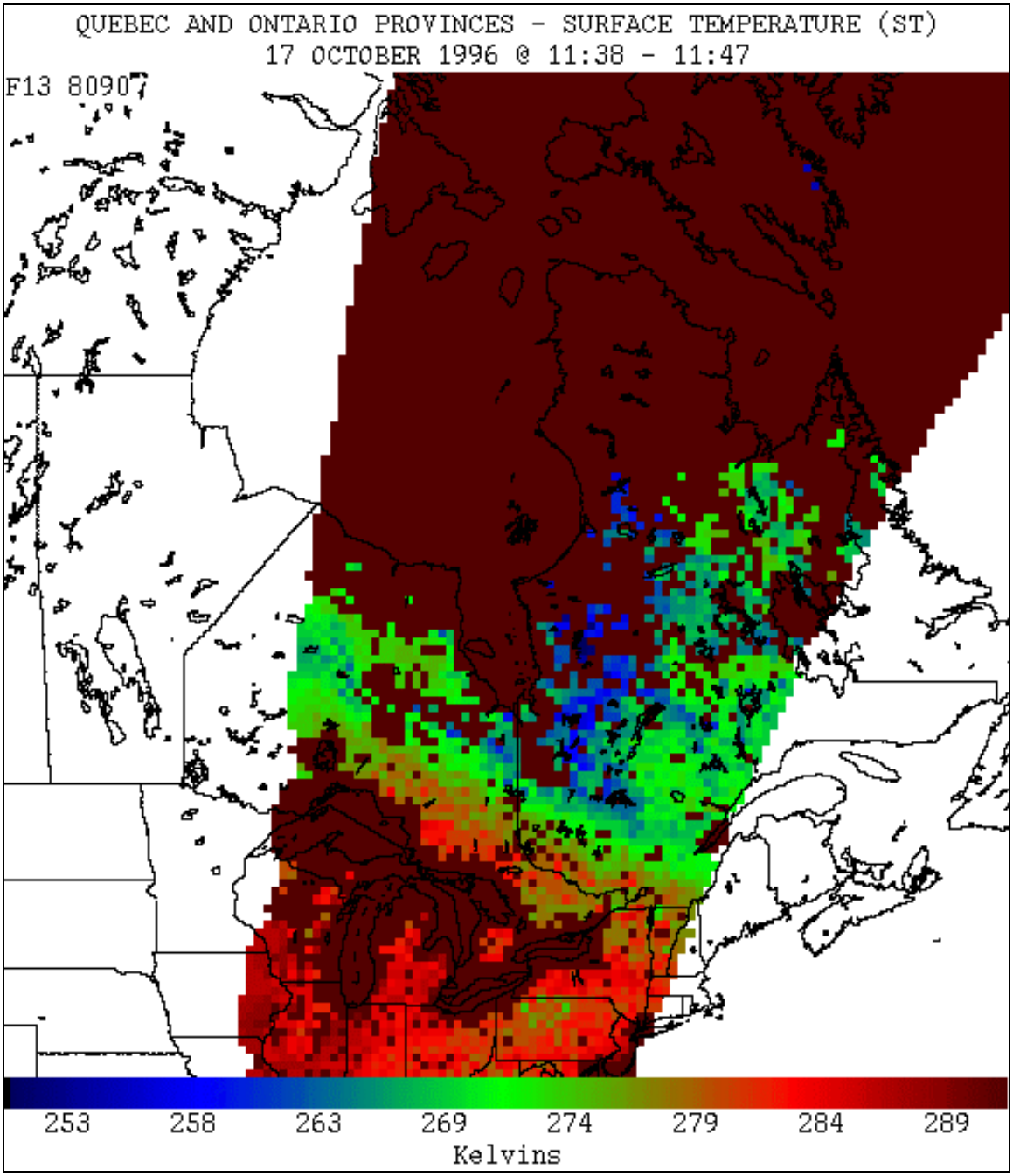

Figure 6.8-1. Surface Temperature (ST) EDR over the Quebec and Ontario provinces, 17 October 1996.

6.9 Snow Depth (SD)

The snow depth EDR gives the depth of snow in millimeters from 0 to 400 mm, quantized in 5 mm increments. While the algorithm gives very good results in conditions of dry snow pack, it is unable to give accurate results under all snow conditions. Knowledge of the area of interest, as well as use of ancillary data, will help the analyst interpret this EDR. The algorithm is based on a single channel: 37 V.

$$SD = 4445 - 17.95 * T(37V)$$

Example of the Snow Depth EDR

Figure 6.9-1 is a snow depth image of the Quebec and Ontario Provinces region. The data shows snow depths ranging from 15 to 290 mm, with the heaviest accumulations near the mouth of the Hudson Bay. This area is known for its snow accumulation and the image corresponds well with the other EDRs shown from this pass: Surface Type (6.3-1), Soil Moisture (Figure 6.4-1), and Surface Temperature (Figure 6.8-1).

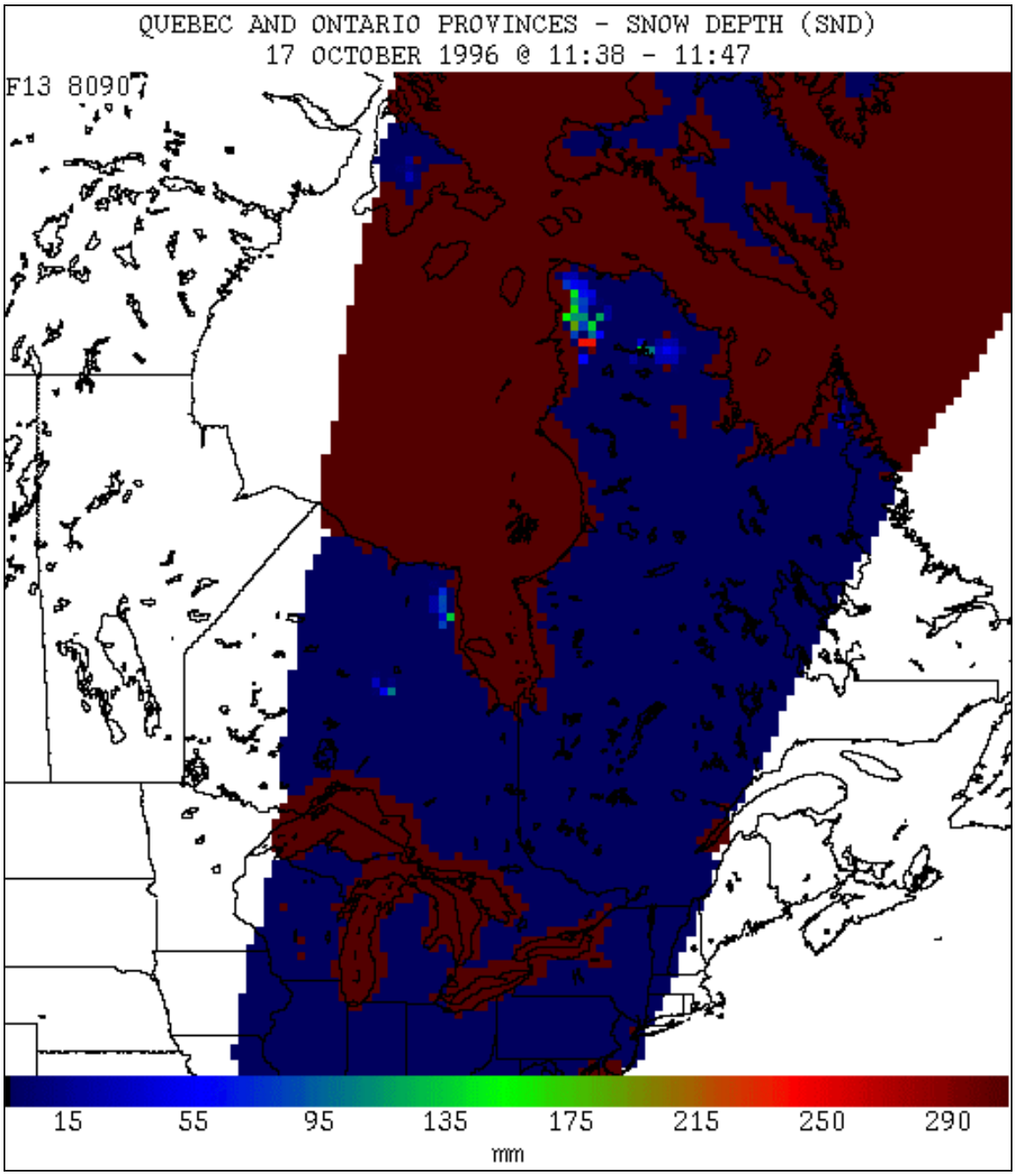

Figure 6.9-1. Snow Depth EDR output for Quebec and Ontario on 17 October 1996.

7. ANALYSIS AND FORECASTING – A CASE STUDY

This case study shows how SSM/I data was used to forecast winds in association with a frontal passage on 25-27 September 1990 at Lajes Field, Azores. Previously, forecasters used surface observations from nearby islands and ships for wind information. The SSM/I provides broad views of wind speeds, enabling forecasters to more accurately predict trends. The data matched well with surface observations from Horta, Flores, and various ship reports. This gave the forecasters confidence in the accuracy of the SSM/I. This confidence, coupled with the wide area view provided by the sensor, enabled the analysts to predict the onset of strong winds on September 25, and to cancel a wind advisory early as the storm moved out on September 27.

The following images show wind speed, the 37 GHz differential, rain rate, and rain flag for passes on September 25, 26, and 27. Wind speeds are in meters/second in the images. In the accompanying text, both knots and m/sec will be provided for wind speeds. Within a reasonable approximation, 1 m/s ≈ 2 knots. When using the wind speed EDR, it is important to cross check the D37, RR, and RF EDRs. These EDRs serve as quality controls on the accuracy of the WS values. See Section 6.6 for additional details on the wind speed EDR.

7.1 Day 1: 25 Sep 1990

SYNOPTIC SITUATION

The weather was dominated by high pressure to the west of Lajes Field (Latitude 38.45 North, Longitude 27.05 West), with a low pressure center at 48N, 18W and a front extending NW of Lajes. Aircraft reports indicated a strong jet over Lajes. The forecast supported frontal passage between 0600Z and 1200Z. Vorticity analysis indicated positive vorticity advection through 36 hours with the vorticity center and low remaining just to the east. Satellite imagery (visible and IR) showed deep convection to the north and evidence of a strong cold air push in a large field of open and closed cell stratocumulus behind the front. The pressure gradient between Lajes and Flores was 2.4 mb at 0600Z and continued to increase to a maximum of 10 mb at 0000Z.

SSM/I IMAGERY (Figure 7.1-1)

The winds in the vicinity of Lajes ranged from 25 to 27 knots (13-14 m/s, bright green) with a broad area of 17 to 23 knot (9-12 m/s, dark blue to bluish-green) winds to the west. Winds to the north were in the 29 to 35 knot (15-18 m/s, bright green to reddish-green) range. The 37 GHz differential values ranged from 38 to 47 in the immediate vicinity of the field, and from 50 to 54 to the north. These values indicate the wind speed is accurate to within 4 knots (~2 m/s).

Two ship reports obtained near the time of the pass verified well with the SSM/I data. A ship at 44N, 27W reported winds of 40 knots (21 m/s). The SSM/I pixel at 43.83 N, 26.98 W reads 40 knots (21 m/s). Area statistics show a mean of 36 knots (19 m/s), maximum of 42 knots (22 m/s), and minimum of 32 knots (16 m/s) in the region immediately surrounding the ship's location. The second ship was located at 38 N, 32 W and reported 15 knots (8 m/s). The SSM/I indicated 14 knots (7 m/s).

The SSM/I readings helped the forecasters predict the onset of strong winds. All weather advisories were issued with the desired lead-time and all were verified.

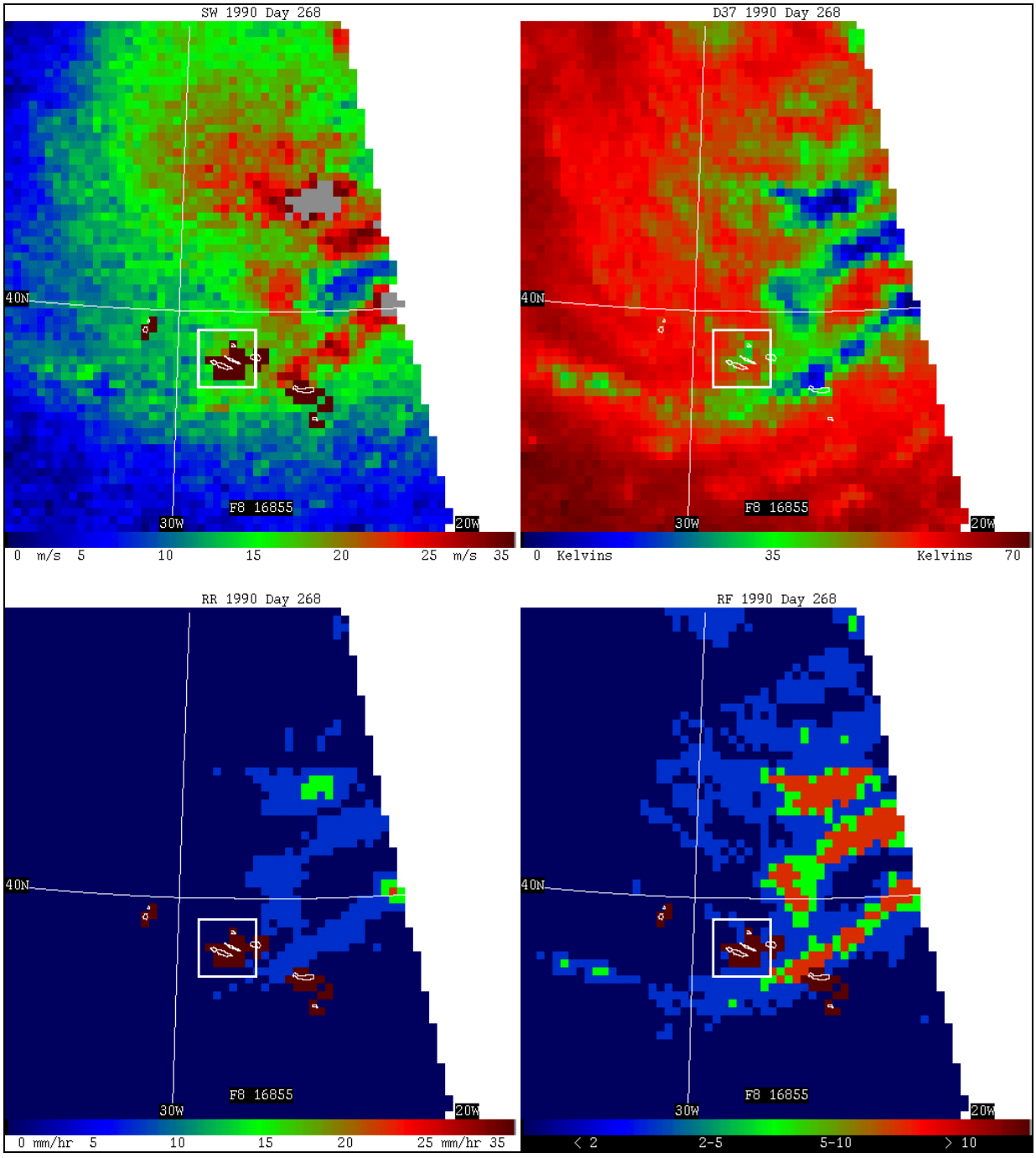

Figure 7.1-1. SSM/I data from DMSP F8, 25 Sep 90 over the eastern Atlantic. The Azores are indicated by the white square. Clockwise from upper left: Surface Wind EDR (m/s), 37GHz differential (D37), Rain Flag EDR, and Rain Rate EDR (mm/hr).

7.2 Day 2: 26 September 1990

SYNOPTIC SITUATION

The surface low was now to the ENE with a strong upper level low cutoff to the east. A strong low zonal jet with a 150 knot maximum just to the east of Lajes was supporting the development of the longwave trough to the east. A number of vorticity lobes were rotating around the low causing periods of enhanced rainshower and thunderstorm activity. A strong gradient between the high and low continued to keep Lajes and the entire archipelago in an area of strong winds.

SSM/I IMAGERY (Figure 7.2-1)

The winds in the vicinity of Lajes ranged from 29 to 35 knots (15-18 m/s), with D37 values from 41 to 55 (reds). The D37 values support a high degree of reliability for the wind speed values. The rain flag and rain rate areas match well with the lower D37 values (greens and blues). The wind speed accuracy suffers in these regions.

In addition, recent studies have shown that very cold 85H brightness temperatures embedded within warmer surrounding temperatures signify vigorous convection. The 85H data from this pass (not shown) clearly showed the enhanced areas of convection associated with the vorticity lobes rotating around the low and matched up perfectly with the OLS data.

Surface observations for Flores, Horta, and Lajes at 0800Z were 30 knots (15 m/s) gusting to 47 (24 m/s), 20G41 knots (10G22 m/s), and 20G30 knots (10G15 m/s), respectively. Ship reports tied very closely with the SSM/I data. Ships at 43 N 34 W, 42 N 34W, and 37 N 30 W measured the wind at 20 knots (10 m/s), 35 knots (18 m/s), and 35 knots (18/m/s), respectively. The corresponding SSM/I observations were 19 (10), 37 (19), and 35 (18) knots (m/s).

Again, the SSM/I data validated the fact that Lajes was in a large area of strong winds and gave forecasters confidence to issue the weather advisories and warnings for long periods of time. All advisories and warnings verified, except one for runway surface winds gusting to 50 knots (26 m/s). A gust to 48 knots (25 m/s) was observed.

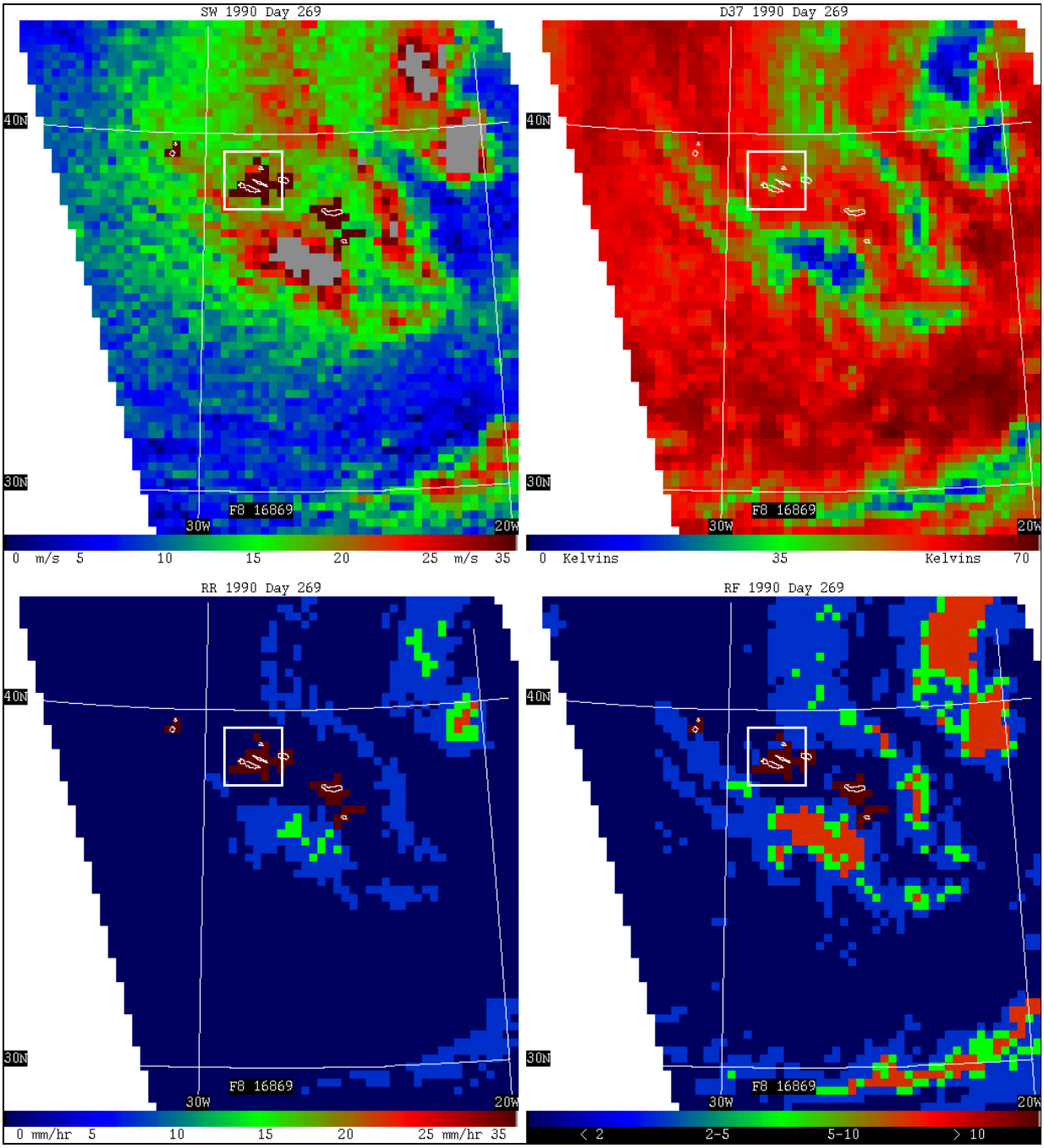

Figure 7.2-1. SSM/I data from DMSP F8, 26 Sep 90 over the eastern Atlantic. The Azores are indicated by the white square. Clockwise from upper left: Surface Wind EDR (m/s), 37GHz differential (D37), Rain Flag EDR, and Rain Rate EDR (mm/hr).

7.3 Day 3: 27 September 1990

SYNOPTIC SITUATION AND SSM/I IMAGERY (Figure 7.3-1)

By early morning on 27 September, it was clear to the forecasting staff that the storm was on its way out, but they expected the winds to remain above the weather criteria [30 knots (16 m/s) for the runway, 40 knots (21 m/s) for the tower] until 1200Z. The 0700Z pass, however, showed the winds just upstream of Lajes had dropped below 30 knots (16 m/s). The SSM/I provided conclusive data which helped convince the forecasters to cancel the wind advisory three hours earlier than previously planned, despite 35+ knot (18+ m/s) winds still being reported on the island of Flores, one of Lajes traditional indicators of pending strong winds. The winds dropped below advisory criteria within an hour after the DMSP pass and continued to weaken throughout the day. As seen in the images, winds in the vicinity of Lajes are in the 22 to 34 knot (11-18 m/s) range, with D37 values ranging from 45 to 55, indicating good wind speed accuracy.

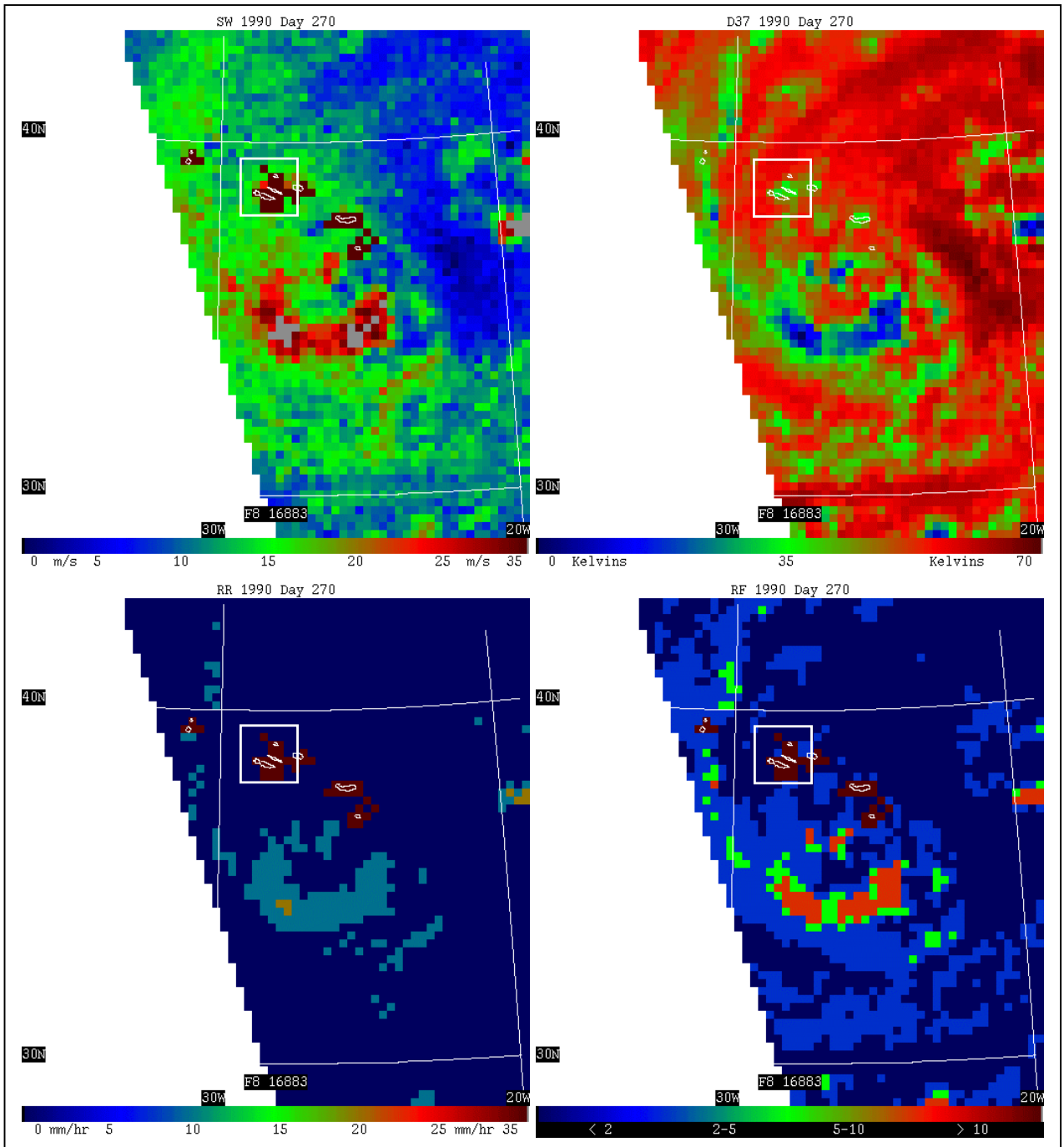

Figure 7.3-1. SSM/I data from DMSP F8, 27 Sep 90 over the eastern Atlantic. The Azores are indicated by the white square. Clockwise from upper left: Surface Wind EDR (m/s), 37GHz differential (D37), Rain Flag EDR, and Rain Rate EDR (mm/hr).

8. GLOSSARY AND ACRONYM LIST

A - Angstroms (1 A = 10^{-10} m)

Absorption - The process by which incident radiation is converted to another form of energy (usually thermal).

AFWA - Air Force Weather Agency, formerly Air Force Global Weather Central (AFGWC) (located at Offutt AFB, Nebraska).

Albedo - The ratio of radiant energy of the total solar spectrum reflected from a surface to that incident on it.

Antenna temperature - Value obtained by converting the received radiance to a temperature via calibration.

APC - Antenna Pattern Correction. This is the process in which the received radiance is corrected to remove the effects of neighboring scene stations.

AVHRR - Advanced Very High Resolution Radiometer. A multichannel infrared/visible sensor system carried aboard NOAA meteorological satellites.

A/D - Analog-to-Digital.

Bandwidth - The range of frequencies which can be received.

Blackbody - A theoretical object which absorbs all energy which falls upon it. In order to maintain thermal equilibrium, it also radiates at all frequencies.

Brightness temperature - Radiometrically corrected antenna temperature.

Cold load - Reflector to cold space used as a calibration reference target on the SSM/I

CW - Cloud Water Content.

DEF - Data Exchange Format. A standard weather data format.

Detector - Electronic device to convert incident radiation to a signal (usually a voltage).

DMDM - Direct Mode Data Message. A data stream broadcast by the DMSP satellite containing ephemeris information.

DMSP - Defense Meteorological Satellite Program. EDR - Environmental Data Records. Earth located environment parameters.

EM - Electromagnetic.

Emissivity - The ratio of radiant energy from a body to that from a blackbody at the same temperature.

Ephemeris - A file containing satellite position vectors.

ESMR - Electronically Scanned Microwave Radiometer.

Exitance - radiant power into a hemisphere per unit emitter area. Units are W/m2 for total exitance and $W/(m^2 \cdot \mu m)$ for spectral exitance.

FNMOC - Fleet Numerical Meteorology and Oceanography Center (located in Monterey, California).

Frequency - The number of occurrences of an event in a given time interval. For electromagnetic radiation, the frequency is the number of wave cycles that pass a point in one second, and is given in Hertz (1 Hertz = 1 cycle per second).

FY - First year sea ice.

GHz - Gigahertz. One billion (10^9) cycles per second.

GOES - Geostationary Operational Environmental Satellite.

Hot load - Heated near-blackbody used as a calibration reference target on the SSM/I.

IA - Ice Age (first year or multiyear).

IC - Ice Concentration.

IR - Infrared. This is the region of the electromagnetic spectrum with wavelengths between 0.76 and 30 micrometers.

ITCZ - Inter-Tropical Convergence Zone.

K - Kelvins. The Kelvin temperature scale measures temperature above absolute zero (0 K = -273.18 degrees Celsius). A one Kelvin difference is equal to a one degree Celsius difference.

MHz - Megahertz. One million (10^6) cycles per second.

Micrometer - 10^{-6} m.

Microwaves - Electromagnetic radiation with a wavelength from 1 mm to l m.

MISTIC - Mission Sensor Tactical Imaging Computer. The SSM/I processing and display system in use at tactical sites.

MY - Multiyear sea ice.

NASA - National Aeronautics and Space Administration.

NESDIS - National Environmental Satellite Data Information Service.

NOAA - National Oceanic and Atmospheric Administration.

Normal - Perpendicular.

NRL - Naval Research Laboratories.

OLS - Operational Linescan System. The visible/infrared sensor onboard DMSP spacecraft.

QDR - Quality Data Records. Files containing information on the health of the SSM/I sensor.

Polarization - The state of electromagnetic radiation when transverse vibrations take place in some regular manner.

Polarization difference - The arithmetic difference between the horizontal and vertical channels at one frequency.

Position vector - The location of a satellite at a specific time, given in terms of subpoint latitude, subpoint longitude, and spacecraft altitude.

RF - Rain Flag.

RMS - Root mean square.

RR - Rain Rate.

RTNEPH - Real Time Nephanalysis. This is the automated cloud analysis system currently in use at AFGWC.

SC - Surface Characteristic.

SDHS - Satellite Data Handling System.

SDR - Sensor Data Records. Calibrated, Earth located, antenna pattern corrected brightness temperatures.

SM - Soil Moisture.

SMIEPE - SSM/I Environmental Parameter Extraction. A program which converts Sensor Data Records into Environmental Data Records (environmental parameters).

SMIRCH - SSM/I Relational Channel History. A program which reads data from the AFGWC eighth mesh polar stereographic EDR/SDR database and updates the SSTDB

SMISDP - SSM/I Sensor Data Processing. A program which converts raw SSM/I data into Sensor Data Records (calibrated, Earth located, antenna pattern corrected brightness temperatures).

SMISHM - SSM/I Sensor Health Monitor. A program which unpacks sensor health information from the SSM/I data stream and generates Quality Data Records.

SMMR - Scanning Multichannel Microwave Radiometer.

SSM/I - Special Sensor Microwave Imager.

SSTDB — Seasonal Surface Type Data Base.

ST - Surface Temperature.

Subpoint - The point on the Earth' s surface directly below a satellite.

TDR - Temperature Data Records. Calibrated, Earth located brightness temperatures.

Thermometric temperature - The true physical temperature of an object (as measured by a thermometer).

Visible - The region of the electromagnetic spectrum (wavelengths from 0.39 to 0.76 micrometers) in which the radiation is perceptible to the human eye.

Wavelength - The length of one period of a recurring signal. For electromagnetic radiation, the wavelength is the distance from one peak of the wave to the next.

WS - Wind Speed.

WV - Water vapor.

9. REFERENCES

Benincasa, F., G. Maracchi, S. Paloscia, P. Pampaloni, and G. Zipoli: Remote Sensing of Vegetation with Microwave Radiometers.

Burke, H. K., C. J Bowley, and J. C. Barnes, 1984: Determination of Snowpack Properties from Satellite Passive Microwave Measurements, *Remote Sensing of the Environment*, **15**, 1-20.

Comiso, J. C., 1983: Sea Ice Effective Microwave Emissivities From Satellite Passive Microwave and Infrared Observations, *J. Geophys. Res.*, **88**, 7686-7704.

Comiso, J. C., 1986: Characteristics of Arctic Winter Sea Ice From Satellite Multispectral Microwave Observations, *J. Geophys. Res.*, **91**, No. Cl.

DMSP SSM/I Cal/Val Team, coordinated by James Hollinger, 1989: DMSP Special Sensor Microwave/Imager Calibration/Validation Final Report. Vol. I., Naval Research Laboratory, Washington, D.C.

DMSP SSM/I Cal/Val Team, coordinated by James Hollinger, 1991: DMSP Special Sensor Microwave/Imager Calibration/Validation Final Report. Vol. II., Naval Research Laboratory, Washington, D.C.

Ferraro, R.R., 1997: SSM/I derived global rainfall estimates for climatological applications. *J. Geophys. Re*s., **102**, 16,715-16,735.

Gaut, N. E., and E. C. Reifenstein III, 1971: Interacton model of microwave energy and atmospheric variables. *ERT Tech. Rep. No. 13*, Environmental Research and Technology, Inc., Waltham, MA.

Grody, N. C., 1988: Surface Identification Using Satellite Microwave Radiometers, *IEEE Transactions on Geoscience and Remote Sensing*, **26**, No. 6.

Grody, N.C. and A. Basist, 1996: Global identification of snow cover using SSM/I measurements. *IEEE Trans. Geo. Rem. Sens.*, **34**, 237-249.

Hamill, T. M.; R. P. D'Entremont, and J. T. Bunting, 1992: A Description of the Air Force Real-Time Nephanalysis Model, *Weather and Forecasting*, **7**, 288.

Hollinger, J. P. (ed.), 1990: Special Issue on the Defense Meteorological Satellite Program (DMSP): Calibration and Validation of the Special Sensor Microwave/Imager (SSM/I), *IEEE Trans. Geosci. Rem. Sens.*, **28**.

Liebe, H. J., G. A.Hufford., T. Manabe, 1991: A model for the complex permittivity of water at frequencies below 1THz, *Int, J. IR & MM Waves*, **12**, 659.

Meeks, M. L., and A. E. Lilley, 1963: The microwave spectrum of oxygen in the Earth's atmosphere, *J. Geophys. Res.*, **68**, 1683-1703.

Mugnai, A., H. J. Cooper, E. A. Smith, G. J. Tripoli, 1990: Simulation of Microwave Brightness Temperatures of an Evolving Hailstorm at SSM/I Frequencies, *Bulletin of the American Meteorological Society*, **71**, No. 1,

Pampaloni, P., S. Paloscia, and G. Zipoli, 1983: Microwave emission of soil and vegetation at X and Ka bands, Proceedings of IGARSS'83 (International Geoscience and Remote Sensing Society Symposium), vol. II, FP-5, 2. San Francisco, 1983.

Pandey, P. C., E. G. Njoku, J. W.Waters, 1985: Measuring Clouds with Microwaves and IR, National Aeronautics and Space Administration Technical Brief, Vol. 9, No. 1, Item # 48.

Parkinson, C. L., J. C. Coniso, H. J. Zwally, D. J. Cavalieri, P.Gloersen, and W. J. Campbell, 1987: Arctic Sea Ice. 1973 - 1976: Satellite Passive Microwave Observations, National Aeronautics and Space Administration SP-489.

Petty, G., 1993: in Proceedings Shared Processing Network DMSP SSM/I Algorithm Symposium Monterey, CA 8-10 June 1993 [Available from FNMOC, Monterey, CA]

Schmugge, T., P. E. O'Neill, and J. R. Wang, 1986: Passive Microwave Soil Moisture Research, *IEEE Transactions on Geoscience and Remote Sensing*, Vol. GE-2, No. 1.

Troy, B. E., J. P. Hollinger, R. M. Lerner, and M. M. Wisler, 1981: Measurement of the Microwave Properties of Sea Ice at 90 GHZ and Lower Frequencies, *J. Geophys. Res.*, **86**, No. C5

Ulaby, F. T., R. K. Moore, and A. K. Fung, 1982-6: Microwave Remote Sensing 3 vol., Addison - Wesley Publishing Co., Reading, Mass.

Weng, F, N. Grody, R. Ferraro, A. Basist, and D. Forsyth, 1997: Cloud liquid water climatology from the Special Sensor Microwave Imager, *J. Climate*, **10**, 1086-1098.

Vincent, J. D., 1990: Fundamentals of Infrared Detector Operation & Testing, John Wiley & Sons, New York.